Optical studies of impurities in quantum wells

Harris, C. I.

Award date:
1991

Awarding institution:
University of Bath

Optical Studies of Impurities in Quantum wells

submitted by C.I.Harris
for the degree of PhD
of the University of Bath
1991

C.Harris

ProQuest LLC
789 East Eisenhower Parkway
P.O. Box 1346
Ann Arbor, MI 48106-1346

Auch in Wissenschaften kann man eigentlich
nichts wissen, es will immer getan sein.....
Maximen und Reflexion 415, Goethe

Abstract

The properties of intentional dopants in semiconductor quantum wells have been studied using various photoluminescence techniques. The presence of impurities in the quantum well structure is found to have diverse effects on the optical properties of the system. The confinement of carriers in the quantum well structure is defined by the band offset between alternate layers; in the presence of ionised impurities this confinement is distorted by the associated Coulombic field. This situation is well recognised in modulation doped structures, we show in this work that it can also be a dominant effect in the centre-doped case. Much of the behaviour of impurities in the confined case can be understood by making a comparison with bulk material. The larger binding energy of the impurity in the quantum well however results in important differences particularly in the development of the PL spectra with increasing doping density. In particular the effect of impurity screening on excitons in a quantum well is found to be negligible in contrast to bulk GaAs where the exciton is quenched at relatively low doping densities. The importance of exciton recombination in confined systems is now well recognised and correspondingly is one of the major themes considered in this work. In addition to the screening action of impurities on excitons, they are also able to act as traps which bind the exciton to form a bound exciton. The interaction of excitons with impurities has been studied using picosecond time-resolved photoluminescence employing a streak camera. The exchange of excitons between the bound site and a free population via capture and thermal release is found to be an important mechanism in determining the observed recombination rate. Excitons can also be localised in the strong potential fluctuations due to, for example a high doping density or to defects at the interface. These bound states are not well defined in energy as are the

Coulombic states of the isolated impurity, but have a spread of binding energies which result in a low energy tail to the exciton recombination. Exciton localisation also strongly affects the interaction of the free exciton with the impurity. The interplay of localisation in determining the exciton interaction, is used in this work to demonstrate a novel method for determining the impurity binding energy in a narrow quantum well.

Acknowledgements

The work described in this thesis has been carried out entirely at the Max-Planck-Institut für Festkörperforschung in Stuttgart, Germany. This opportu nity was made possible by the support and encouragement of many people both at the University of Bath and at the Max-Planck-Institut itself. In particular I would like to thank Dr Jörg Weber within whose group I have had the pleasure to work, and Prof. H.-J. Queisser as head of the department without whom none of this would have been possible. I would also like to thank Dr. W. Clark for his support in the early stages of my battle against mountains of unsuccumbing bureaucracy!

As to the science, I'd like to start by thanking both my supervisors, Dr Jörg Weber for introducing me to the art of photoluminescence, for teaching me so much about the optical properties of defects in semiconductors and for countless discussions as to the whys and wherefores of it all! Secondly Dr Bill Clark my internal supervisor at Bath whose regular visits and whose difficult task of support from afar were invaluable to me.

I would also like to thank in particular Prof. Bo Monemar (Linköping University, Sweden) for his enormous support and encouragement of my work and with whom many of the ideas presented here have undergone their necessary filtering and refinement! Dr Heinz Kalt (MPI and University Kaiserslautern, Germany) for introducing me to time-resolved photoluminescence and the perils of picosecond spectroscopy and also for many useful discussions. Dr Gerhard Brunthaler for his guidance on the intricacies of MATLAB and calculations done therewith and also many insights into the world of the DX centre! Dr Klaus Köhler (Fraunhofer Institut für Angewandte Festkörperphysik, Freiburg) for the generous donation of many samples. And also the group at Quest (University of Santa Barbara) for the indirect supply of

samples. In addition I would like to acknowledge the many useful discussions with visiting scientists at the Max Planck Institut ; Dr H. Sigg (Paul Scherrer Institut, Zürich), Dr J. Donegan (Trinity College, Dublin), Dr J. Svensson (Linköping University, Sweden), Dr W. Sawyer (Mobil Solar, U.S.A.), Dr. J. Hartung (Kings College), Dr P. De'ak (Budapest, Hungary), Dr N. Pulsford (MPI) and many others. Many thanks also to my friends and colleagues not mentioned above, to name but a few, Andrew Peck, Deborah Cecere, Annedore Vierhaus, Rainer Ehmann, Gerhard Hofmann, Thomas Prescha, Thiery Zundel, Karsten Weronek, Dirk Bohne, Gerd Pfeiffer .....

As with any final product, the preparation of this thesis has also been made possible by the people in the background supporting it all, the technical staff. It is a pleasure to thank Wolfgang Heinz, Werner Krause, Klaus Rother and Heinrich Klann for their assistance in all matters technical! I also wish to acknowledge the service groups of the Max-Planck-Institut including Technologie, Kristallpräperation, Tieftemperatur, Photolabor and Bibliothek.

Finally I must thank my parents and grandmothers for their love and encouragement over the years. A special thanks goes also to Ute for her love and support.

Contents

Figure Captions

Chapter 2

Chapter 3

Chapter 4

Chapter5

Chapter 6

Chapter 7

Chapter 1

Introduction

1.1 Motivation

The past 40 years, since the invention of the transistor by W. Shockley, has seen a revolution in science and technology through the development of semiconductors. The increase in the physical understanding of these materials has lead to their utilization in a spectrum of devices encompassing every aspect of our daily life. The main "work-horse" of this developing era has been the material silicon. The ease of production techniques and the important high purity of this material have maintained its dominant position despite the development of many new materials. This situation looks certain to continue for digital devices well into the next century [1.1].

Silicon is an example of an "indirect-gap" semiconductor, the implication of this is that the recombination of electron and hole charge carriers is a relatively inefficient process. Demand for opto-electronic devices and higher switching speeds has motivated an ever increasing interest in the group III-V compound semiconductors, in particular those which are "direct gap" and hence exhibit highly efficient recombination. Despite the advantages of the compound semiconductors, their overall succession over silicon has not yet occurred. The problems encountered with these new materials have been considerable, in particular when comparing production techniques, the III-V compounds are extremely difficult to handle. In addition the purity of compound semiconductors is poor in comparison with that of silicon. The problem of impurities and defects in the native material has hindered their characterization and the understanding of their basic properties. The investigation of the exact

nature of these defects has enabled some progress to be made in the production of higher quality material [1.2]. A significant step forward in our understanding has been made in recent years with the development of thin film epitaxial techniques which have allowed the growth of high quality single crystal layers. The state-of-the-art development of thin film techniques now allows near atomic-layer resolution control in the growth of layers. Metal Organic Chemical Vapour Deposition (MOCVD) [1.3] and Molecular Beam Epitaxy (MBE) [1.4] are the two most common examples of these high resolution growth methods, which have opened the possibility of designing multi-layer semiconductor structures where each layer is typically of a few nm in thickness. A layer of thickness comparable to the mean free path and de-Broglie wavelength of the charge carriers will exhibit quasi two dimensional behaviour of its charge carriers. Such quantum confinement conditions have been achieved in multi-layer semiconductor structures grown, using the MBE and MOCVD growth techniques [1.5]. To date the most commonly investigated of such structures has been that formed by the layer combination AlGaAs-GaAs-AlGaAs. The aluminium content of the ternary alloy AlGaAs is chosen such that the band offset in both conduction and valence bands confines the charge carriers to the active GaAs layer. Band-gap engineering of this kind was first proposed by Esaki and Tsu as early as 1970 [1.6]. They also highlighted the possibility of modulation doping, in which the dopant is placed in the larger band-gap material with the result that the dopant is then ionised and the carrier lost to the quantum well. The carriers separated from the ionised scattering centre are able to achieve extremely high mobility within the 2D layer. The high quality of such systems has allowed the investigation of new physical phenomena such as the Integer and Fractional Quantum Hall effects [1.7]. One further consequence of confinement is an effective increase in the Energy gap of the confined layer, this tuning of the gap allows an accurate control of the

photon energy of a semiconductor laser made from such a structure. As a result of these developments there has been considerable technological interest in the design of high-speed switching devices and optical elements based on the selectable bandgap and excitonic non-linearities of such systems.

The situation for which the dopant appears in the well and not the barrier (anti-modulation doping) has received considerably less attention, although also of potentially important technological interest. The possible effects of an impurity within the well are manifold: the provision of carriers for conduction; the ability to act as a scattering site, thereby limiting mobility, and as a centre for radiative or nonradiative recombination of electrons and holes.

The use of optical techniques in the study of impurities in semiconductors has a long standing history [1.8]. Excitation of the material with photons of energy larger than the fundamental bandgap creates free electron-hole pairs. The subsequent relaxation and recombination of these carriers can occur via impurity related states. When recombination takes place radiatively the resulting emission is characteristic of the relaxed state. In this way, analysis of the photo-induced luminescence (photoluminescence) is a powerful tool to directly study impurity states.

1.2 Scope of Thesis.

The basic physical properties of a crystalline semiconductor are for the most part determined by the regular periodic nature of its atomic potentials. It is therefore not surprising that the presence of an impurity or defect, interrupting the regular lattice has diverse and significant effects upon the behaviour of the semiconductor. The work reported in this thesis reflects this diversity in response and considers a number of effects of an impurity in a quantum

confined structure. Many of the properties discussed have a direct counterpart in bulk material, while others are specific to layered structures.

The main theoretical framework for the thesis is set out in chapter 2. The simple text book example of the ideal square well is described in terms of its application to real quantum structures. An approximate technique based on a Transfer Matrix treatment is also discussed as a means of calculating the eigenvalues for an arbitrarily shaped well. The section continues by considering the presence of impurities in a confined system and their treatment using the Effective Mass Approximation. A brief review is given of the effects of high doping in a semiconductor, in particular with regards to the Mott transition and the localisation of carriers in a random potential. Finally the different recombination mechanisms which occur for a direct bandgap material, specifically those prominent in a confined system, are discussed.

Chapter 3 reviews the experimental techniques and equipment that have been used in this work. The basic principles of the photoluminescence technique described in the first section are further discussed in the context of application of the method. The use of a tunable photon energy excitation source is highlighted as a means of probing specific transitions within the QW, so called selective excitation. An extension of this idea is the technique of excitation spectroscopy in which we examine the dependence of a single recombination channel upon tunable excitation at higher photon energy. The mechanisms by which carriers excited at high energy are able to relax to a local potential minima before recombination are of significant importance in understanding the electronic structure of a system. These dynamic processes can be studied by using a time-resolved photoluminescence technique, the principles of which are also discussed in chapter 3.

Chapter 4 looks at the importance of the Coulombic potential of an impurity in perturbing the confinement in a single quantum well. At high doping densities

the superposition of the potential due to a large number of ionised dopants, upon the band profile is found to dictate the observed subband energy levels. The influence of the impurity potential in turn leads to a strong dependence on the excited carrier density and distribution. The final section of this chapter looks at the effect of hydrogen passivation in GaAs/AlGaAs n-type quantum wells. In particular the dramatic effects discussed in the earlier part of the chapter as due to depletion by deep surface states are shown to be totally removed following passivation, a result which provides strong support for the original model. The effect of hydrogen in passivating shallow defects is also briefly discussed.

Chapter 5 studies in greater detail the high doping density limit in a quantum well. Interaction between dopants increases with concentration; the Coulombic potential of each impurity overlaps to an increasing extent until a carrier can no longer be considered as bound to a single core but is shared amongst many such centres. This "washing out" of the bound state leads progressively towards a quasi bound state (the so called impurity band in which carriers are still localised in the vicinity of an impurity) and on to an eventual free carrier. This phase change is usually referred to as the Mott transition and describes the change over from insulating to metallic type behaviour. The increased binding energy of a carrier to an impurity resulting from confinement implies an increased density limit for the Mott transition to occur. The observation of such a transition in a confined system is discussed in comparison to the 3D case. In addition a high doping density also effects the mechanisms by which recombination takes place, non radiative processes (such as Auger) in particular are enhanced.

Time-resolved measurements in the picosecond range are a particularly powerful technique to study the recombination kinetics for impurity related

transitions in a quantum well. Chapter 6 describes an extensive study of the interaction between free and bound excitons in narrow doped quantum wells. The observed decay of the exciton luminescence is discussed in terms of the determining contributions of capture and thermalisation to and from the bound site. The total kinetics can be modelled using a series of coupled differential equations, which also allows a more accurate analysis of both the radiative lifetime and the capture and thermalisation terms. The second half of this section considers the localisation of excitons either at interface roughness or by the random potential produced by impurities at high doping density.

The degenerate limit is again considered in chapter 7. The large number of free carriers present in a degenerate semiconductor leads to a strong interaction and scattering of charge. As a result of this interaction we can no longer consider the properties of a system in terms of the behaviour of each individual charge and instead are required to view the properties as a collective response. Such systems are said to exhibit "Many-Body" effects. In this chapter we examine one example of a Many-Body related phenomena, the so called Fermi-Edge Singularity (FES). The FES is an enhancement in the oscillator strength for transitions in the vicinity of the Fermi-level, and results from the correlation of a photo-excited hole with the total Fermi electron sea (in n-type material). This effect has been extensively studied in modulation doped systems, but a similar effect in centre-doped structures has not been discussed in the literature to date. The FES in modulation doped structures is compared and contrasted with the effects observed in the current work.

Finally chapter 8 makes an overall summary and conclusion to the work presented and discusses the direction of future work.

Chapter 2

Electronic Structure of Impurities in a Semiconductor Quantum Well.

2.1 Introduction.

2.2 The ideal square well.

2.3 Calculation of the bound states for an arbitrary potential.

2.4 Bandstructure of the bulk III-V compounds.

2.5 Effective Mass Theory.

2.6 Impurity bands and degenerate doping.

2.7 Radiative recombination.

2.1 Introduction.

This first main chapter of the thesis sets out most of the basic theoretical ideas which are drawn upon throughout the discussion of the material in this thesis. It starts by looking at the simple quantum mechanics of the ideal square well. The extension of this text book model to a real system depends on the electronic bandstructure of the materials involved, the relevant electronic properties of the III-V compound GaAs are reviewed. Traditionally the introduction of impurities into the semiconductor lattice has been treated within the framework of the Effective Mass Theory (EMT). Here a single excess valence electron or hole of an impurity in the lattice is considered analogous to the single charge of a hydrogen atom, the impurity state energy levels can be calculated by replacing the free space permittivity with that of the material and taking an effective mass for the charge carrier. This theory is outlined as applied to bulk GaAs. The results of variational method calculations of impurities in the confined GaAs/AlGaAs system using the effective mass approximation are also reviewed. As the doping limit is increased impurities begin to interact leading to the formation of an impurity band. The dependence of the semiconductor bandstructure on doping density is discussed, in particular the criteria for the transition from insulator to metallic-like behaviour is considered. The concentration of impurities is also shown to have important consequences for the localisation of charge. The final section looks at the different mechanisms of radiative recombination for direct gap materials.

2.2 The ideal square well

It is one of the attractions of the physics of 2 dimensional systems that the most basic concepts can be understood from the simplest example solution of quantum mechanics, the ideal square well. The potential profile for a general square well confined by finite barriers of height V_0 is shown in Fig.2.1 , and is described by:

$$V(z) = \begin{cases} 0 \text{ for } \frac{-a}{2} \le z \le \frac{a}{2} \\ V_0 \text{ for } |z| > \frac{a}{2} \end{cases} \qquad (2.1)$$

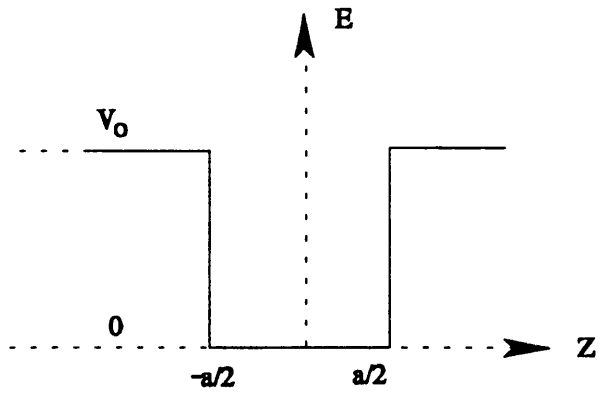

Fig.2.1 Square well potential with finite barrier height.

The eigenvalues and eigenfunctions are found from the solution of the one dimensional Schrödinger equation under the appropriate boundary conditions.

$$\frac{-h^2}{2m}\frac{d^2\Psi}{dz^2} + V(z)\ \Psi(z) = E\,\Psi(z) \qquad (2.2)$$

Since the potential is continuously defined for all z, general solutions of the time independent Schrödinger equation can be expressed as the sum of two travelling waves with opposite directions:

$$\Psi = A\, e^{ikz} + B\, e^{-ikz} \qquad (2.3)$$

with k vector:

$$k(z) = \left[\frac{2m^*(E-V(z))}{h}\right]^{1/2} \qquad (2.4)$$

The wavevector k is therefore defined by the potential in each layer, for an energy below the barrier height V_0 the wavevector in the barrier will be imaginary, giving a real coefficient to the exponent and implying an exponential decay of the wavefunction.

We define the wavefunction in each layer:

$$\Psi_1(z) = A\ e^{ik_1 z} + B\ e^{-ik_1 z} \qquad |z| \leq \frac{a}{2}$$

$$\Psi_2(z) = C\ e^{ik_2 z} + D\ e^{-ik_2 z} \qquad z \leq \frac{-a}{2}$$

$$\Psi_3(z) = F\ e^{ik_2 z} + G\ e^{-ik_2 z} \qquad z \geq \frac{a}{2}$$

Physically it is clear that the wavefunction must be finite for all z, hence $z \rightarrow -\infty$ implies D=0 and similarly $z \rightarrow +\infty$ implies F=0 (given k_2 real). The boundary conditions require the continuity of the wavefunction and its derivative at the interfaces; however the latter condition can in fact be more generally defined by the continuity of the particle current, which allows for a change in effective mass giving:

$$\frac{1}{m_1}\frac{d\Psi_1}{dz} = \frac{1}{m_2}\frac{d\Psi_2}{dz} \qquad (2.5)$$

Applying the boundary conditions and the normalisation of the wavefunction across all space leads to the eigenvalue equation:

$$\cos k_1 a + \frac{1}{2}\left[\frac{k_2}{k_1}\frac{m_1}{m_2} + \frac{k_1}{k_2}\frac{m_2}{m_1}\right] \sin k_1 a = 0 \qquad (2.6)$$

a solution for which exists only at discrete energies E. Alternatively we can simplify the algebra slightly by making use of the known symmetry of the potential. The solutions to a symmetric potential must be either symmetric or anti-symmetric (due to the arbitrary definition of the z direction). At the well centre (centre of symmetry, z=0) therefore, either the wavefunction (anti-symmetric) or its first derivative (symmetric) must be zero. Given these additional constraints we derive the simplified eigenvalue equations:

$$\tan k\, a/2 = i\left(\frac{k_1}{k_2}\frac{m_2}{m_1}\right) \qquad \text{(symmetric)} \qquad (2.7)$$

$$\tan k\, a/2 = \left(\frac{k_2}{k_1}\frac{m_1}{m_2}\right) \qquad \text{(anti-symmetric)} \qquad (2.8)$$

The first three solutions to which are plotted in Figure 2.2.

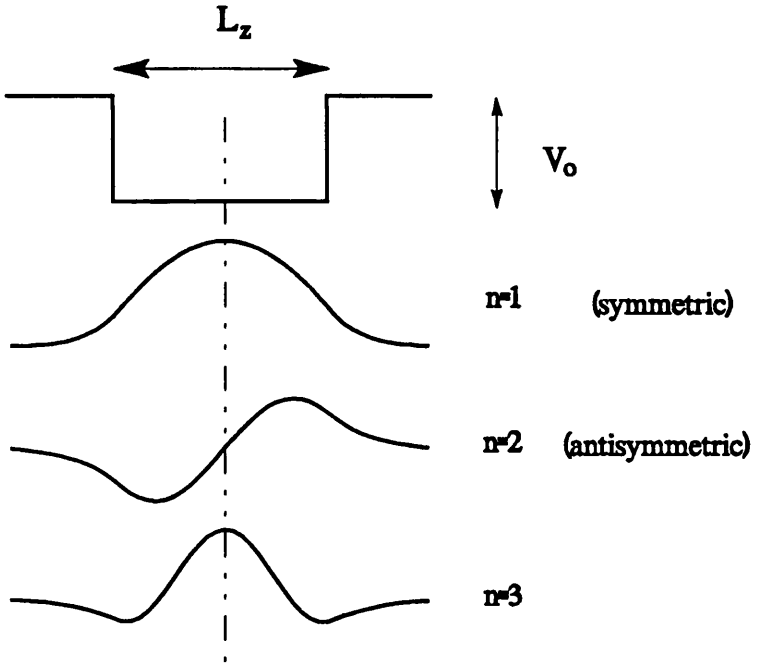

Fig 2.2 First three solutions to the square well problem with finite barrier height Vo.

The simple potential of the square well is in many cases no longer a realistic approximation to the actual potential shape. Unfortunately there exists no analytical solution for the bound states of an arbitrary shaped potential and various approximate methods have been developed for the numerical solution in these cases. In particular the presence of charge in a given potential will result in a perturbation due to the additional Coulombic field. This charge can be introduced for example by the presence of impurities. Perhaps the most important and easily recognisable example of this is modulation doping. A shallow donor/acceptor placed in the barrier will lose its extra valence electron/hole and becomes ionised. The lost charge is transferred to the well and in the process causes an internal electric field to be set up between itself and the ionised impurity centre. The resulting potential is illustrated in Fig.2.3.

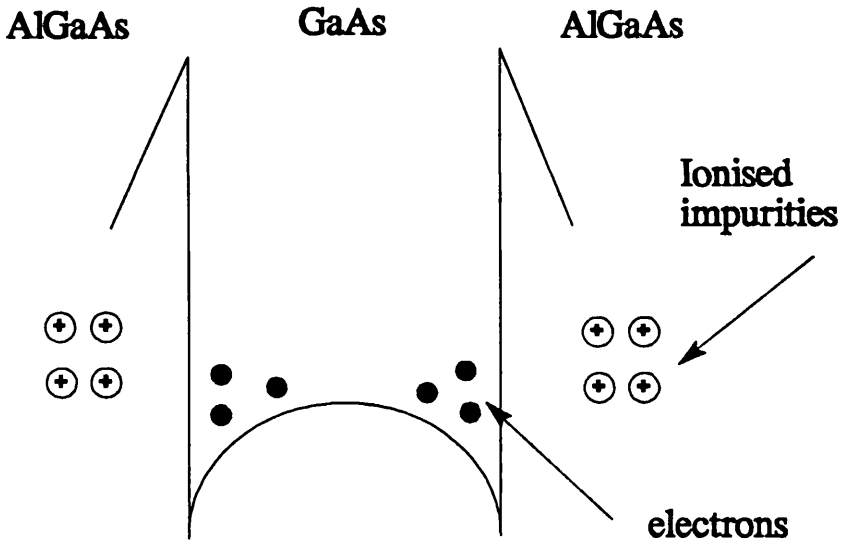

Fig 2.3 Symmetric Modulation doped structure.

The present work has looked not at modulation doping but at the presence of impurities in the centre of the well. In this case the impurity is not automatically ionised and in the neutral state does not make a significant perturbation to the potential. The important effect in this case is the additional confinement of the impurity bound state which enhances the binding energy, this process is

discussed in more detail in the following section. If on the other hand the impurity becomes ionised the resulting Coulombic potential can dramatically distort the square well profile. This effect should be observed for example as a shift in the confinement energies for the well. A detailed calculation of the potential shape and the resulting system of eigenvalues and eigenfunctions requires a self consistent approach, which is able to calculate the complex charge distribution in such a system. An in-depth calculation of this kind has not been attempted in this work and to the author's knowledge has also not been presented in the literature. It has however been useful as a guide to the analysis of the results of chapters 4 and 5 to make some guide-line calculations of the expected energy levels in a system with a potential shape estimated to be appropriate. A suitable technique for such a calculation is potentially quite complex since we face the problem of an arbitrary potential as was discussed previously. The method described here is chosen for it's simplicity but also it's versatility. Strictly speaking it is appropriate only to the treatment of periodic systems but can be applied to single potentials in the weakly coupled limit.

2.3 Calculation of the bound states for an arbitrary potential.

The motivation behind this calculation has been to try and estimate how an impurity related potential might distort the confinement from a simple square well system. The criterion imposed has been to try and make as realistic as possible an approximation to the expected potential, but at the same time retain a high degree of flexibility in the analysis. The routine used does not account for either correlation effects or the possibility of band mixing and hence does not deal with exciton states. A good qualitative analysis of the subband shifts and the distortion to the carrier wavefunctions is however possible.

The technique used is analogous to the Transfer Matrix Method [2.1], and uses the same approach in analysing a structure by considering the transmission matrix at each interface. We start by assuming a one dimensional periodic barrier for which we can specify the transmission and reflection coefficients (Fig.2.4).

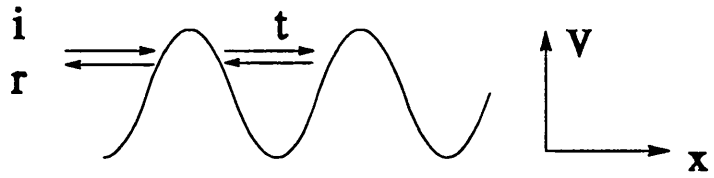

Fig 2.4 Transmission coefficient defined for single barrier of periodic structure.

Such a structure can then be analysed using a Kronig-Penney type treatment for which we can derive the following relation between the allowed energies and the transmission for a single barrier [2.2]:

$$\frac{\cos(Ka+\delta)}{|t|} = \cos(ka) \qquad (2.9)$$

where $K=(\sqrt{2mE})/h$, $|t|$ is the magnitude of the transmission $t=|t|\, e^{i\delta}$, δ being the resulting phase change, a is the period of the structure and k is the Bloch wavevector. The allowed energies are defined by the fact that cos(ka) must lie within the limits ± 1.

The analysis so far has made no assumptions as to the barrier shape and therefore, given that the transmission is known, can be arbitrarily defined. The confined system is analysed by choosing an appropriate form for the barrier, for example a square well has a corresponding rectangular barrier. The analysis of any defined barrier can be made by approximating the potential shape by a

series of steps (see Fig.2.5). The total transmission for the structure is then given by the product of the appropriate step transmissions.

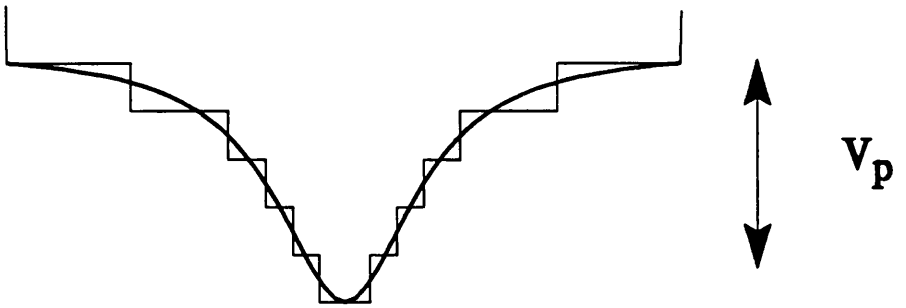

Fig 2.5. Approximation to potential by series of steps.

The transmission at a step is given by the standard derivation applying the boundary conditions at the interface which require the continuity of the wavefunction and its derivative. We define the wavefunctions on either side of the interface by:

$$\Psi_1(z) = A\ e^{ik_1 z} + B\ e^{-ik_1 z} \qquad z \leq a$$

$$\Psi_2(z) = C\ e^{ik_2 z} + D\ e^{-ik_2 z} \qquad z \geq a$$

Applying the boundary conditions leads to the coupling matrix M^c where:

$$M^c \begin{bmatrix} A \\ B \end{bmatrix} = \begin{bmatrix} C \\ D \end{bmatrix} \tag{2.10}$$

For the total structure this implies:

$$\prod_i M_i^c \begin{bmatrix} A \\ B \end{bmatrix} = \begin{bmatrix} C \\ D \end{bmatrix} \tag{2.11}$$

Assuming a wave incident from the left i.e. travelling in the direction of positive z, the transmission is given by the ratio of the coefficients C/A [2.3]. Substituting this result into the Kronig-Penney criterion for the allowed energies

provides a general method for the analysis of the confinement levels in a potential described by an arbitrary locus of points. It is clear that the technique strictly applies only to periodic structures, however by choosing the barrier to be suitably wide we can approximate the single well as the weakly coupled limit. Chapter 4 uses the results of such calculations to illustrate the change in the electron-hole wavefunction overlap for an impurity distorted potential.

2.4 Bandstructure of the bulk III-V compounds.

The III-V compounds including GaAs in general crystalise in the Zinc-blende structure (with some exceptions for example GaN), this is similar to the diamond structure of Si but with Ga and As (in the GaAs case) occupying adjacent sites. The bonding is tetrahedral with each Ga being surrounded by four As and similarly each As surrounded by four Ga in the perfect lattice (see Fig. 2.6). The lattice can be seen to consist of two interpenetrating face-centred-cubic (f.c.c.) lattices displaced from one another by a quarter of the main cubic diagonal (the tetrahedral spacing).

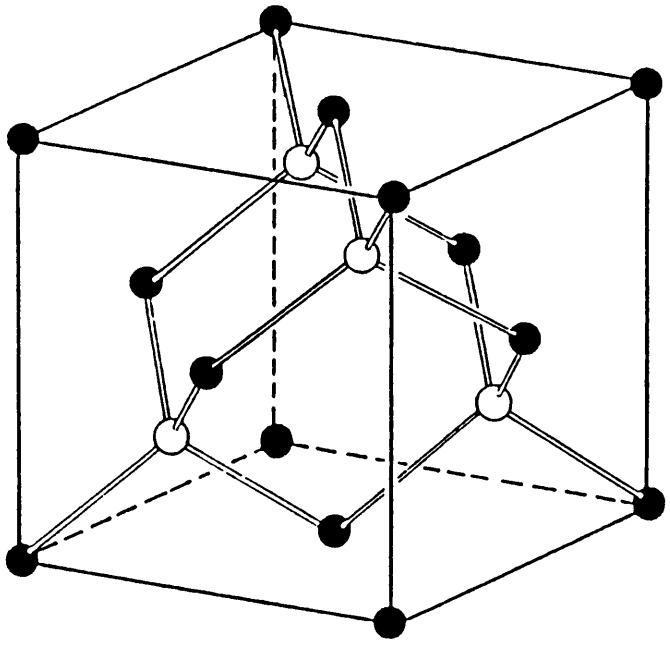

Fig 2.6 Arrangement of atoms in Zinc-blende structure.

The Bravais lattice of the zinc-blende structure is not the illustrated cell as this contains more than one lattice point, but is f.c.c. The corresponding reciprocal lattice is a body- centred cubic and the first Brillouin zone a truncated octahedron (Fig. 2.7). The high symmetry points X (square face centre), L (octahedral face centre) and the zone centre Γ are marked.

The chemical bonding in the binary III-V compounds is formed from the 8 outer valence electrons associated with each unit cell (for GaAs 3 from Ga and 5 from As). Electron orbitals between neighbouring atoms (for example Ga with As) hybridize to form two levels, the bonding and anti-bonding states. Due to the interaction of a large number of unit cells the states broaden to form bands. The bonding levels are normally filled, the s-like levels are deeply bound and contain 2 electrons per unit cell, the remaining 6 electrons are filled into the p states. The anti-bonding states are empty, the conduction band being formed from the lowest lying of these levels, normally the s state.

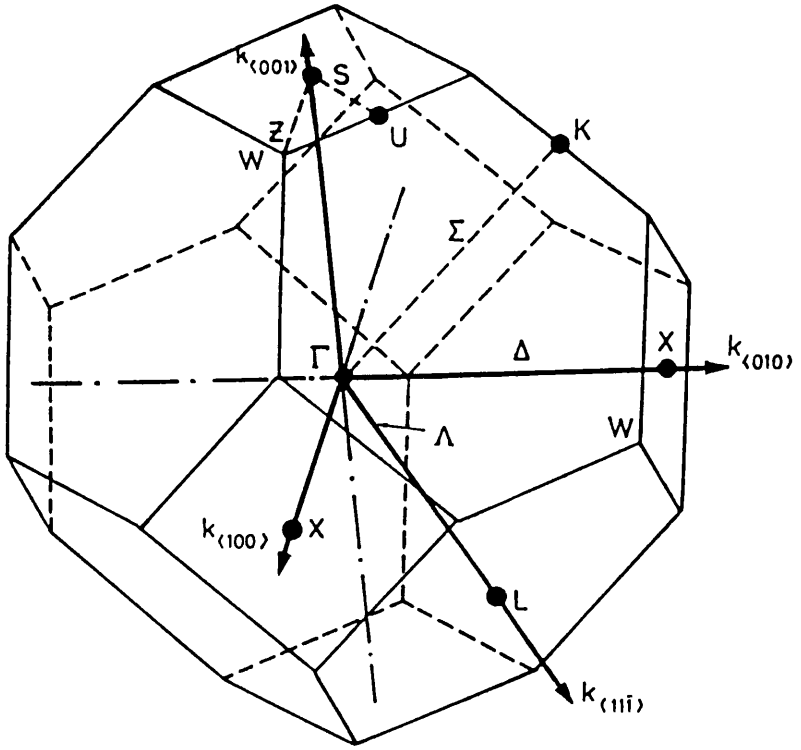

Fig 2.7. Brillouin zone for Zinc-blende structure (fcc unit cell).

The valence band maximum is found at the zone centre (Γ) for all the III-V compounds (see Fig. 2.8) [4], in the absence of spin-orbit coupling the three p orbitals are degenerate at the Γ point. This degeneracy is lifted in the presence of spin-orbit coupling, so that a fourfold Γ_8 level and a twofold Γ_7 (split-off) level is formed [2.5].. In a two dimensional confined system the Γ_8 degeneracy is further lifted so that one distinguishes a "heavy" and "light" hole.

The conduction band edge is situated either at the Γ point (GaAs) or close to the X or L points. the location of this minimum can in fact be related to the ionicity of the chemical bond formed [2.6].

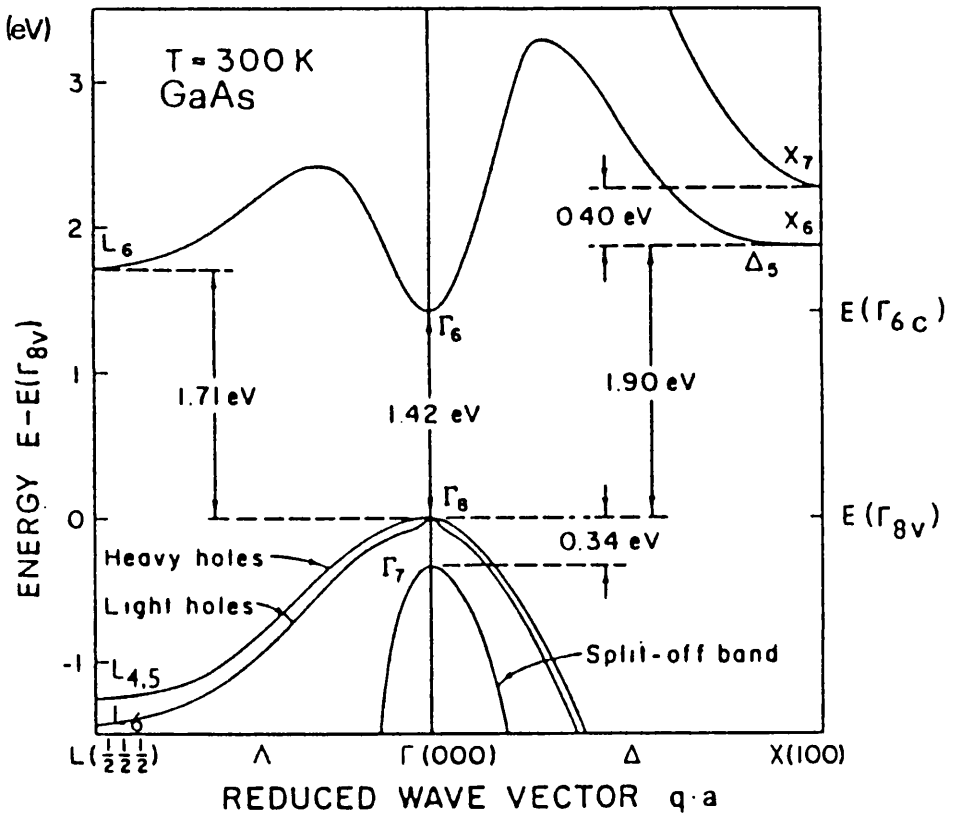

Fig 2.8 Band structure for GaAs in vicinity of zone centre.

The III-V elements are also able to form ternary alloys (e.g. AlGaAs) in which one of the lattice sites is randomly occupied by one of two species. The random identity of the atom at a particular lattice site is reflected in the atomic

potentials, this disorder results in a blurring of detailed features. In particular the lack of exact translational symmetry results in scattering from the Bloch states creating band tails and localisation. The dependence of the definition of the fundamental bandgap, effective masses etc. on the alloy composition depends strongly on the relative lattice mismatch between the parent binary compounds (e.g. AlAs and GaAs for AlGaAs). In general for a well matched system the alloy bandgap demonstrates a close to linear dependence on the parent compound ratio. If however, the bandstructure is significantly different between the two binary compounds, for example AlAs with a conduction band minimum at the X point and GaAs with a Γ minimum, then the alloy will show a non-linear dependence in its bandgap irrespective of lattice match.

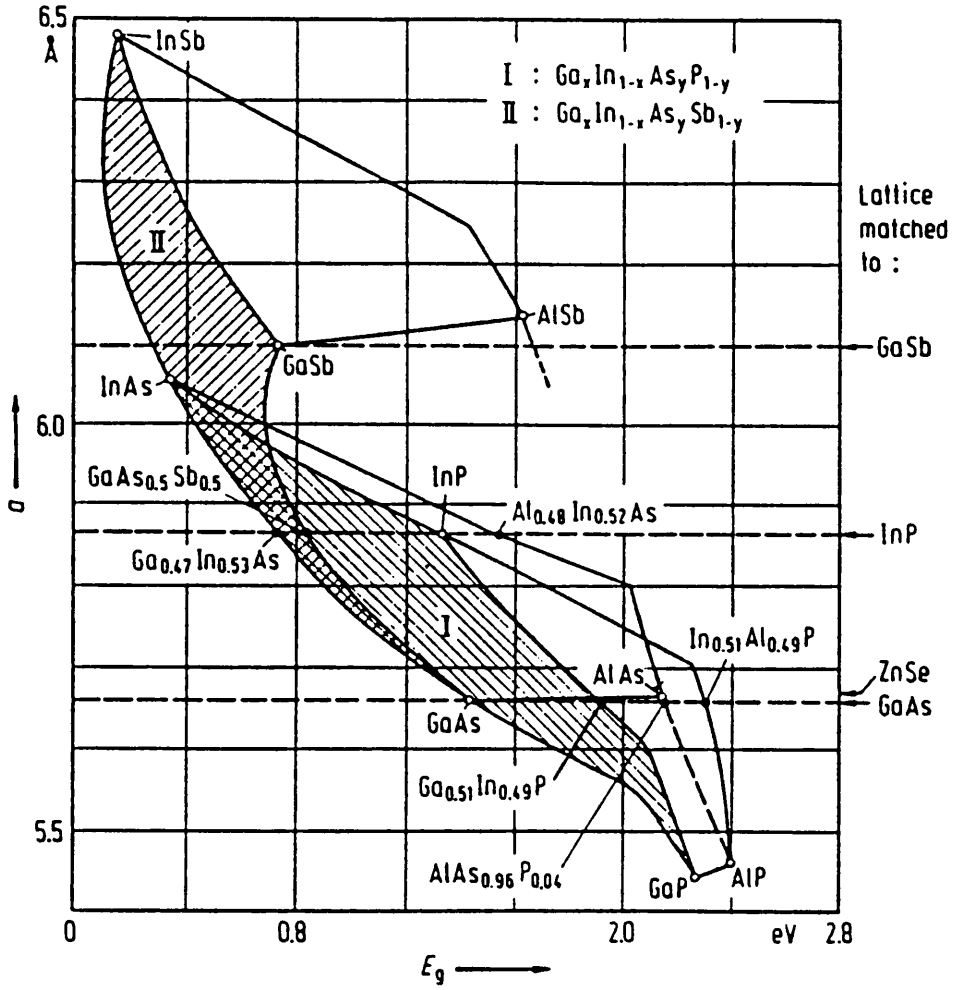

Fig 2.9 Lattice constant versus energy gap for various III-V compounds.

The lattice mismatch between compounds is also of critical importance in determining the band structure of a heterostructure. An interface between non-lattice matched material will be highly strained and distorts the local bandstructure. The accommodation of this strain will in fact determine whether a useful heterojunction can be formed or not. So called Strained-Layer-Superlattices (SLSs) using non-lattice matched materials have been developed which specifically make use of the distorted bandstructure in designing devices. Figure 2.9 illustrates the lattice match between various III-V binary and ternary alloys.

2.5 Effective Mass Theory.

A detailed review of this model is not given here, as numerous accounts exist in the literature, and the results of such a calculation are not explicitly discussed in any depth in this work (the following review articles are in particular well presented [2.7] [2.8] [2.9]). The model starts from the pretext that in the case of a donor impurity the one extra positive nuclear charge can be considered analogous to an isolated hydrogen nucleus. The impurity binding energy can then be derived from the Bohr model simply by substituting a reduced effective electron mass and a Coulombic interaction screened by the material dielectric. Using this hydrogenic approximation the donor bonding energy is given by:

$$En = \frac{1}{n^2}\frac{R_0 m^*}{\varepsilon^2 m_0} \qquad n=1,2,3..... \qquad (2.12)$$

where m^* is the effective mass, ε is the static dielectric constant and R_0 is the hydrogen Rydberg (13.6eV). The justification of this simple model has been shown from a quantum mechanical derivation by Kohn and Luttinger [2.10]. Their derivation follows an Envelope Function Approximation in which the

bound state wavefunction is expanded in terms of free Bloch-type functions modulated by a hydrogen-like envelope.

One consequence of the effective mass treatment is that all donors will have the same set of bound states. The deviation from this result in real systems is due to the fact that close to the impurity the potential is no longer simply Coulombic. A tightly bound donor state is strongly affected by this near-centre field, whereas a weakly bound donor, i.e. with large Bohr radius (for example r_B=103Å, as for GaAs) is only weakly affected. This difference in binding energy from the effective mass picture is often referred to as the central cell correction. For a donor in GaAs, the Bohr radius is extremely large and as a result the bound states are found to be totally effective mass like with no significant central cell correction.

The application of effective mass theory to shallow impurity centres in quantum well structures has been carried out by a number of groups, in most cases using a variational method of solution. The first such calculation was performed by Bastard [2.11], who considered a donor state associated with the first subband. His calculation assumed the well to be infinitely deep, an argument justified by the fact that the conduction band offset is considerably larger than the donor binding energy. This has the effect of excluding penetration of the barrier by the impurity wavefunction. Using this approach he was able to study the binding energy as a function of well width and also the donor position within the well. The extension of this work in removing the approximation of infinite barrier height was subsequently carried out by Greene and Bajaj [2.12] and also by Mailhiot *et al* [2.13]. A series of following papers made successive improvements to the approximations used. Chaudhuri and Bajaj [2.14] looked at the effects of a non-parabolic conduction band; Tanaka *et al.* [2.15] looked at the binding energy dependence of asymmetric barriers. Chaudhuri [2.16] has also considered the effect of variable barrier width i.e. the coupling between

wells on the donor states. It is interesting to note that the electron can still remain bound to the donor even when the donor is located within the carrier. Tanaka *et al.* have shown that for the GaAs/$Al_xGa_{1-x}As$ system the donor still maintains a binding energy of approximately 0.3 effective Rydbergs even between two and three effective Bohr radii into the barrier. The effect of external electric or magnetic fields has also been studied by Greene and Bajaj [2.17], Kleinmann [2.18] and by Brum *et al.* [2.19]. The acceptor case has received proportionately less attention due to the more difficult description of the hole. The electron is considered to be made up from Bloch type states that derive from a single band, while the hole wavefunction is formed from several valence bands which are degenerate at k=0 for the bulk material. A calculation of the acceptor binding energy has been carried out by Masselink *et al.*[2.20]. It is interesting to note that for very narrow wells the heavy and light hole bands are well separated and the effective mass of the "heavy-hole" is actually lighter than that of the "light hole". In the limit of sufficient separation the same method of calculation as for the donor could be used i.e. a straightforward substitution of hole effective mass appropriate to the well.

The results of the above calculations show that the binding energy of the impurity increases with confinement (see Fig. 2.10, 2.11) This can be understood for example for the donor in terms of the relative shift of impurity and conduction band states. As the well is made narrower, the conduction band is raised in energy due to the confinement of the electron. The impurity state is however already confined by the Coulombic interaction and as a result is less affected by the presence of the barriers. The increase in energy of the bound electron state is therefore less, leading to a proportionately larger binding energy. The binding energy of the impurity is in fact found to have a maximum at non-zero well width (see Fig. 2.10, 2.11).

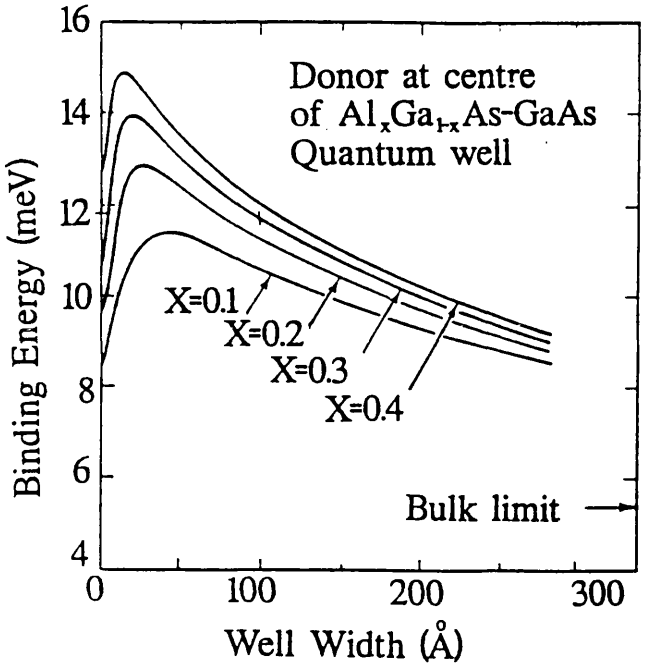

Fig 2.10 Dependence of donor binding energy on well width (donor placed at well centre).

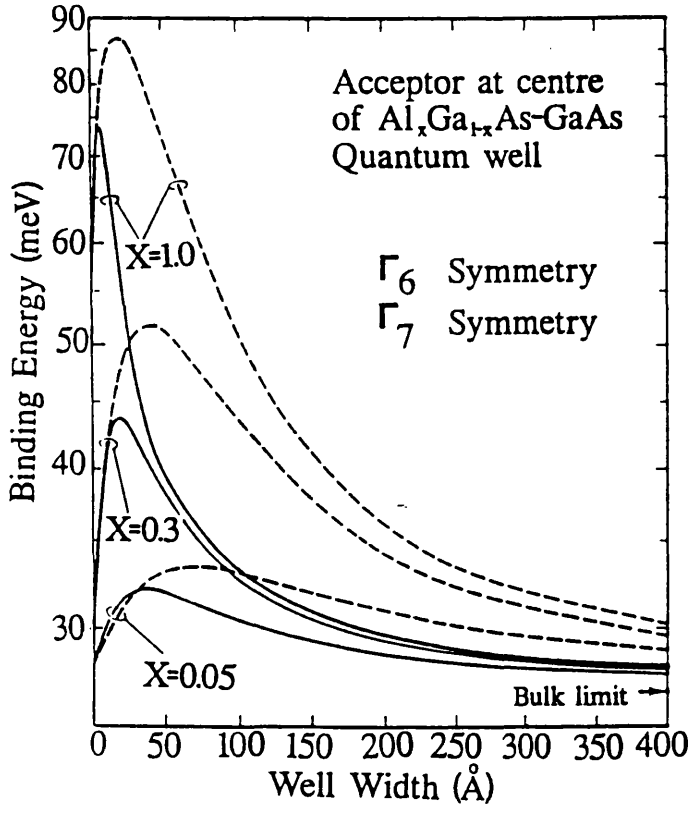

Fig 2.11 Dependence of acceptor binding energy on well width (acceptor placed at centre of well).

This point is a consequence of the penetration of the barrier by the impurity wavefunction and was therefore not realised in the original work of Bastard. The dependence of the binding energy on the impurity location within the well illustrates a further consequence of the barrier interaction. The edge-positioned donor is found to be less strongly bound in comparison to that at the centre. The barrier effectively pushes the wavefunction away from the impurity centre i.e. it becomes increasingly non-symmetric which decreases the Coulombic interaction (see Fig. 2.12 in comparison to Fig 2.10).

In general, the results of the above theoretical calculations have provided excellent agreement with experimental results measured by a number of different techniques (Photoluminescence [2.21] [2.22], Raman [2.23] and Far-Infra-Red [2.24]).

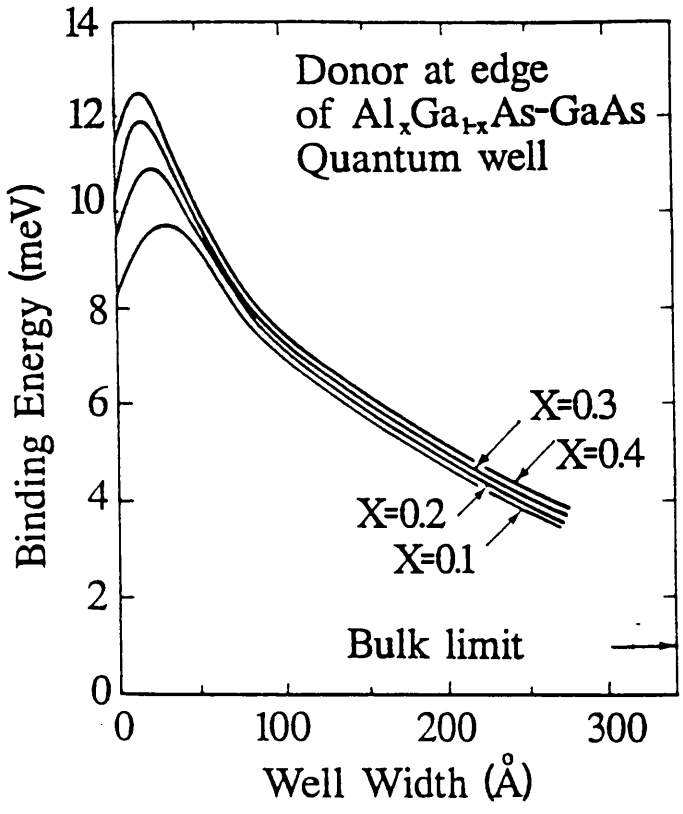

Fig 2.12 Dependence of binding energy for donor placed at edge of well.

2.6 Impurity bands and Degenerate Doping.

So far the picture presented for an impurity present in the semiconductor lattice has discussed a unique ground state energy level (Fig. 2.13 (a)). It turns out that this description is only appropriate when the impurity atoms can be considered as isolated centres. In terms of concentration this would correspond to the lightly doped limit.

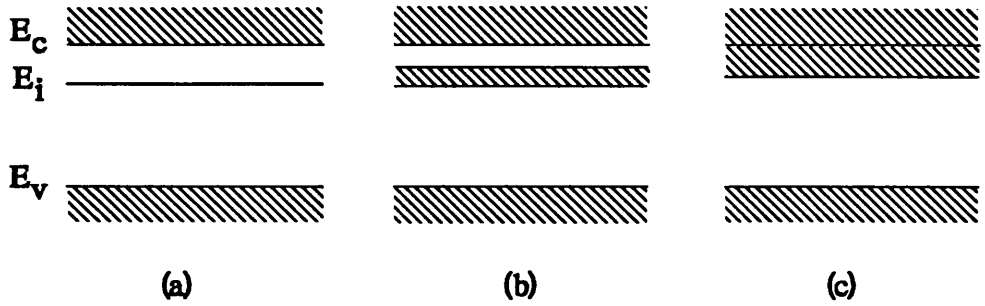

Fig 2.13 Broadening of impurity level with increasing doping.

As the density is increased the orbits of the electron/hole bound at the impurity begin to overlap. As this overlapping increases so the discrete level of the isolated atom broadens to from an impurity band. This is somewhat analogous to the transition from the distinct levels of an individual atom to the formation of bands in the crystal. The picture should however, not be taken too far, since the impurities are not periodically arranged as are the atoms in a crystal. An important consequence of this non-periodicity is that standing wave Bloch states are not formed. As a result the term "impurity band" is perhaps rather loosely applied, since we do not imply any relationship between energy and crystal momentum.

The energy diagram for a moderately doped semiconductor consists of an impurity band separated from an "intrinsic" (free carrier) band by a forbidden gap (Fig. 2.13 (b)) [2.25]. The width of the impurity band increases with doping concentration; experimentally this can be quantitatively observed as a decrease in the thermal activation energy for the transfer of electrons (referring to n-type)

to the conduction band [2.26]. At a particular concentration this energy gap goes to zero and the impurity band can be considered as overlapping with the intrinsic band (Figure 2.13 (c)) [2.27]. This transition is usually referred to as the Mott-transition, however, since the degeneracy of the impurity electrons with the intrinsic band also implies that the material will exhibit basically metallic behaviour, it is often also called the Metal-Insulator Transition (MIT). A detailed review of the MIT is given in references [2.28] and [2.29]. The critical concentration at which the this transition occurs n_{cr} (assuming uncompensated material) was deduced by Mott [2.30] to follow the numerical criterion:

$$a_o(n_{cr})^{1/3} \cong 0.25 \qquad (2.13)$$

where a_o is the Bohr radius for the impurity. The values measured in many materials for the critical density give an approximate agreement with the Mott value of 0.25 [2.31]. The Mott condition is derived by considering the limit at which, given all the electrons to be free, the screening in the system prevents the formation of a bound state. In a two dimensional system the effects of screening are considerably weaker. It is also the case that for a two dimensional system electronic bound states are found to exists no matter how small the localising potential [2.32]. As a result the criterion for the degenerate limit in a confined doped system will be very different to that deduced for the bulk. This idea has not been considered extensively in this context in the literature to date [2.33]. Chapter 5 briefly considers the degenerate limit under such conditions and demonstrates that indeed the critical concentration is distinctly higher than for bulk material.

Finally we consider the influence of a highly doped semiconductor upon the movement of carriers within the material. The inhomogeneous nature of the impurity distribution gives rise to a weakly fluctuating random potential in the

lattice. Anderson in 1958 [2.34] was the first to analyse the electron states in such a system and to distinguish whether an electron in a particular state will be mobile or localised. Again the question of the existence of localised states was shown to be governed by a critical quantity, in this case the ratio of the maximum potential fluctuation to a measure of the bandwidth of energy assuming a periodic and not random lattice. These arguments were subsequently extended by Mott [2.35], who argued that for a given band this criterion could be met by those states in the tail of the band but not necessarily throughout the band, thus giving rise to a so called mobility edge between localised and delocalised states. This model applied in two dimensions to the context of Landau levels is one of the basic mechanisms for understanding the Integer and Fractional Quantum Hall effects.

The presence of a second compensating impurity in a material greatly enhances the potential fluctuations and hence the degree of localisation (see Fig. 2.14). Such systems of strongly fluctuating potential are referred to as disordered and include a large range of materials such as glasses, alloys, heavily doped semiconductors, amorphous materials etc. A more in depth discussion of Anderson Localisation is given for example in references [2.35] and [2.36]. The idea of localisation in a random potential is referred to in a number of contexts throughout this thesis. In particular in Chapters 5 and 7 high doping density is considered for the centre doped quantum well and Chapter 6 looks at localisation at interface roughness.

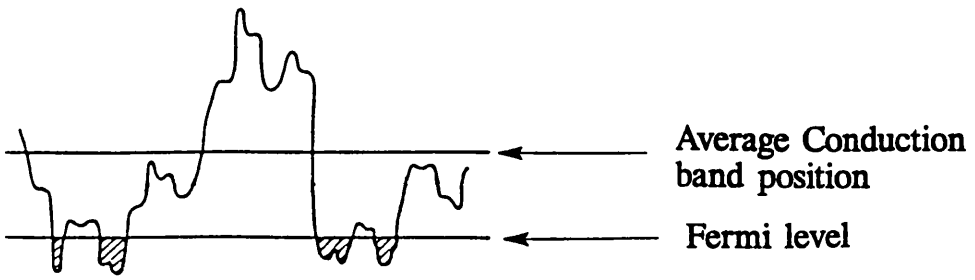

Fig. 2.14 Localisation in a random potential.

2.7 Radiative recombination

This section briefly reviews some of the more important mechanisms by which a semiconductor existing in an excited state (following illumination or some other excitation process) is able to relax to the ground state of the crystal by recombination resulting in the emission of electromagnetic radiation. The mechanism by which relaxation will occur is strongly dependent on both the material and also the external conditions applied to it. Partly for this reason the radiative recombination in a confined system can be very different from that of the bulk material. Probably the most important distinction to make in discussing radiative recombination in a particular material is whether the bandstructure is direct or indirect. For a direct bandgap material the minimum of the conduction band lies at approximately the same wave vector as the maximum of the valence band [Fig.2.15 (a)]. In the indirect gap case the band extrema are misaligned [2.15 (b)]. Since the momentum associated with a photon is negligible in comparison to the Brillouin zone size, the indirect radiative transition requires the simultaneous transfer of the excess momentum of the carriers to the crystal lattice. This restriction makes radiative recombination in such materials (e.g. Si) a relatively inefficient process. Carriers occupying states in the band (conduction band for electrons, valence band for holes) are free to move essentially independently. The Coulomb interaction between the singly charged free electron and hole can be considered analogous to that of the hydrogen atom and indeed is able to form a bound state. In other words the electron and hole move together as a correlated pair. This is the so-called exciton state (more strictly the Wannier-Mott exciton, however the distinction with Frenkel type excitons is not discussed here).

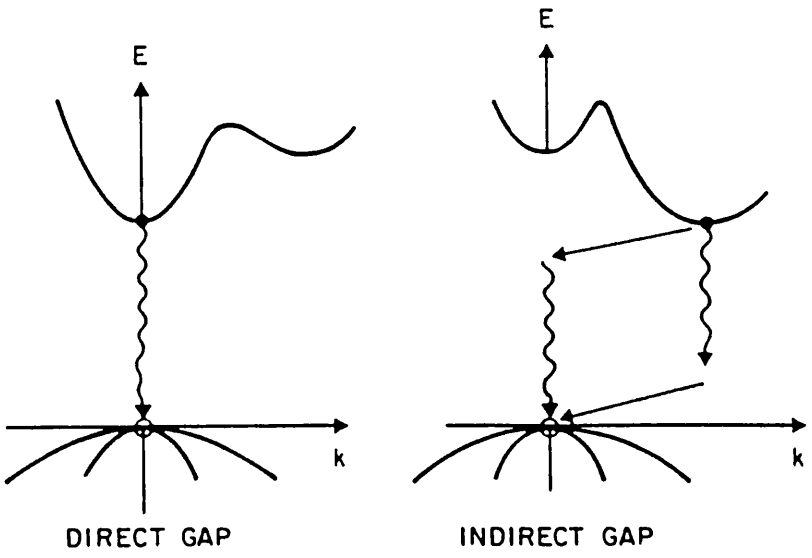

Fig 2.15 Direct and Indirect transitions in k-space.

The formation of the free exciton results in a lowering of the total energy with respect to the unpaired carriers by an amount corresponding to the exciton binding energy. The exciton state demonstrates a series of excited states which again follow the hydrogen-like description suggested above. A point not often realised is that the exciton can only be optically excited at 'critical points' within the bandstructure. Since the electron and hole must move with the same translational velocity the restriction:

$$\left[\frac{dE}{dk}\right]_{electron} = \left[\frac{dE}{dk}\right]_{hole} \qquad (2.14)$$

must apply to the momentum space available to the exciton state [37]. This restriction is of course guaranteed at the conduction band minima in a direct gap material. A scattering event in which the exciton is given momentum implies that for the translational velocity to remain the same for both electron and hole the momentum for the two is different i.e. the electron and hole are scattered to different points in k-space. At high excitation densities free excitons are further

able to condense to form more complex excitonic molecules (e.g. the bi-exciton). At still higher densities the excitons condense to form an electron-hole liquid. At low temperatures and low to moderate exciton densities (the exact limits are material dependent) the optical spectra are typically dominated by transitions from exciton related states and from impurity related levels (to be discussed below). Free carriers under these conditions relax into the lower lying states associated with excitons and impurities, hence the direct recombination of a free electron with a free hole is not usually observed at low temperatures. Since for the conditions used in the work to be reported here the direct band to band transition is not seen, it will not be discussed further. The effects of electron-hole interaction in addition to the formation of a bound state have a strong effect on the absorption spectrum for free carriers. Fig. 2.16 illustrates the enhancement in the ionisation continuum (i.e. free carrier excitation, above the fundamental absorption edge) when this interaction is taken into account. The relative increase in the absorption coefficient is referred to as the Sommerfeld factor.

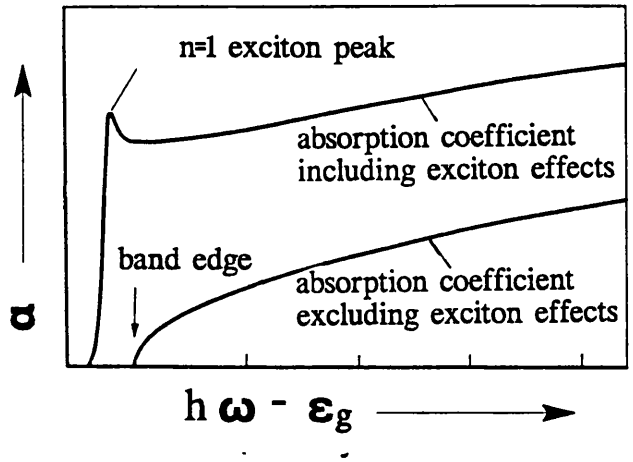

Fig 2.16 Enhancement of absorption due to correlation effects.

Excitons in a confined semiconductor are found to be strongly enhanced in comparison to their bulk counterpart and hence dominate the optical spectra observed at low to moderate excitation densities. This effect can be associated with the increased overlap of the electron and hole wavefunction (and hence greater Coulomb interaction) due to the confinement, which results in a factor four increase in the exciton binding energy (in the truly 2D case). Partly as a result of this exciton recombination is observed even up to room temperature.
In a doped material (or in the presence of lattice defects), trap related states can exist in the forbidden gap. Free carriers or excitons can therefore relax to these states before recombining. The observed radiative recombination in a material will result from the interaction of both the intrinsic states (excitons, free carriers) with the various impurity related extrinsic levels and including possible coupling with phonons or Auger related excitations. As a result the investigation of the luminescence from a material can provide detailed information as to the electronic processes which are taking place in that material. A summary of the basic radiative transitions is given in Fig. 2.17 and will be discussed specifically below.

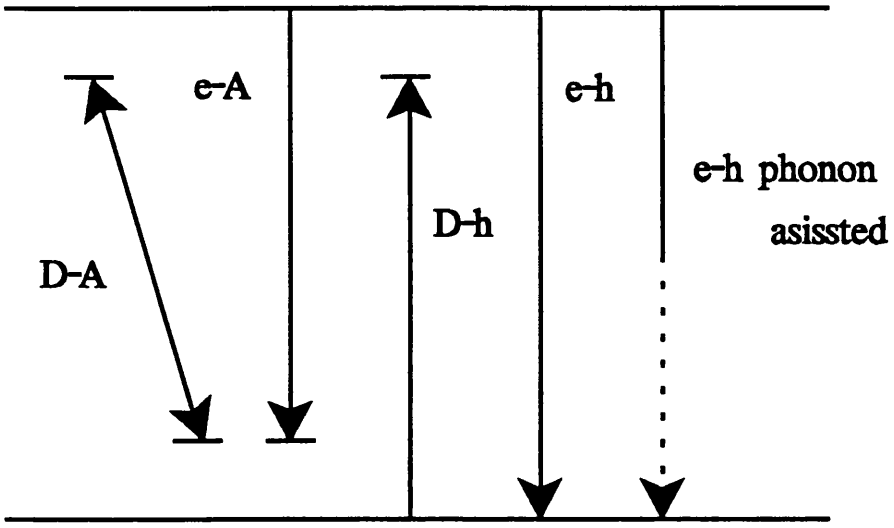

Fig 2.17 Radiative transitions in a semiconductor.

The main considerations in the formation of free excitons have already been pointed out above, however it is worth briefly mentioning the distinctions between the 2D and 3D model which are important to the understanding of the results in the confined case. Furthermore the discussion is restricted to the direct gap case as is appropriate to the work presented in this thesis. The interpretation of free exciton spectra in direct gap materials is governed by the coherent nature of the interaction between the exciton and the photon. As a result the absorption of light resonant with the exciton state cannot be described as the simple transformation of a photon into an exciton. Instead, a mixed state is formed referred to as the free-exciton-polariton. The exciton and photon propagate through the crystal as a mixed mode; the character of this polariton can be either photon or exciton like depending on the total momentum. The polariton nature of the exciton spectra has been observed for many direct gap semiconductors (GaAs [2.38], CdS [2.39]). The exact nature of the polariton luminescence is however determined by for example impurity scattering or phonon interaction and is difficult to fully assess. The polariton picture is however not strictly appropriate in the two dimensional case. This is because of the two dimensional nature of the exciton, which implies that efficient coupling with the photon can only occur in a so-called surface mode excitation. These excitations have an electric field which decays exponentially far from the well [40]. Such a surface polariton mode can only be excited under special excitation conditions e.g. in the presence of a grating on the sample [2.41].

The observation of excitonic molecules has also been reported in both the 3D and the 2 dimensional case. The dependence of bi-exciton formation on the presence of dopant impurities has been studied for the first time in the present work.

2.7.1 Free to bound transitions

In the presence of a single impurity type in a material, the simplest extrinsic transition is the radiative capture of a free carrier to the impurity bound state. In the case of a donor these transitions correspond to the recombination of a free hole at the neutral donor or the capture of a free electron at an ionised donor site. The latter process has however a low radiative efficiency, since its energy is relatively small and phonon emission is a favourable alternative. The corresponding transitions for the acceptor involve the capture of a free hole at the ionised acceptor and the recombination of an electron with the neutral acceptor.

2.7.2 Donor-acceptor-pair transitions

Typically a semiconductor will contain impurities of both donor and acceptor type. In such a situation at low temperatures, the donated electron can be passed to the acceptor, leaving both centres ionised. Under these conditions the material is said to be compensated. The energy gained in the capture of an electron from the donor to the acceptor is typically lost radiatively and results in a characteristic emission series depending on the donor-acceptor pair separation. Since the separation between lattice sites is well defined for a crystalline structure, the line spacing between transitions will in some cases allow the lattice site of the impurity to be determined. The corresponding transitions in a QW have not been identified to date, although there is some speculation on this point in chapter 5. Reference [2.42] provides a detailed review of this recombination mechanism and the information which can be derived from it.

2.7.3 Bound excitons

The formation of a bound exciton can be viewed in two ways, either the alternate capture of both an electron and a hole at a single impurity centre, or the direct capture of a free exciton. In both cases, the result is a correlated electron-hole pair weakly bound to an impurity or defect. It is in fact clear that any elementary multiparticle excitation of the impurity could be described in this way, by convention the term BE is usually applied only in the case that the electronic structure can be distinguished from that of the excitation localised at the impurity centre. The nature of the bound site is found to determine the observed electronic structure of the bound exciton. For example, the potential which binds the exciton can be either hole or electron attractive. Even in the case that the centre is electrically neutral, the short range interaction can be sufficient to localise one of the carriers, the second is then bound via the Coulomb interaction. This model of BE capture at a neutral defect is due to Hopfield, Thomas and Lynch who together were responsible for much of the early work on bound excitons [2.43]. Excitons bound to ionised centres are found to exist only under particular conditions depending on the relative carrier masses of electron and hole. Since their discovery some 30 years ago bound excitons have been studied in a large number of materials under various applied conditions [2.44]. There exists a vast body of literature on the subject and a number of well written reviews have been made. The recombination of bound excitons is discussed further in chapter 6. A more detailed discussion of the electronic structure is given in the following references [2.45] [2.46].

Chapter 3

Experimental Approach and Techniques

3.1 Introduction

3.2 Emission spectroscopy

3.3 Excitation spectroscopy

3.4 Time resolved photoluminescence

3.5 Sample preparation

3.1 Introduction

The experimental techniques used in this work are all based on the principle of photoluminescence. A light source (in most cases a laser) is used to excite the sample, for photon energies larger than the bandgap of the material, this implies the creation of free electron-hole pairs. The photo-excited carriers lose energy through interaction with the lattice, in particular via impurity and defect states, before recombining. When this recombination is radiative we observe a photoluminescence signal which is characteristic of the relaxation that has taken place in the crystal. In this way we can derive detailed information about the materials properties, both those related to the electronic structure of the host lattice and also those of the impurities and imperfections present in the material. The interaction of the excited carriers with lattice vibrations (phonons) implies that the relaxation mechanisms are strongly temperature dependent. In order to observe many of the detailed interactions it is necessary to perform the experiments at extremely low temperatures to minimise phonon scattering, typically liquid Helium temperatures.

This chapter reviews the experimental arrangements used for the measurement of photoluminescence. The first half looks at a time integrated system, which uses cw laser excitation and a photon counting method of data collection. The second part looks in more detail at a picosecond time-resolved setup with which it is possible to probe the mechanisms of relaxation. The instrumentation used in this technique is fairly complex and a more detailed description is given.

3.2 Emission spectroscopy

Luminescence emission spectroscopy is in fact a family of techniques which differ only in the manner in which the luminescence is originally excited. Independent of whether high energy electrons (electroluminescence,

cathodoluminescnce) or photons (photoluminescnce) are used the resulting spectra is one of intensity versus photon energy. The observed luminescence is the result of a radiative electronic transition between an excited state and the ground state of a centre or molecule (the different recombination mechanisms have been looked at in chapter 2). Additional information is derived from an emission measurement by examining the dependence of the luminescence on the application of different external conditions to the material examined. There are numerous parameters which can be controlled, the most obvious of which are temperature, pressure and electric and magnetic fields. Measurements using the external perturbation of pressure or a magnetic field have also been looked at during the current work, however as a topic of work in progress the results are not presented in this thesis but are reffered to in the description of future work (section 8.2).

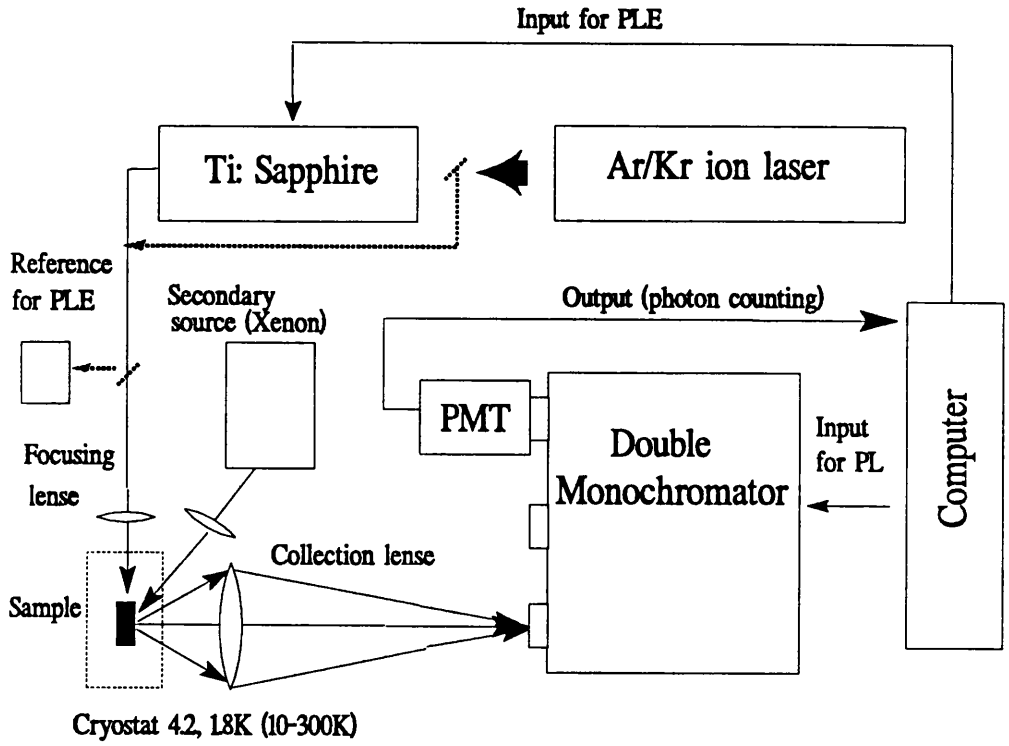

Fig. 3.1 Basic experimental setup for Photoluminescence measurement.

The basic experimental set-up for both photoluminescence (PL) and photoluminescence excitation spectroscopy (PLE) is shown schematically in Fig. 3.1. PL measurements are made by exciting the sample with monochromatic laser light, a monochromatic source is favourable since it provides a well defined initial energy for the excited system. The photon energy of the exciting light is typically chosen to be larger than the semiconductor bandgap, thus a single absorption process results in the formation of a free electron-hole pair. Below bandgap excitation has also been used to resonantly create excitons without directly producing free carriers. The use of resonant excitation to selectively excite specific transitions is sometimes referred to as selective photoluminescence (SPL). Two sources of cw excitation have been used, either directly using specific lines of a gas ion laser (Ar^+ at 5145Å, or Kr^+ at 6740Å) or with a tunable laser pumped using one of the gas lasers.

The earlier part of the work has used a Dye laser with LD700 dye and pumped using the Kr^+ laser as pump, the results in the later part were taken with a Titanium-Sapphire laser using the Ar^+ laser as pump laser [3.1]. The samples are mounted in one of two cryostats, a helium bath cryostat allowing measurements at either 4.2K, or when the overpressure on the He is pumped down to take it below the lambda point, at approximately 1.8K. A cold finger cryostat was also used to provide measurements in the range from 8K up to room temperature. The luminescence excited is collected using a lens and focussed onto the entrance slit of a double monochromator. The use of a double monochromator (Czerny Turner configuration [3.2]) reduces the problem of interference of stray light with the real signal (a point which is particularly important for selective excitation and for PLE). The PL signal is detected using a GaAs cathode photomultiplier using a photon counting technique.

In addition to the conventional technique described above we have also made

use of a novel dual-excitation technique to probe specific properties of our samples. Briefly, a secondary source provides excitation at higher photon energy and is thus able to excite transitions not accessible to the main source. This additional excitation is able to change the electronic bandstructure of the sample and so control the emission produced by the primary source. The intensity of the second control beam is typically a small fraction of that of the main source, a few μWs in comparison to mWs, this small intensity is in itself unable to excite significant luminescence. This technique has been employed in chapter 4, where we study an optically induced charge transfer mechanism which can be accessed in exactly this manner.

3.3 Excitation Spectroscopy

Photoluminescence excitation spectroscopy (PLE) is a complimentary technique to PL and provides information regarding states at higher energy than a particular observed emission. The principle of the technique lies in the assumption that particles excited at higher energy than the detected transition will at least in part relax back to this state before recombining. By detecting within a particular luminescence peak we should be able to measure the relative absorption efficiency into all states lying at higher energies. This is in fact only partly true, since the relaxation mechanism between absorption and re-emission can play an important role, the transfer mechanism can for example be dependent on the excited state. It is important to note this point when interpreting PLE spectra and to draw the distinction with standard absorption measurements; this point is made specifically in chapter 7. PLE has however two major advantages over absorption, firstly in examining epitaxial layers there is no need to remove the substrate and secondly it is more sensitive when looking at weak absorption in thin layers. The observed PLE intensity

(photons/s) can be expressed as a product of the terms corresponding to the above mechanisms:

$$I(\omega)= I_0(\nu)\cdot A(\nu)\cdot T(\nu \rightarrow \omega)\cdot L \qquad (3.1)$$

where I_0 is the incident light intensity, $A(\nu)$ is the absorption term, $T(\nu \rightarrow \omega)$ the relaxation and L a luminescence constant. The last two terms can be combined to express what is referred to as the luminescence quantum efficiency Q i.e. the ratio of phonons absorbed to the number emitted by the radiative species. For Q frequency independent PLE is essentially equivalent to an absorption measurement.

The experimental set-up for the PLE is equivalent to that shown for PL in Fig. 3.1 Tunable excitation is provided either by the Titanium sapphire laser or the Dye laser. The intensity of the excitation is calibrated during the measurement by using a beam splitter to sample a fraction of the laser light. The measured luminescence is then normalised to this laser intensity. This procedure is in fact non-ideal since it assumes a linear variation in luminescence with excitation intensity, which is in general not the case. Such an approximation is justified only in the case where the variation in intensity over the excitation range used is small. For this reason measurements are often checked using a procedure where the laser intensity is fixed at a constant level using crossed polarisers to provide continuous control of the laser attenuation. Fig. 3.2 illustrates a typical pair of spectra for both PL and PLE taken here for an acceptor doped quantum well. By choosing the detection point on the low energy side of the peak we scan through the emission maxima with the excitation, thus gaining the most information about the near to resonance condition and in particular the possibility of a shift to lower energies between the absorption and emission maxima (the Stoke's shift).

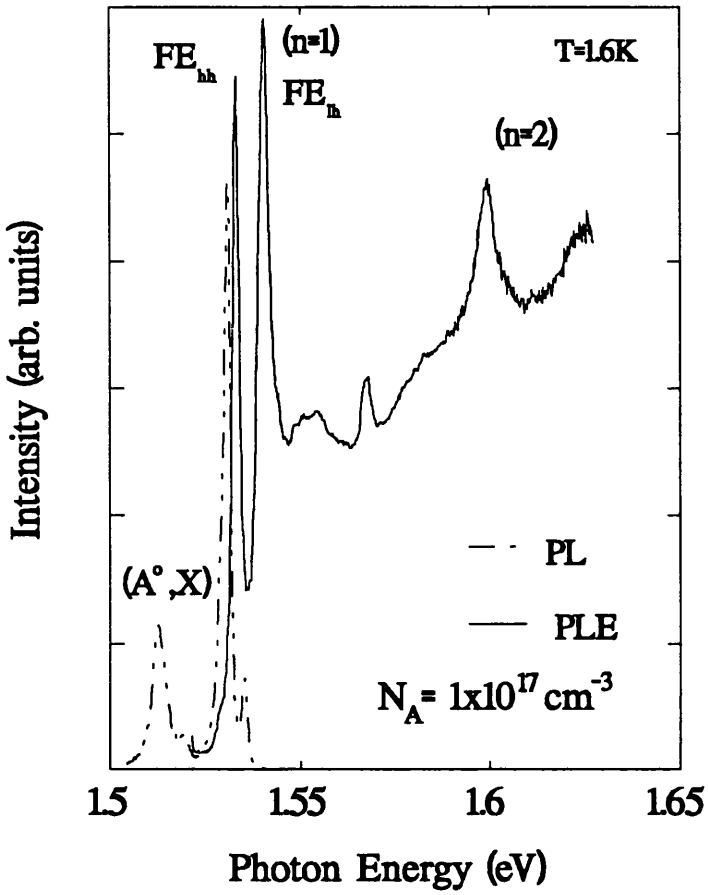

Fig 3.2 Typical PL + PLE spectrum for a doped QW sample

3.4 Time Resolved Photoluminescence

Time resolved measurements have made perhaps the most dramatic advance in the last ten years or so of all the luminescence methods. The time scale over which measurements can be resolved is now approaching the 10^{-14} s range [3.3]. The heart of the time resolved measurement is made possible by our ability to generate very short light pulses of variable length, duration and repetition rate. Various techniques have been developed which make use of pulsed excitation to measure the lifetime of electronic transitions, the reader is referred to references [3.4] and [3.5] for a general review of these methods. The technique employed in this work is perhaps the most direct measurement, the sample is excited with an extremely short pulse and the repetition time

between pulses is chosen to be larger than the typical lifetime to be measured. The decay in the excited population is then monitored via the subsequent decay in the luminescence intensity. The luminescence is measured either using a box-car integration technique, a transient recorder or as in the present technique using a streak camera [3.6]. It is a well matched technique for use with mode locked lasers and has proved to be a powerful method for measurements down to better than 10^{-11} s resolution. A schematic diagram of the setup used is shown in Fig 3.3.

3.4.1 Generation of picosecond laser pulses.

Laser pulses in the sub-nanosecond time range can be generated using a technique referred to as mode locking. Modulation of a light wave of frequency ν_o at a frequency f will result in additional Fourier components at $\nu_o \pm nf$ (where n=1,2,3....), the relative intensity of which depends on the details of the modulation [3.4] (see Fig 3.4). The modulation element can be either a Pockels cell [3.7], which makes use of the Kerr effect, or an opto acoustic modulator which uses diffraction of the light beam at an ultrasonic wavefront to modulate the beam [3.8]. The latter has been used in the current set-up; this modulator is then placed directly in the laser resonator (Fig. 3.4(a)). When the frequency f is chosen equal to the optical cavity mode separation ($\Delta\nu = \frac{c}{2d}$, where d = cavity length) then the sidebands generated will also correspond to modes of the laser resonator. The phases of these laser modes are coupled by the modulation frequency. Within the gain bandwidth $\delta\nu$, a total of 2p+1 coupled modes will oscillate. The superposition of these phase coupled modes leads to a net instantaneous field [3.8] :

$$C(t) = \sum_{m=-p}^{+p} Am\, e^{i(\omega o + m\Omega)t}, \qquad 2p+1 = \frac{\delta\nu}{\Delta\nu} \qquad (3.2)$$

where $\omega_0 = 2\pi\nu_0$, $\Omega = 2\pi f$ and Am is the amplitude of the mth mode.

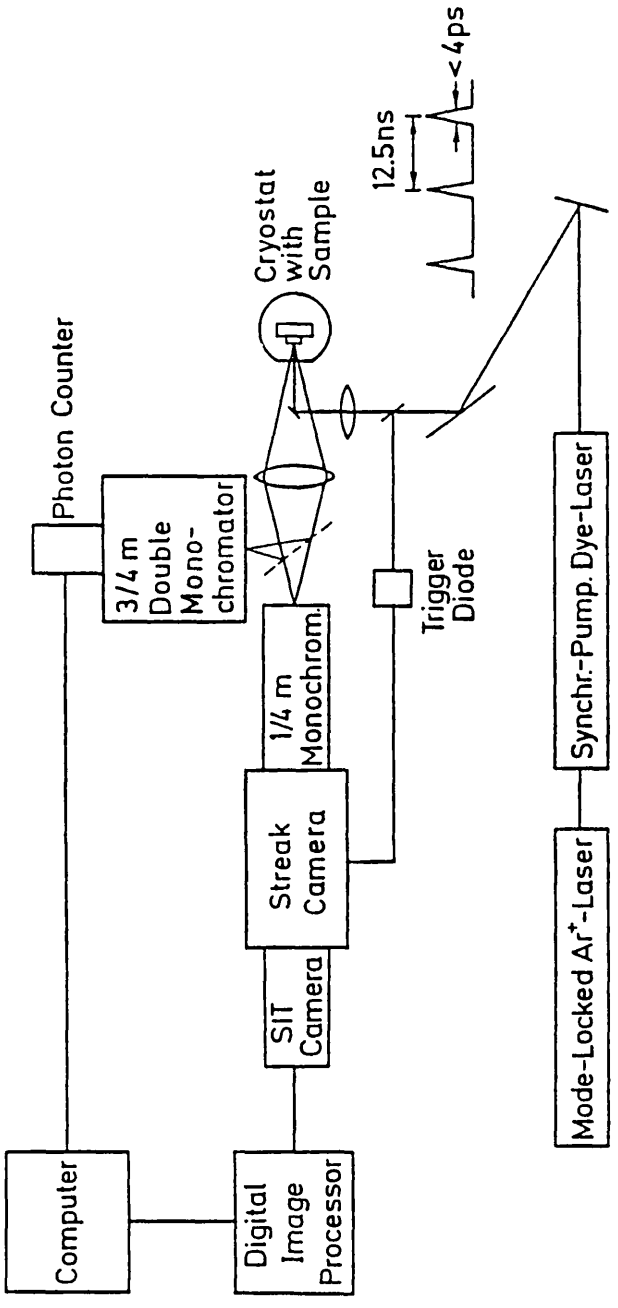

Fig 3.3. Experimental setup for ps time resolved luminescence measurement.

The resultant laser intensity is then given by the complex product $I(t) \propto C(t)*C(t)$ (see Fig 3.4(c)):

$$I(t) \propto A^2_0 \frac{\sin^2[(2p+1)(\Omega/2)t]}{\sin^2[(\Omega/2)t]} \qquad (3.3)$$

It is worth noting that this pattern is analogous to the interference of waves from an optical grating. The grating formula describes the interference of stationary coherent waves in *space* while the mode locking equation represents the interference of phase coupled waves in *time*. The use of internal modulators is an example of *active* mode locking, so called passive mode locking is also possible using saturable absorbers but is not discussed here [3.9].

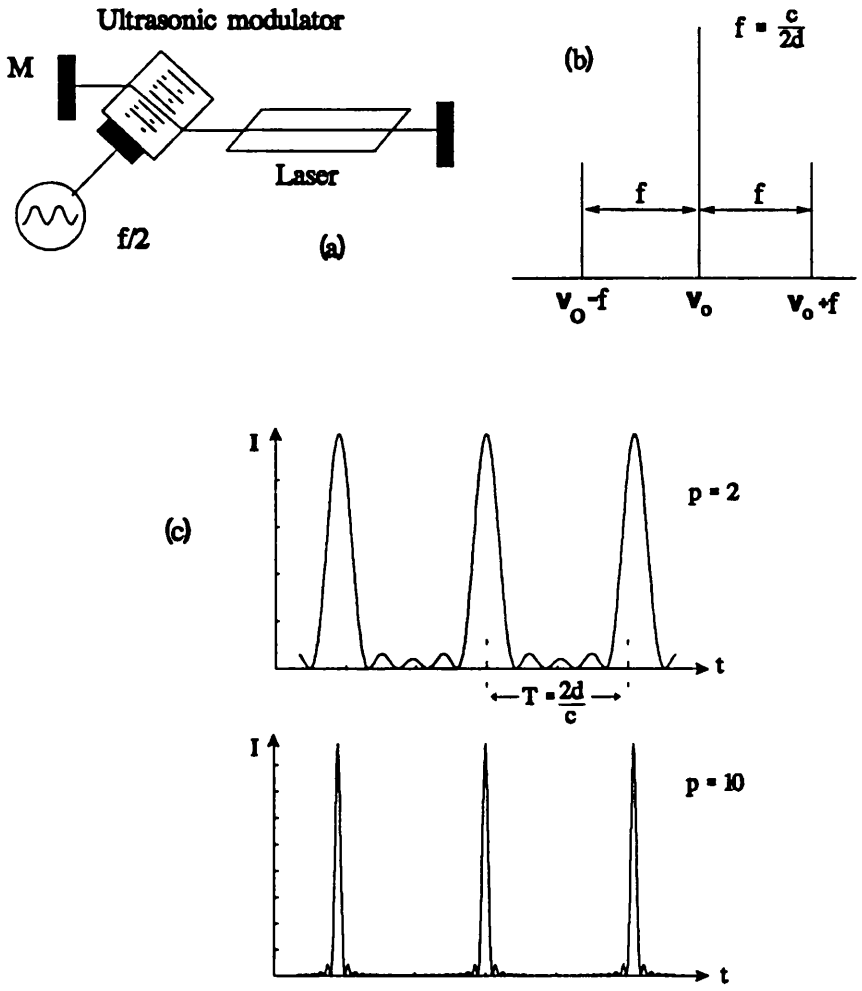

Fig 3.4 Details of mode locking using an acousto-optic modulator.

The production of pulses at tunable wavelength is possible using a cw dye laser which is synchronously pumped using a mode locked laser [3.10]. The optical

cavity of the dye laser is then matched to that of the pump laser (Fig. 3.5). Using such a system we have produced pulses of approximately 5ps length and using Styryl 8 dye in the tuning range from 7200 Å to 8100Å.

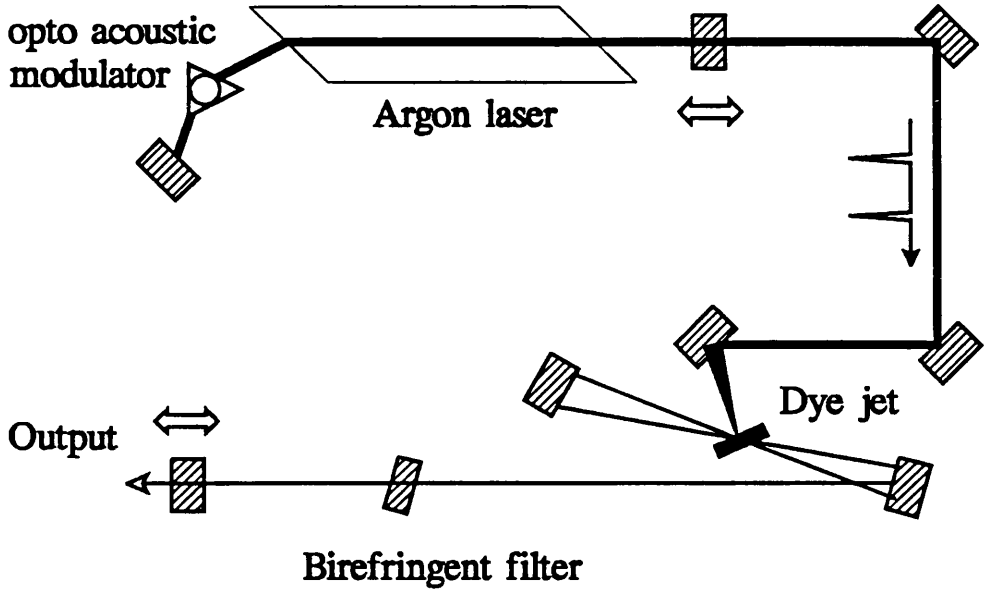

Fig. 3.5 Experimental arrangement for synchronously pumped Dye-laser.

3.4.2 The Streak Camera

The streak camera is used to record the decay in the luminescence signal following excitation with a short laser pulse. The system operates by translating time information into spatial information in the form of a 2D array of intensity points. This conversion is achieved by essentially combining the operating principles of a photocathode with that of an oscilloscope i.e. photoemission of electrons followed by a means of electron beam steering and finally phosphoresence [3.11]. Briefly, photons striking the photocathode produce an emission of electrons in proportion to the incident intensity, these electrons are accelerated and then swept using the electrostatic fields at a known rate over a known distance thus converting time into spatial information (see Fig 3.6). The pattern of electrons formed first undergoes multiplication via secondary

emission using a microchannel plate, the total electron beam then impinges upon a phosphor screen which gives the final optical signal detected using a video readout system.

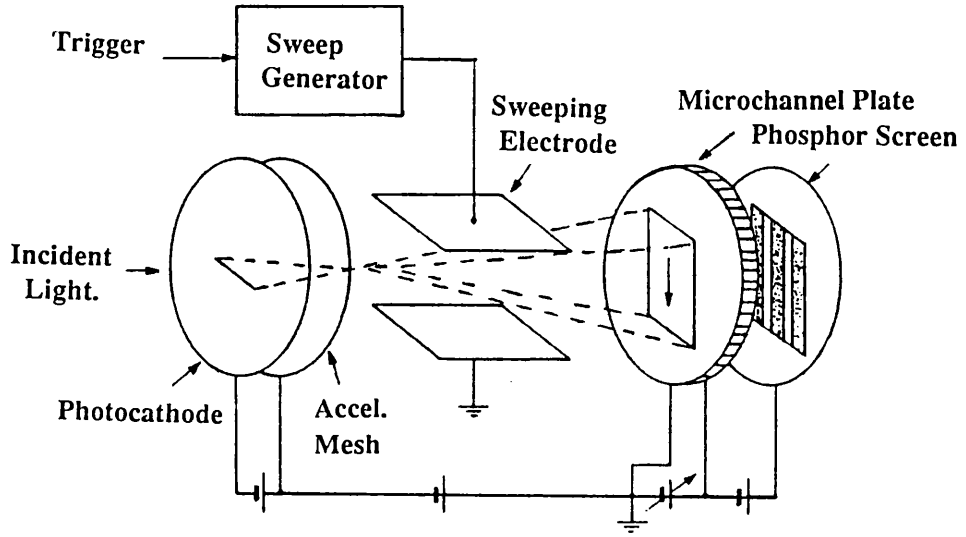

Fig 3.6 Schematic diagram of operation of Streak Camera

An example of such a 2D image is shown in Fig 3.7, the intensity of each pixel corresponding to the emission intensity at a particular time and energy of the original luminescence signal. In this way a temporal resolution of approximately 10ps can be achieved, This resolution is limited by the triggering of the electrostatic sweep coinciding with the onset of the laser pulse, the so called jitter performance.

Analysis of the streak camera data requires a calibration of the intensity of each screen element. This array of values can then be manipulated using a computer to select either the total decay at a single photon energy or the total photoluminescence spectra at a given time *t* after the centre of the laser pulse (t=0).

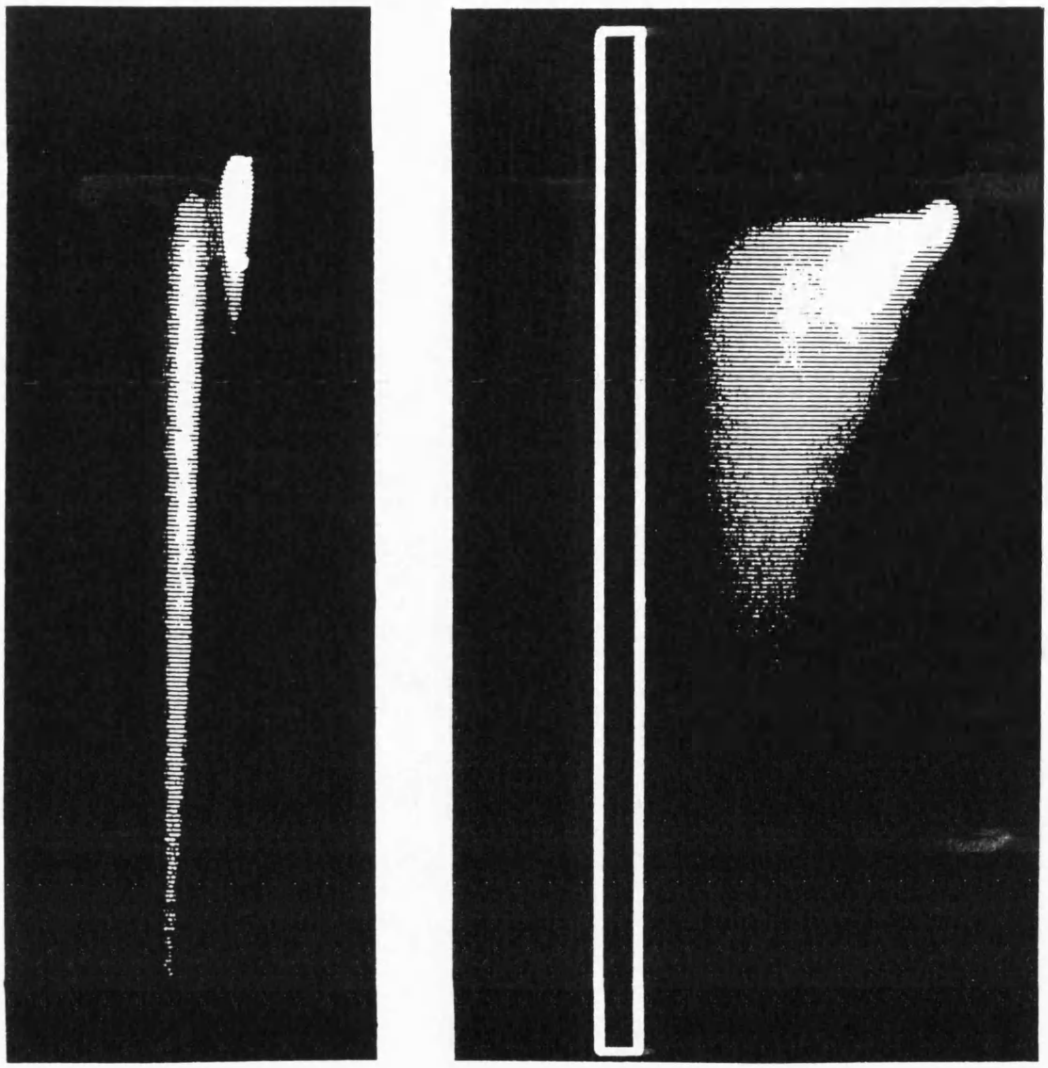

Fig 3.7 Typical Streak Camera trace showing development in time of PL signal

The long open rectangle of Fig 3.7 illustrates how a window is used to define part of the spectrum across which the signal is integrated, to give the temporal development of an emission with a defined spectral linewidth. One problem with this kind of analysis, when the window is restricted to a definite number of channels, occurs if the luminescence broadens or relaxes to lower energies during the emission. In this case a window centred on the emission at t=0 can lose intensity at longer times as the emission emerges beyond the window limits. This problem is discussed more specifically in chapter 6, but highlights the importance of well chosen and defined limits in the analysis.

3.5 Sample Preparation

The samples used in this investigation have all been prepared using molecular-beam epitaxy (MBE) on a semi-insulating GaAs substrate. Two different sets have been used according to the kind of experiment being performed, the layer sequence in both is however essentially similar. An initial wide GaAs buffer layer followed by a short period superlattice (SPS) have been grown in order to minimise the background carbon level, before commencing growth of the active QW layers. Set A consists of a series of 7 single quantum well samples doped with silicon at various levels in the central 50% of the well. The QW structure itself consists of a single 100Å GaAs well sandwiched between 300Å $Al_{0.34}Ga_{0.66}As$ barriers (see Fig. 3.8). The growth temperature was chosen at 680°C, for which segregation effects, which smear the doping profile in the growth direction, are minimised at the expense of poorer interface quality. A relatively wide central 50 Å of the well is chosen to provide a large number of donor sites, the dopant being added concurrently and not using interrupted growth. All the other layers in the structure are nominally undoped. Samples have been prepared with a range of doping levels from $2.5x10^8$ cm^{-2} (essentially undoped) to $2.5x10^{12}$ cm^{-2} (above the degenerate limit). A detailed discussion of the specific changes in the PL spectra for these samples observed for increasing doping levels is given in chapter 5.

Set B consists of the corresponding series to that of set A for acceptor doping with Be. The samples in this case are multiple quantum wells (MQWs) and the doping is restricted to the central 20% of the well only. The layer sequence is again shown in Fig. 3.8.

Set A has been grown by Dr. K. Köhler at the Fraunhofer Institute für angewandte Festkörperphysik (Applied Solid-State Physics) in Freiburg. Set B

is from the group of A.C. Gossard at the Center for Quantised Electronics (QUEST), University of California at Santa Barbara.

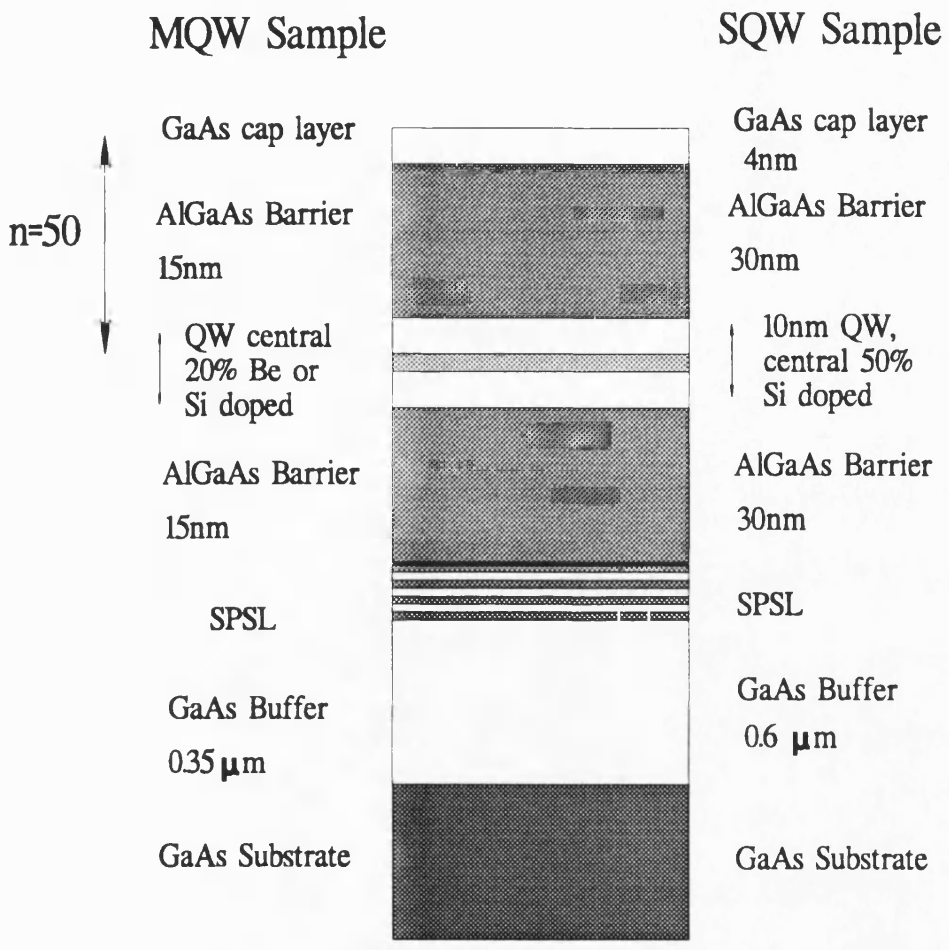

Fig. 3.8 Structure of QW sample for series A (SQW) and B (MQW).

Chapter 4

Optically Induced Carrier Transfer in a Silicon Doped Single Quantum Well.

4.1 Introduction.

4.2 Experimental procedure.

4.3 Results and Discussion

4.4 Conclusions

4.1 Introduction

The potential producing confinement of carriers in a quantum well is defined by the absolute energy difference between the band edges in the well and barrier material. In the presence of shallow impurities this well defined offset can be modified by the additional contribution of the associated Coulombic potential. This effect becomes significant in the limits of high impurity concentration and if a large number of the impurity centres are ionised. Under these conditions the subband energy levels are modified according to the shape of the combined potential. This picture is most commonly applied to modulation doped structures where the barrier impurity is normally in an ionised state having lost an electron (in n-type) to the well (Fig.4.1.). The situation of centre doping in the quantum well has received less attention in terms of the possible effects of the impurity on confinement, although potentially an important question for device structures [4.1]. Vasil'ev *et al.* [4.2] have looked at the problem of δ doping, in which the dopant is placed in a narrow high density spike (Fig.4.2.). In this case they find even additional confined levels associated with the deep Coulombic potential produced by a narrow degenerately doped layer. The analogous effect for bulk GaAs has been studied by Zrenner and Koch [4.3].

One further consequence of the impurity contributed charge is the ability to alter the local potential according to the charge state of the impurity. Such an effect was first demonstrated in the modulation doped case by Chaves *et al.* [4.4] and has also been studied by Delalande *et al* [4.5] . This mechanism in particular is examined in the current chapter for the centre doped structure. We find that the unintentional depletion of charge via surface related states can have a major effect on the confining potential. In turn this depletion can be reversed using an optically induced charge transfer and allows a fine control of the internal field in the structure.

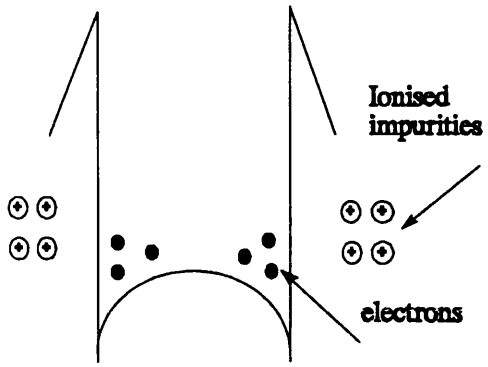

Fig 4.1 Distortion of band structure due to ionisation of impurities in a modulation doped structure.

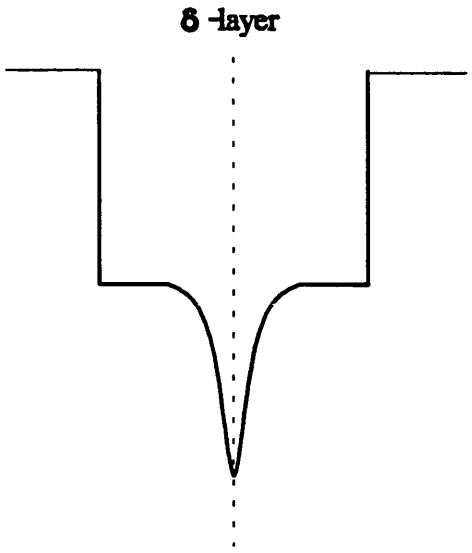

Fig 4.2 Delta doping spike in quantum well.

4.2 Experimental procedure.

The samples used in this investigation are those referred to as set A in the description of chapter 3. Two samples from the series of 100Å single quantum wells are discussed, although the arguments apply to the general behaviour observed for each of the samples, a low doped sample with approximately 2.5×10^{8} cm^{-2} and a high doped sample (but below the degenerate limit of 7.5×10^{11} cm^{-2}).

Time integrated photoluminescence measurements have been carried out in the temperature range from 1.6K up to room temperature. A number of different excitation sources were used to cover the excitation energy range of interest; at "high" photon energy either by the 5145Å (2.41eV) line of the Ar^{+}-ion laser or at low intensity (up to25μW) by filtering the emission of a high power Xenon lamp through a 0.32m monochromator. A tunable dye laser using LD700 dye and pumped using a Kr^{+}-ion laser was used to provide excitation in the longer wavelength range 7250-8050Å (1.71-1.54eV). The excited luminescence was

focussed onto the entrance slit of a Spex double monochromator and detected using a cooled GaAs cathode photomultiplier. Excitation spectroscopy has been made using the dye laser to scan the excitation in the range 7250-8000Å.

Picosecond time-resolved PL measurements have been carried out using a synchronously pumped, mode-locked dye laser with a repetition rate of 80MHz and a pulse width of 5ps. A Styryl 8 dye was used to give a tuning range from 7400 to 8100Å and to allow resonant PL excitation. The luminescence was dispersed through a 0.32m spectrometer and detected using a Hamamatsu streak camera giving the total luminescence as a function of both time and energy. The temporal resolution of the system is approximately 10ps.

Further PL transient data have been measured using an acousto-optic modulator to provide excitation pulses of 10ms duration, the luminescence being detected using a box-car photon counting technique on the time integrated equipment described above. Luminescence decay on a ms time scale has been measured.

4.3 Results and Discussion

4.3.1 Photoluminescence under different photon energy excitation

The low temperature steady state photoluminescence spectra for the two different samples at low (a) and high (b) doping concentration is presented in Fig. 4.3. Excitation at high and low photon energy is contrasted. For the low-doped sample under high photon energy excitation, we observe a typical single, strong exciton transition. Under the lower energy excitation, the sample shows a significant down-shift in energy of the main exciton peak and a second well-resolved peak at lower energy.

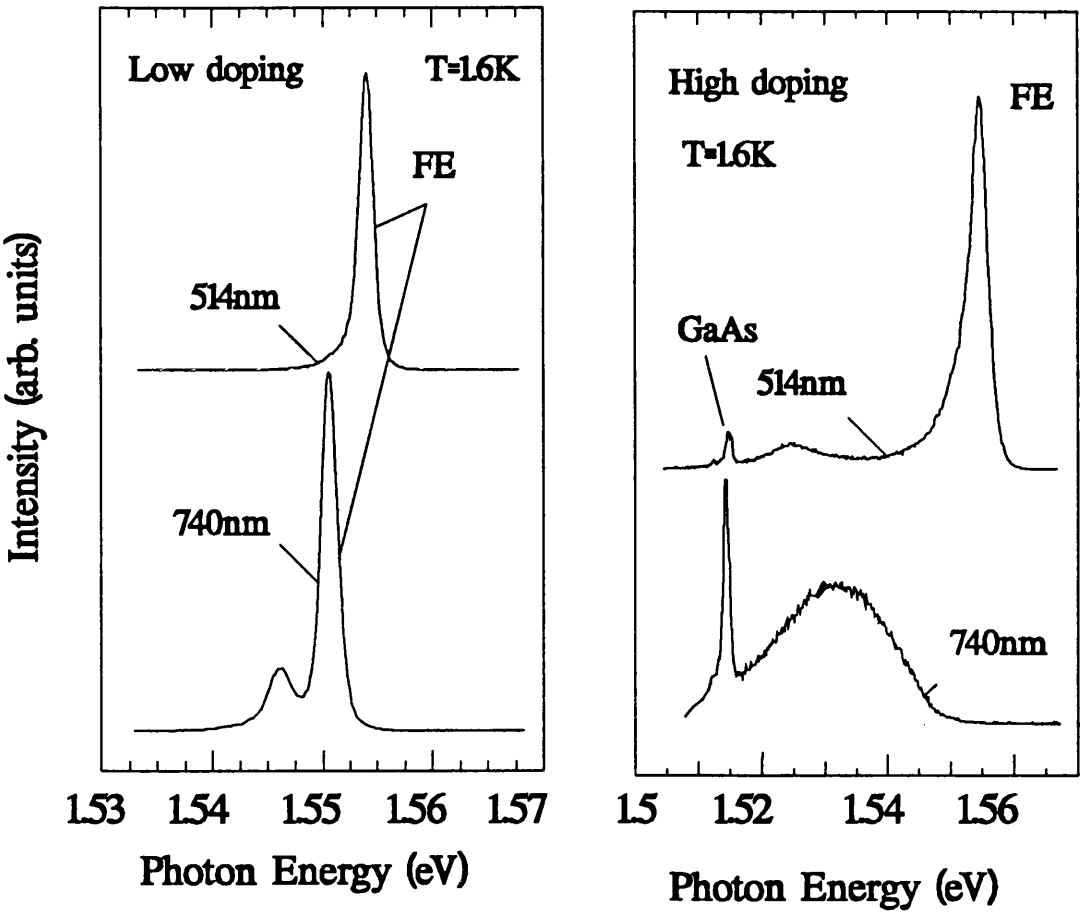

Fig 4.3 Comparison of PL spectra for low and high doped sample under the different excitation conditions discussed in text.

The high-doped case under the same comparison of excitation conditions demonstrates a corresponding but more dramatic difference. At high photon energy excitation a single peak is again observed however the low energy excitation in this case gives no distinct exciton recombination and only a broad luminescence extending to lower energies is observed. An estimate of the strength of the mechanism resulting in the contrasting PL spectra can be made from a two source excitation experiment. The main excitation is given by the Kr^+ laser (6740Å), the secondary illumination is tunable over a range of photon energies higher than that of the primary source, in this case using a Xenon lamp filtered through a small 0.32m monochromator. The results of illumination with

high photon energy of variable intensity are given in Fig. 4.4.

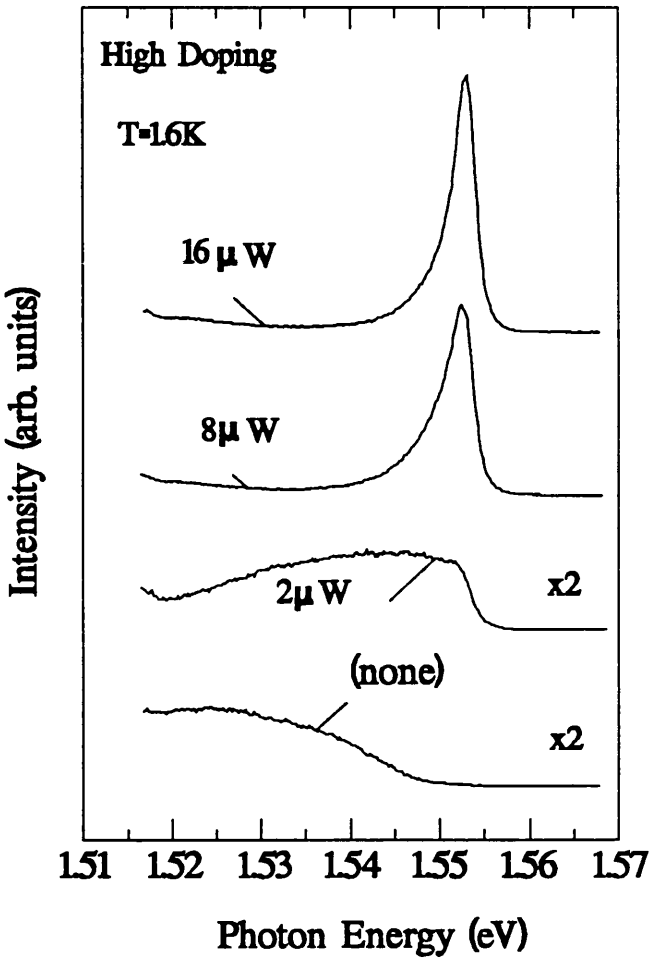

Fig 4.4 Variation of PL with intensity of high photon energy excitation.

Results will be discussed here for the high-doped case, but a corresponding transition between the limits of Fig. 4.3 can be shown for the low-doped sample. The high photon energy intensity necessary to restore the exciton character of the luminescence is of the order of a few $\mu W/cm^2$, compared to the 0.1W cm^{-2} typically used for the low photon energy intensity. The mechanism responsible for the transition from weak to strong exciton recombination is therefore a highly efficient one. If the photon energy of the low intensity component is varied we observe a relatively abrupt transition to the strong exciton case as the excitation energy is increased above the AlGaAs band gap

(see Fig. 4.5). The implied mechanism is clearly dependent upon the generation of free carriers in the AlGaAs barrier material. The mobile charge generated in the barrier will move under the influence of a local field and given sufficient field strength the photogenerated electron-hole pair will become spatially seperated. A redistribution of charge can therefore occur following excitation in the barrier, in turn the movement and seperation of charge will alter the confining potential of the well. Note that if both the electron and hole were to move into the well, the two would contribute to the total recombination, but would not affect the confining potential. Transfer of a single carrier type only must therefore occur if we are to associate the spectral change with a corresponding change in the confining potential.

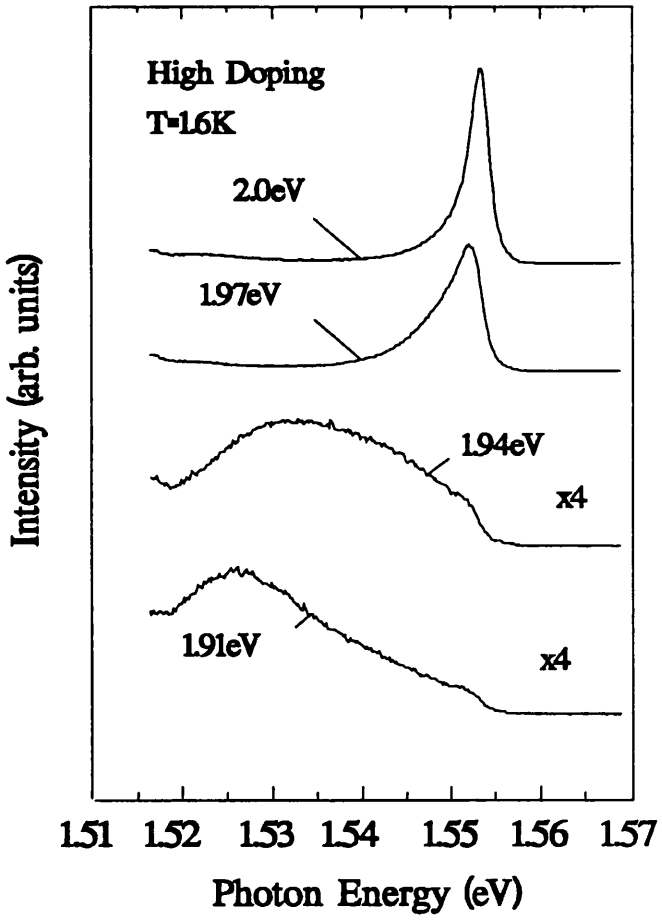

Fig 4.5 Dependence of PL spectra for high doped sample on photon energy of secondary excitation.

The idea of optically induced carrier transfer has been discussed by a number of authors. The control of the two-dimensional electron density via optical excitation in a modulation-type doped structure has been considered by Chaves *et al* [4.4]. They observe a shift in the energetic position of a QW band to band transition and interpret this as a change in the local band bending and correlation energy of the system. Similarly Plaut *et al.* [4.6] have also observed a reduction in electron density under specific photon energy excitation in a single GaAs/AlGaAs heterojunction. The results in both these cases were associated with a decrease in the electron concentration, as expected from the band bending profile which exists in the modulation doped system. The effect of a change in the electron concentration in a quantum well on the optical spectra can be more readily observed by using a field-effect-transistor configuration [4.7,4.8]; such a system allows a well defined control of the charge density and has enabled a detailed correlation of the optically-observed many-body effects with carrier density.

In contrast to the majority of the systems described above, the QW structure under investigation here is centre-doped (anti-modulation) and at low temperatures has essentially no free carriers (degenerate doping is not considered in this chapter). The Fermi-level for n-type doped samples will nominally reside at the donor level high in the band gap. The barrier material in this case is undoped, however, the dominant background impurity in AlGaAs is usually the carbon acceptor, hence the barriers are weakly p-type and as a result there is a certain amount of compensation between well and barrier. The distribution of charge in this structure is, however, additionally complicated by the close proximity of the surface to the quantum well region. The high density of defect states at the surface pins the Fermi-level at approximately 0.6eV below the bulk GaAs conduction band [4.9]; as a result there is a further

transfer of charge to the surface and a depletion of the donors in the well at room temperature [4.10]. The equilibrium distribution of charge, therefore, results in band bending, which strongly distorts the confining potential of the system. Exactly what proportion of the donors are ionized is not easily deduced, however it is clear from the highest doped samples that there exists what appears to be a strong Moss-Burstein shift [4.11].

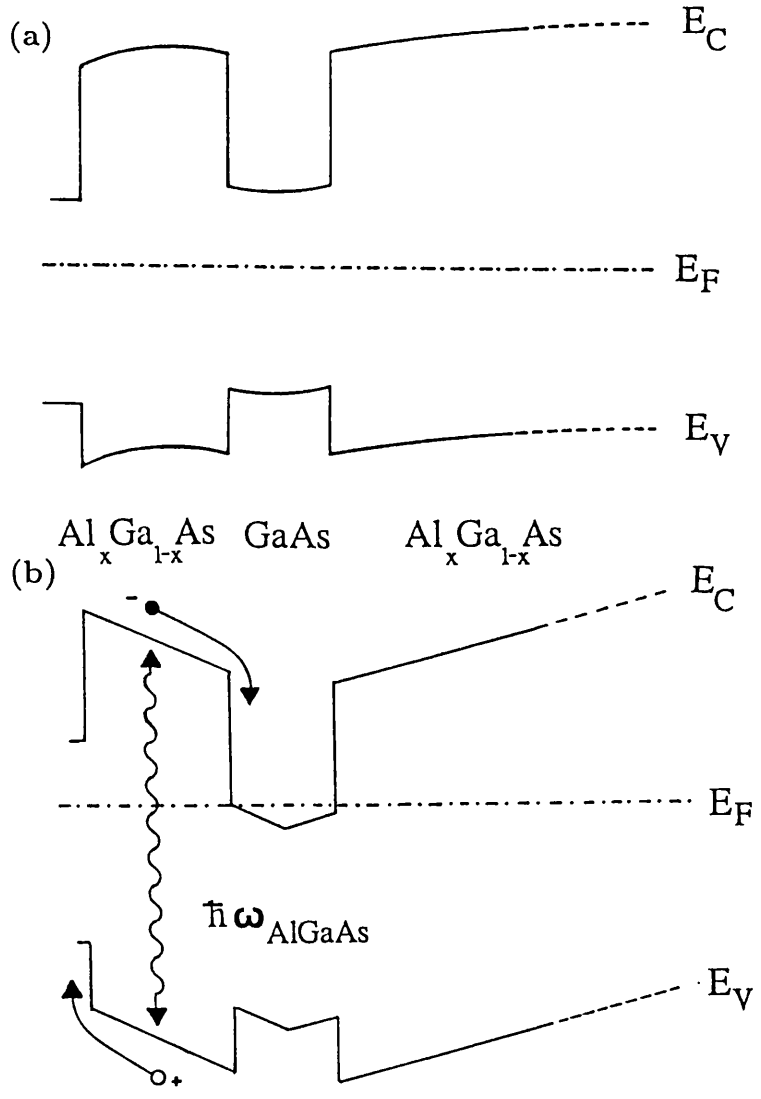

Fig 4.6 Schematic diagram of proposed band bending scheme for the low and high doped single quantum wells

The limit on the depletion of the well (approximately 10^{18} cm^{-3}), which is apparent from the onset of band filling as the high energy emission tail shifts to higher energies, is in good agreement with a simple calculation of the carrier density, given that the internal field must approximately align the Fermi-level pinned at the surface with the subband edge in the well. It is reasonable to assume, on the basis of the strength of the observed depletion for higher doped samples, that low-doped samples may be essentially totally depleted.

A potential energy diagram showing the band bending for both the light and heavily doped cases is given in Fig. 4.6. We have assumed for the high-doped samples that the donors are not entirely depleted and the Fermi-level is, thus, resident somewhere in the donor band. In the next section we develop a model of charge transfer based upon the proposed band structure which accounts qualitatively for the results observed in the emission spectra.

4.3.2 Carrier Transfer model.

Excitation at energies above the band gap of the AlGaAs barrier will result in the formation of free electron-hole pairs. Under the influence of the internal field the charges are swept in opposite directions, the electron being drawn towards the well where it is trapped by a positively charged donor (Fig. 4.6), while the hole is lost to the surface or towards the substrate. At low temperatures this process of charge re-balance will continue, given sufficient photo-generated carriers, until flat band conditions exist between well and barrier i.e. no internal field exists across the well. The size of the internal field is dependent upon the number of ionized donors and therefore increases for higher doping (up to the depletion limit). At higher doping and hence high fields the exciton PL spectra are strongly perturbed.

The reason for the distinct threshold for carrier transfer associated with the

barrier band gap is not immediately apparent. The high density of electrons bound at the Fermi level at the surface implies that it is possible even with low photon energy excitation to excite electrons with kinetic energy larger than the AlGaAs barrier (although momentum considerations imply a relatively low transition probability), and hence for them to move into the well under the influence of the internal field. Similarly, and as we shall argue later, an electron bound to a donor within the well can be excited with sufficient kinetic energy to escape to the surface. The dynamic equilibrium set up by these two processes is that observed under low photon energy excitation. The difference for AlGaAs excitation is interpreted in terms of the role of the photo-generated hole. The behaviour of the hole in the AlGaAs in the adjacent layers above and below the well is not equivalent. An electron-hole pair generated in the near surface AlGaAs is rapidly spatially separated, the hole moving to the surface where it recombines with an electron. The surface reservoir of electrons due to defect states prevents an accumulation of holes at the expense of depletion. Holes generated in the AlGaAs layer below the well are swept towards the substrate; the absence of any electron 'reservoir', however, means that the holes tend to accumulate and carrier transfer to the well is rapidly reduced. We therefore propose that the dominant processes are taking place in the near surface region.

The influence of an externally applied field perpendicular to the well plane has been examined by a number of groups [4.12-4.14]. The work of Mendez *et al.*[4.13] demonstrated a reduction in PL intensity with increasing field, which they interpreted as due to the spatial separation of carriers within the well. The same work also noted, under low fields, a second peak in addition to the main exciton transition associated with the recombination of ground-state electrons with a carbon (acceptor) impurity (e,A^o). The presence of an electric field would appear to relatively enhance the free-to-bound transition.

In direct analogy to the external field case, we are able to make a similar interpretation of the results presented here in terms of the internal field. The presence of a static electric field will have multiple effects upon the exciton transiton energy [4.14]:

(1) The effective band gap of the bulk semiconductor (Eq. 1) is reduced through tilting of the band edges, the Franz-Keldysh effect [4.15].

(2) The binding energy of the exciton (B_{ex}) will be modified by the relative difference in effect upon the motion of the electron and hole [4.16].

(3) The local distortion of the well will cause a variation in confinement energies of the electron (E_e) and the hole (E_h).

The exciton transition energy is then given by:

$$E_{ex1}=E_G+E_{h1}+E_{e1}-B_{ex1} \qquad (4.1)$$

The observed shift in the exciton transition energy with different excitation energies (Fig.4.3(a)) can be interpreted predominantly in terms of the latter two effects. The reduction in luminescent intensity leading to total quenching of the exciton in the high doping case (Fig.4.3(b)) with 740nm excitation can be partly explained as due to the spatial separation of the carriers in the well. The recombination probability of the electron and hole, either directly or through first forming an exciton, is reflected in the overlap of the respective wave functions. At zero field the wave functions are symmetric about the well centre and their overlap is at a maximum. In general, in the presence of an electric field the distribution of electrons and holes is polarized in opposite directions, this reduces the wave function overlap and the effective recombination probability. The polarisation in carrier distribution is not equivalent for both carrier types and is relatively stronger for the heavy-hole [4.13]. In the present case, the 'sagging' potential of the high-doped sample illustrated in Fig. 4.6(b),

has the effect of more strongly localising the hole wave function at the edge of the well, while we interpret the effect on the electron distribution to be less extreme (see later calculation). The reduced overlap in electron-hole wave functions implies that a photo-excited electron has a greater chance to relax and be captured at an ionized donor site. As a result we observe under low energy excitation and hence high fields what we believe is either an enhanced donor to valence band transition or an exciton bound to a ionised donor. It is difficult to make a definite assignment on the basis of comparison with calculated donor binding energies [4.17] since the local well potential is not well defined; the separation to the exciton peak ($\approx$ 2.7meV) is, however, approximately consistent. A similar interpretation of an enhanced free to bound transition supports the assignment of Mendez *et al.* [4.13] of an acceptor-related transition under external field conditions.

4.3.3 Excitation spectroscopy measurements

The above internal field model is strongly supported by photoluminescence excitation spectroscopy measurements. Dual excitation has again been used to control the internal potential and probe the resulting band structure. Fig. 4.7 shows the development in excitation spectra for the highly doped sample under increasing intensity of the high photon-energy component excitation, under comparable conditions to Fig. 4.3. In the absence of any secondary excitation the n=1 heavy-hole exciton resonance is strongly reduced while the light-hole exciton strength is apparently unperturbed. For increasing illumination with high energy excitation the heavy-hole exciton is recovered. The shift in energy of the light-hole exciton between zero and saturation is some 4meV, while for the heavy-hole there is a significantly smaller shift. If we compare the shift in the light-hole exciton with the theoretical calculations of Brum and Bastard

[4.12] the predicted field strength is greater than 100kV cm^{-1}; a field of this magnitude is on the field-ionisation limit of the heavy-hole exciton and may partly account for the strong reduction.

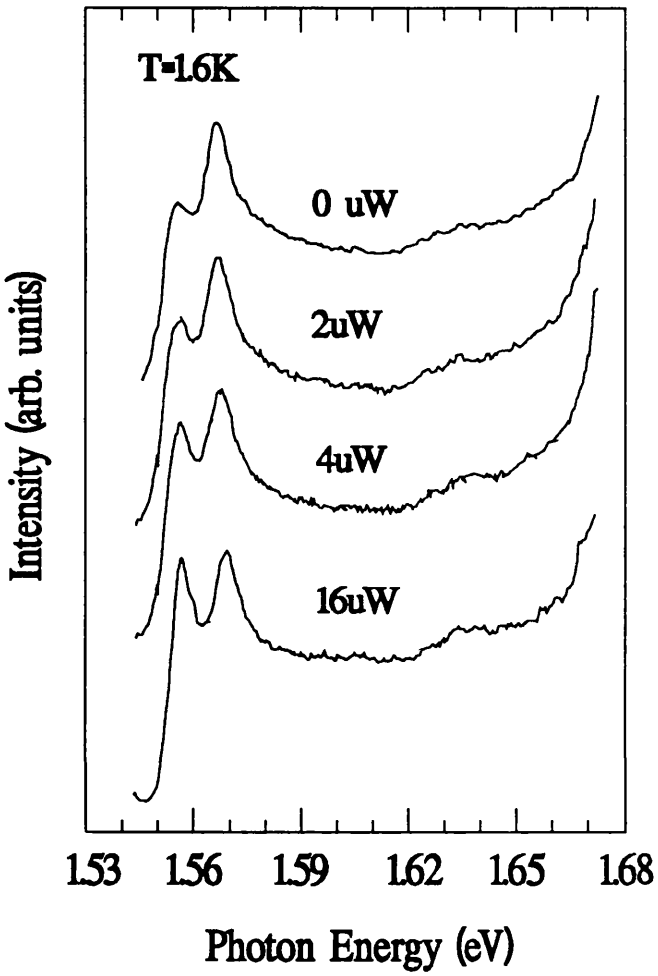

Fig 4.7 Excitation spectra for high doped quantum well showing recovery of heavy hole exciton with increasing intensity of high photon energy excitation.

It is not clear why there should be a reduced shift in the heavy-hole exciton resonance, however, this may be an artifact of the changing potential shape to which it is strongly susceptible, as pointed out earlier. It is interesting to further note that there is effectively no perturbation of the n=2 exciton resonance/band edge. If indeed the observed shifts are due to changes in the electron and hole confinement energies then corresponding shifts should be observed for higher

subbands. However, if the shifts are predominantly due to changes in exciton binding energy the effects for higher subbands are potentially much weaker, the latter case seems to be implied by our results. Furthermore the observed exciton shift in excitation spectra is not reflected in photoluminesence. The Stokes shift in this system is therefore also dependent on the internal field, the larger Stoke shift occuring for larger field strengths. The implication of the internal field model described above is that under high field conditions the hole wave function is compressed towards the edge of the well. Studies of the AlGaAs-GaAs interface [4.18] have highlighted the ability of well width fluctuations (growth steps at interface forming mononlayer islands) to localise carriers, in particular holes. The increased Stokes shift then follows the increased localisation of the hole at the barrier-well interface. The idea of exciton localisation is discussed in more detail in chapter 6.

4.3.4 Calculation of effect of impurity potential on carrier wavefunctions

The proposed model for the distortion of the quantum well by the ionised impurity potential can be examined in more detail by making an approximate calculation of the resulting distortion to the electron and hole wavefunctions. The technique used has already been discussed in section 2.3. We approximate the total potential found for the quantum well as a combination of the simple square well with a Lorentzian like distortion at the centre. For simplicity we maintain the symmetry of the problem. As a larger amount of ionised charge is placed in the well we imagine the depth of this central potential (V_p) to increase. Fig. 4.8 shows the development of the electron (a) and hole (b) wavefunctions for increasing potential depth V_p. The parameters used in this calculation are summarised in Table 4.1 (m^* is the effective mass and V_d the band offset). The effect on the electron wavefunction is found to be relatively

small as can be seen in Fig 4.8 (a) for deeper potentials the electron is increasingly localised towards the centre of the well. For the hole the distortion is significantly more dramatic Fig. 4.8(b), here we consider the heavy hole mass. As suggested earlier the hole is pushed towards the edge of the well with increasing potential depth. Even for relatively small perturbations the hole wavefunction is quite strongly distorted as is seen for the 20meV depth.

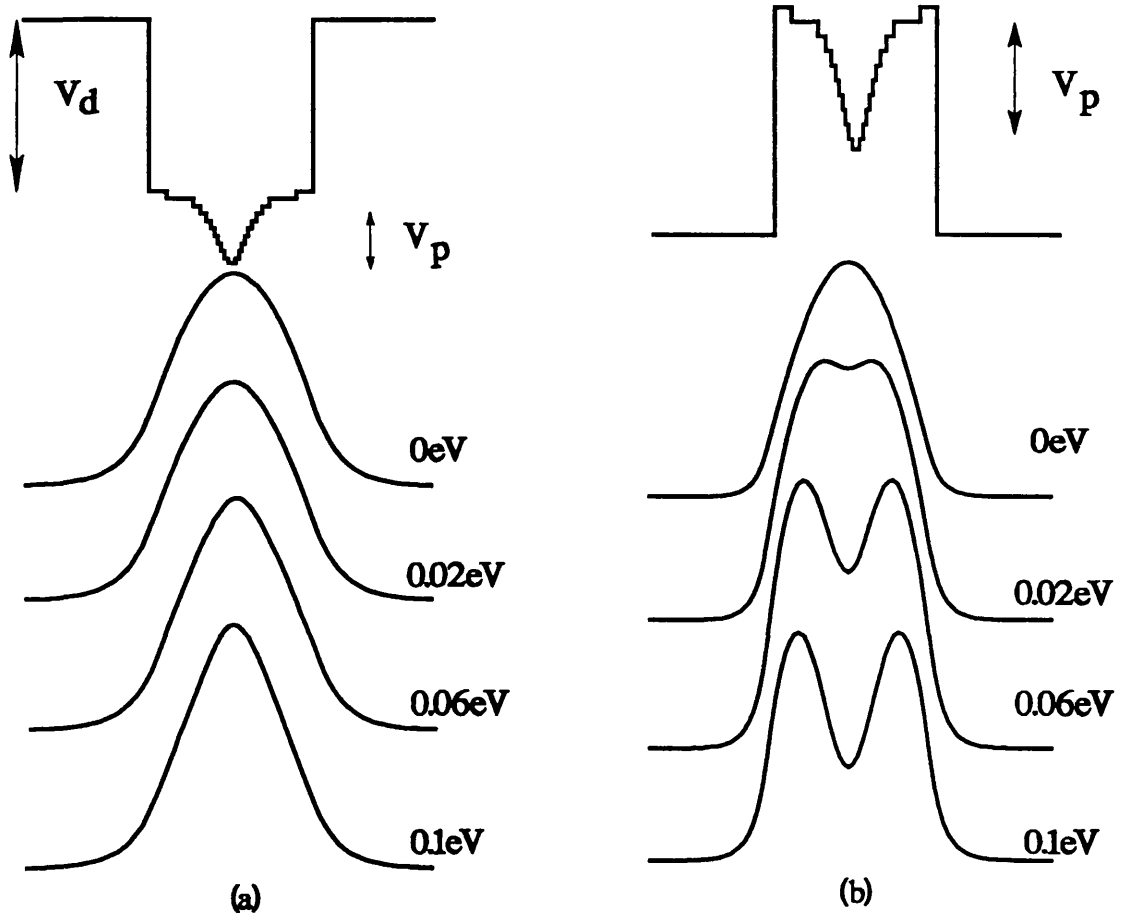

Fig 4.8 Perturbation of electron and hole wavefunctions with increasing depth of impurity potential.

	m^*/m_o	Vd(eV)
electron	0.067	0.24
hole	0.45	0.16

Table 4.1 Parameters used in calculation of wavefunctions in Fig 4.8

This illustrates rather convincingly the ideas put forward regarding the relative distortions of the two carrier distributions. Two further results can be derived from this calculation; Fig. 4.9 illustrates the development in the total confinement for the electron and hole for increasing potential depth i.e. $E_{1e}+E_{1hh}$. Interestingly the change in energy is relatively small, even for a potential depth of 100meV the perturbation to the interband transition $E_{1e}-E_{1hh}$ is only 13meV. Given an associated reduction in the exciton bindig energy this is in fact not an unrealistic value when compared with our measured results.

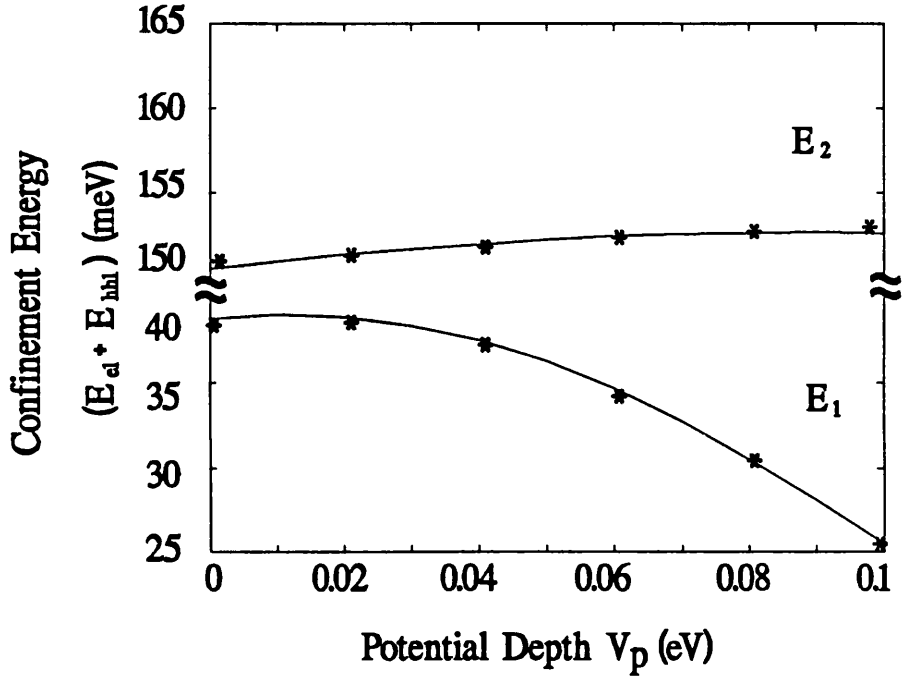

Fig 4.9 Dependence of confinement energy on potential depth.

This indicates that there can indeed be relatively large potentials present in the quantum well profile. Furthermore if we compare the distortion to the second subband transition (labeled E_2) the shift is extremely small ≈2meV for 100meV potential depth. This again fits nicely with the observed data in that we see almost no shift in the n=2 subband levels. Finally Fig. 4.10 shows the change in the e-h wavefunction overlap with increasing potential depth, evaluated simply

as the integral $\int \psi_e \psi_h^* dx$. This is a good illustration that the increasing potential depth reduces the recombination strength as observed experimentally.

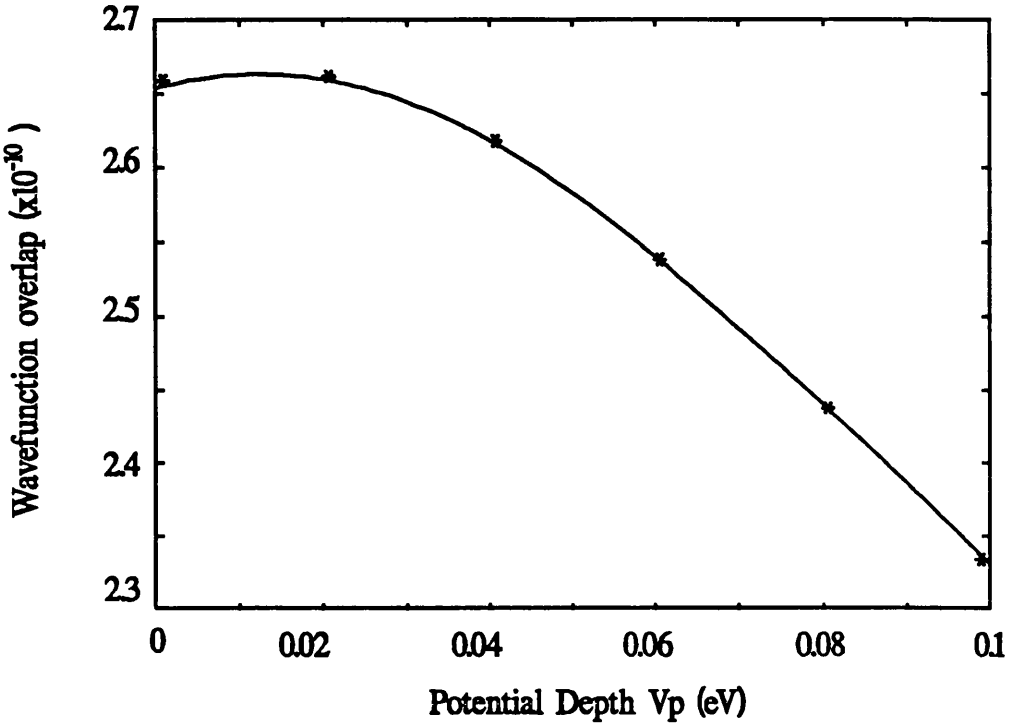

Fig 4.10 Reduction in wavefunction overlap with increasing potential depth Vp

4.3.5 Dynamics of carrier transfer

The transfer and subsequent return to equilibrium of carriers following a high-energy excitation pulse has been studied using a time-resolved photoluminscence technique on a ms time-scale. An acousto-optic modulator has been used to provide the low intensity excitation pulses of a few ms durations. At the same time the sample is continuously excited with the low photon energy illumination following again the dual excitation procedure. Fig. 4.11 shows the temporal development of the exciton spectra. The luminescence shows a sharp onset corresponding to the in-filling of carriers by the high energy pulse. The subsequent relaxation is by comparison extremely long-lived and reflects the slow relaxation of the potential as the carrier distribution returns

to equilibrium under low photon energy excitation only.

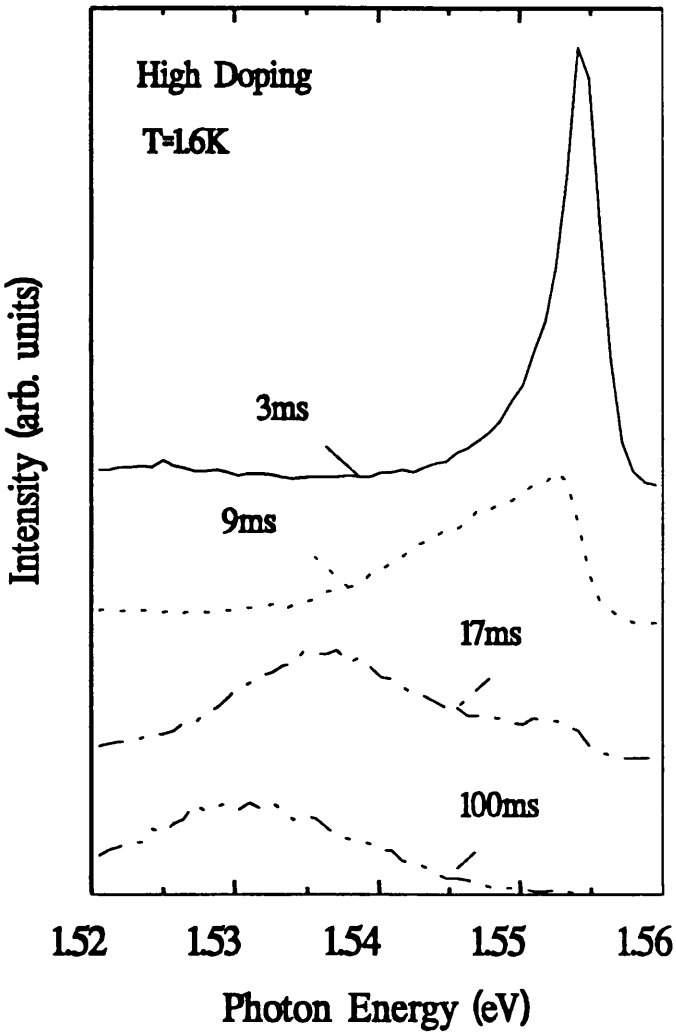

Fig. 4.11 Time dependent luminescence spectra following 5ms pulse at high photon energy but with continuous low energy excitation

Fig. 4.12 shows the decay in luminescence as detected at the exciton transition. On the time scale investigated the onset of exciton character is essentially coincident with the beginning of the laser pulse. A strong dependence of the decay-time upon the intensity of the low energy excitation is found; higher intensity results in more rapid decay. This dependence indicates a direct competition between the processes resulting from the different illumination energies i.e filling of electrons into the well and re-exciting out of the well. In

fact it is likely that the high energy excitation induces both processes, but the in-filling of electrons is by far the more efficient mechanism.

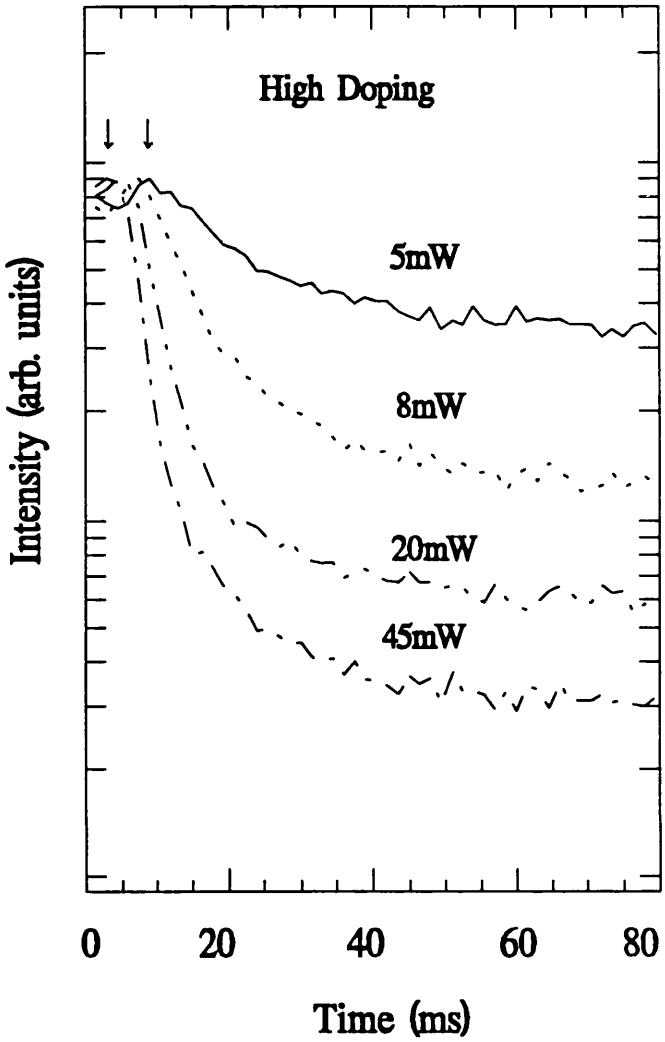

Fig 4.12 Photoluminest transient detected at a photon energy corresponding to the free exciton recombination.

As a result of these two competing processes, we find that the maximum exciton PL intensity occurs at different times dependent on the low energy intensity. Furthermore, the maximum is found to occur after the end of the filling pulse; this is an artefact of the exciton peak shifting down in energy with time. As we have detected below the maximum photon energy the peak energy relaxes through the detection point giving the false maximum observed in the

decay curves (Fig. 4.12). The idea of the intensity dependent rebalance is an apparent contradiction to the proposed model of charge transfer from the AlGaAs barrier, since we have argued that a charge redistribution only occurs for the high photon energy excitation; we must however, consider that following the in-filling of carriers there is a high density of electrons sitting on donor sites high in the band gap. Under illumination electrons are excited high into the conduction band continuum (Fig. 4.13). Although the high energy electrons rapidly relax back into the well, it is possible for a fraction of the electrons to transfer to the surface. We can consider from a statistical argument, that under illumination there exists an average effective distribution of electrons in energy at any particular instant in time. The exact form of the distribution of excited electrons will be a complex function of a number of parameters and cannot be treated simply in a realistic way. However, it is reasonable to assume that the distribution will be exponential in form, given that we expect a rapid falloff at higher energies, and that it can be characterized by a specific electron temperature T_e. From a known distribution we can determine a transfer rate of electrons by considering both a tunneling component and also, by resolving the electron velocity perpendicular to the plane of the well, the direct transfer of electrons with sufficient kinetic energy.

The barrier height presented to electron transfer is itself a function of the charge inbalance and increases as the system returns to equilibrium. As a result an iterative technique is used to calculate the decay in transfer. A derivation of the equations used in this basic analysis is given in the following section. The final governing equation (4.5) can be seen as a prefactor multiplied by a carrier transfer probability, dependent on the total barrier height.

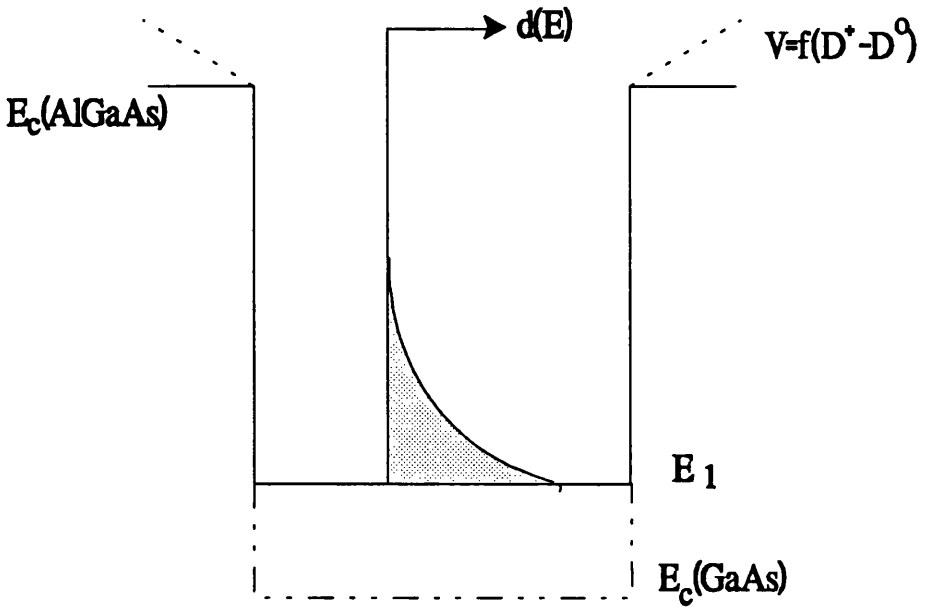

Fig 4.13 Schematic diagram of carrier excitation in well.

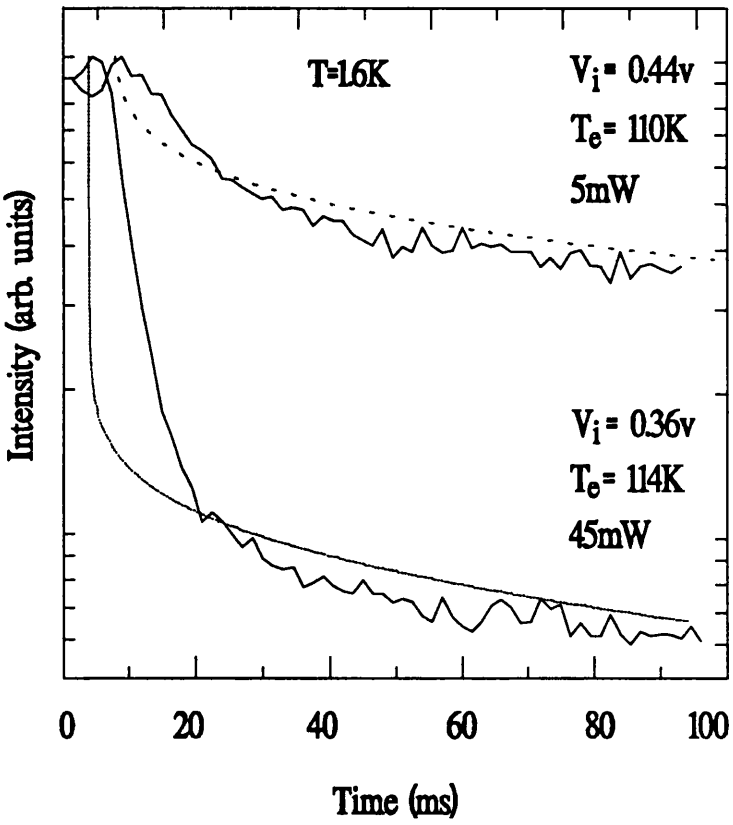

Fig 4.14 Fit to transient data using model described in text.

Fig. 4.14 shows the result of fitting to two of the decay curves. The calculated curve is a measure of how many non-equilibrium (i.e. inbalance from non excited distribution) electrons remain in the well and as such is not directly the measured quantity. In attempting to match the form of the decay we make the basic assumption that the exciton oscillator strength decreases linearly with increasing field. This relationship does not represent the actual dependence, but it allows some qualitative assessment to be made. The aim of the simple model presented here is to demonstrate our ability to understand the gross features observed; the quality of the fit obtained allows some confidence in the picture presented. It is interesting to note that if we use the above results to calculate the field dependence of the oscillator strength we obtain a result qualitatively similiar to the work of Ref.[4.19].

4.3.6 Calculation of electron transfer

The calculation of the loss in photo-excited carriers from the well, follows the assumption that the relative number of electrons with a given kinetic energy at any instant is expressed by a simple Boltzmann type distribution (see Fig. 4.13). This distribution is then characterised by an effective carrier temperature T_e, which is one of the two parameters used to model the carrier flux, the other being the initial field (V_i) which is present following the excitation pulse due to those carriers not refilled into the well by the pulse. We assume a distribution of the form:

$$d(E) = \exp\left[\frac{E-E_0}{kT_e}\right] \qquad (4.2)$$

where E_0 is the zero point energy for the distribution i.e. the boundary between

excited and non excited electrons, in a zero temperature system this would correspond to the equilibrium electron Fermi-level. In this case we consider all the electrons as initially residing at the n=1 band edge and hence neglect any distribution in the electron energies, we thus have a simple zero point defined as E_1. The number of excited carriers in a given energy range dE is thus given by:

$$dn = g(E)\cdot d(E)\cdot dE \qquad (4.3)$$

For simplicity in calculation we assume the density of states to be 3 dimensional, this can be justified in that those electrons which escape are in any case unconfined and whose density of states is therefore essentially 3 dimensional. This gives:

$$dn = \left[\frac{1}{2\pi}\right]^2 \left[\frac{2m^*}{h^2}\right]^{3/2} (E-E_c)^{1/2}\, e^{-\frac{(E-E_c)}{kT_e}}\, dE \qquad (4.4)$$

where E_c is the GaAs conduction band edge. We consider two possible mechanisms for the carrier escape, (1) direct thermal transfer and (2) tunneling through the barrier. Due to the barrier width the second component was found to be negligible and thus only the thermal component will be discussed.
The kinetic energy of the excited electron is given by the difference $E-E_c$.

$$\frac{1}{2} m^* v^2 = E - E_c$$

$$\frac{1}{2} m^* v^2 + E_c - E_1 = E - E_1 \qquad (4.5)$$

We now substitute for this energy difference and resolve the velocity perpendicular (V_x) and parallel (V_y,V_z) to the barrier. We assume that only those electrons travelling towards the barrier with kinetic energy in excess of the total barrier height are transferred. The total barrier height will be a

function of the AlGaAs-GaAs conduction band offset E_{BO} and the internal field (V) due to the charge inbalance. Integrating over those electrons above the minimum velocity for transfer (v_o) and then substituting for the total barrier height gives us an equation for the particle flux:

$$\frac{1}{2} m^* v_o^2 = E_{B0} + Vq - E_c \qquad (4.6)$$

$$J = \int dn\, V_x = \left[\frac{m^*}{h^3}\right] \left[\frac{(kT_e)^2}{2\pi^2}\right] e^{-(qV+E_{BO}-E_1)/kT_e} \qquad (4.7)$$

The internal field V we calculate on the basis of a charge inbalance distributed over a 2D sheet. The conduction band offset E_{BO} has been taken as 60% of the total band gap difference. Our final equation (4.5) essentially represents a prefactor multiplied by a transfer probability. This probability is dependent on the total barrier height as would be intuitively expected.

4.3.7 Picosecond time-resolved spectrosopy

The apparent total quenching in exciton luminescence in highly doped samples observed for excitation at low energy has been further investigated using picosecond time-resolved spectroscopy. The lifetime parameters derived from measurements of this kind are important in understanding the mechanisms of the qualitative model described above. Fig. 4.15 shows the spectral development of the high-doped sample resonantly excited at the n=2 exciton (1.66 eV). Despite the absence of the exciton in the time integrated spectra (Fig. 4.3), the exciton is strongly observed in time-resolved spectra during the excitation pulse. Following excitation, we observe a rapid capture of the exciton, here seen as an increasing rate of decay at higher energies as the

exciton population is transfered to lower energies. The quenching of the exciton PL is apparently in part a consequence of the strong capture present in the system. A high capture probability simply reflects the large number of capture sites available in the high-doped system. The exciton bound at the donor site (either neutral or ionized) is increasingly strongly localized finally being dissociated in the local field, leaving an electron bound at the donor and a spatially separated hole. As a result of this localisation sequence, we observe at time > 500ps only the radiative recombination of donor bound electrons (D, h) in agreement with the time integrated spectra. The localisation of bound excitons is studied in more detail in chapter 6.

The loss in exciton luminescence in the time integrated spectra is a combination of two related effects, the polarisation in carrier distributions leading to reduced oscillator strength, and enhanced capture in the presence of a strong electric field. The mechanism behind enhanced capture we propose is predominantly a statistical one; the larger extension of the exciton wavefunction implied by reduced binding energy means that the number of possible capture sites enveloped is increased. Furthermore enhanced capture may be associated with the relatively higher concentration of ionized donors under high-field conditions, for which the coulombic potential gives an additional capture mechanism. The observed shift in the light hole exciton indicates a field strength consistent with a strong reduction in the oscillator strength. However, the picosecond data suggests a predominant role played by capture in quenching the exciton luminescence. The relative contribution of the two effects is difficult to assess due to their interdependence.

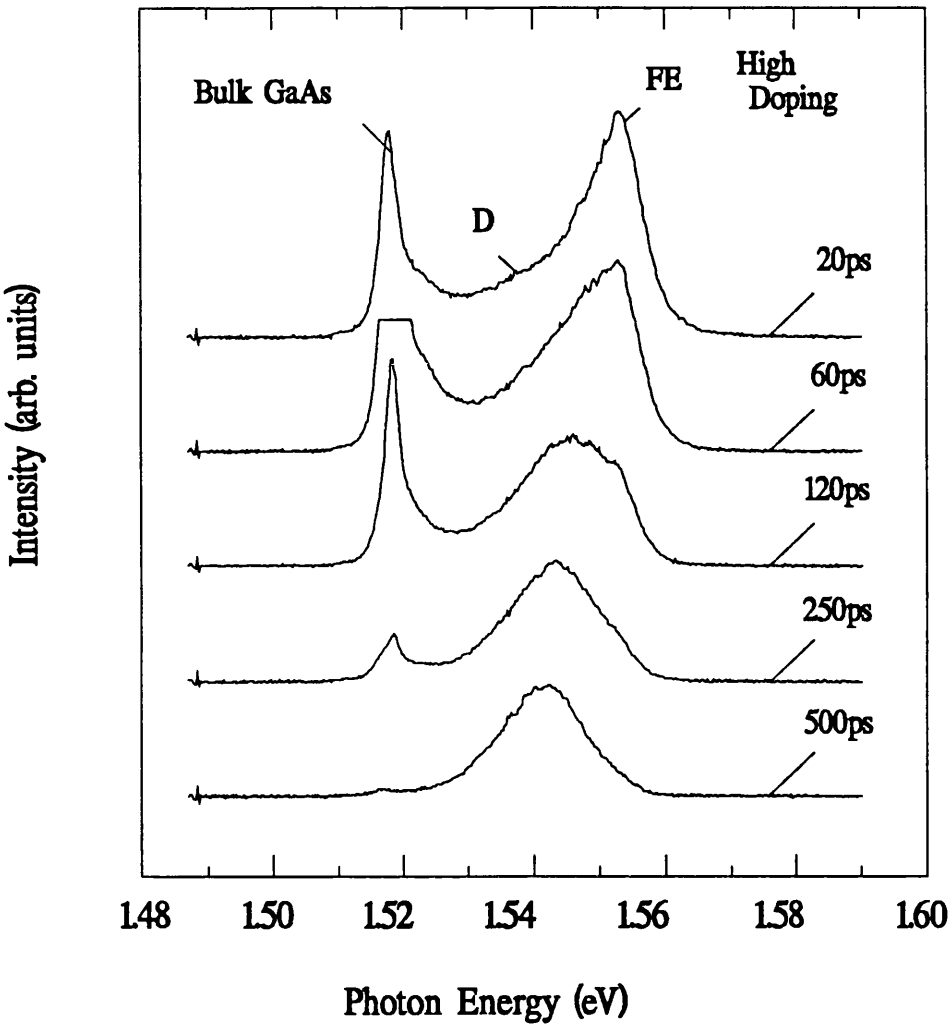

Fig 4.15 Time resolved measurement of the PL for the highly doped sample

4.3.8 Temperature dependent analysis

The importance of capture stressed above has been further examined by investigation of the temperature dependence of luminescence in the highly doped sample. Fig. 4.16 illustrates the change in luminescence with increasing temperature in the range 8K to 200K under single excitation at low photon energy (740nm). We observe at temperatures above 50 K a sudden re-appearance of the exciton transition. In our previous analysis, the occurrence of the exciton in the luminescence spectra has been associated with a change in the local well potential. It is unclear, however, why a significant change in

potential should result singularly from an increase in temperature.

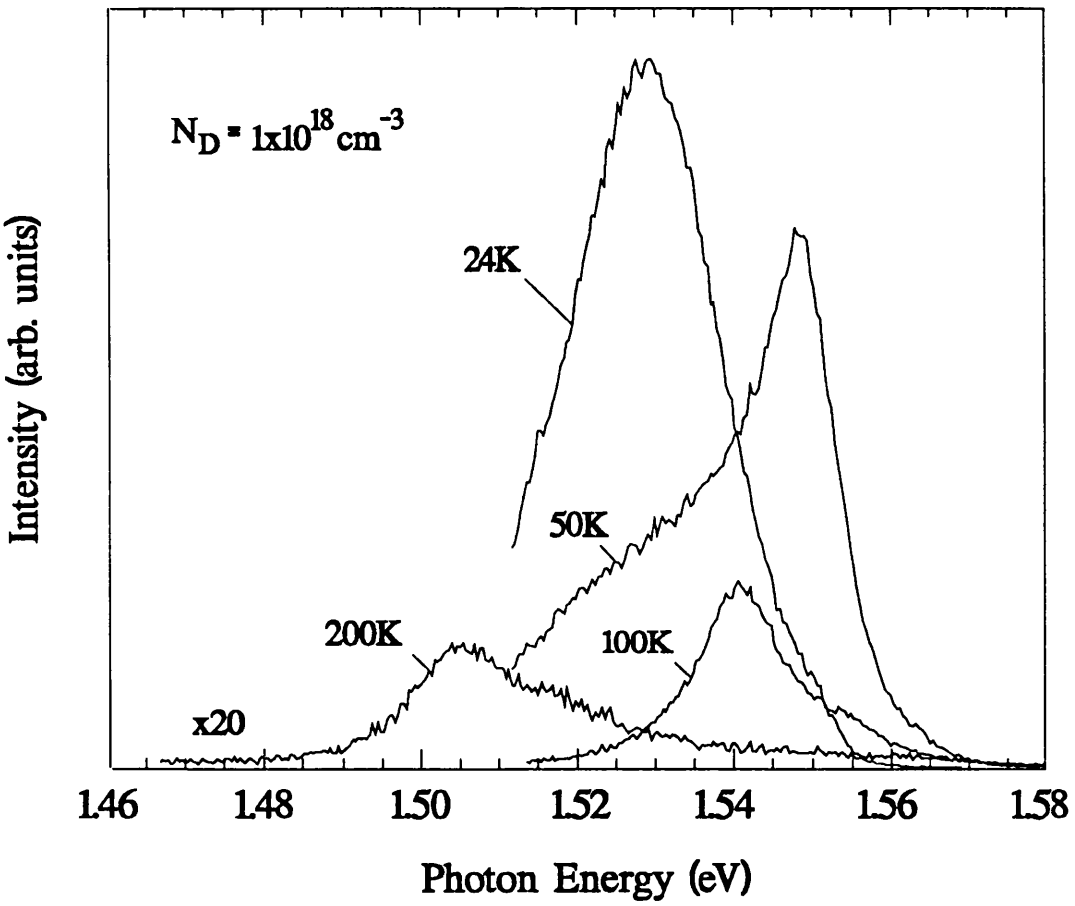

Fig 4.16 Temperature dependence of luminescence for high doped QW.

The large impurity binding energy (E_D=12 meV [4.20]) associated with the strong confinement of the system implies that the effect of thermal ionisation upon carrier concentrations at this temperature should not be significant. We suggest that the observed effect is one of reduced capture at the donor. At elevated temperatures the exciton is less able to be localized to form a bound exciton. If as suggested field ionisation of the exciton does not take place, the reduction in exciton localisation results in enhanced free exciton recombination. This proposal is further supported by picosecond time-resolved data, which indicates slower capture for increasing temperature.

4.4 Hydrogen passivation of GaAs/AlGaAs Quantum wells

The effect of hydrogen on the passivation of defects in semiconductors is a topic of considerable recent interest [4.21]. In particular the passivation of shallow as well as deep impurity levels when the material is exposed to a hydrogen plasma has been demonstrated [4.22]. Hydrogen passivation has been used in this work to again test the hypothesis of charge transfer to the surface. By exposing the samples to a H plasma we hope to passivate the surface related states, thereby preventing the loss of charge from the well which results in the distorted potential associated with the ionised donors. The difference in the PL spectra for different excitation conditions should not be seen for the passivated samples.

The system used for passivation is based on a DC plasma arrangement (see Fig. 4.17). The quartz tube is first evacuated to remove all trace oxygen, a small flow of pure hydrogen gas is then bled into the tube while at the same time maintaining a weak pumping on the chamber. In this way we maintain a constant low pressure of hydrogen under continuos flow. A large electric field ($\approx$1Kv) is placed across the two electrodes so that the H_2 gas is dissociated to form different radical species (H^+,H_2^+ + electrons). The sample is mounted on a seperate electrode a short distance away which is held at a small potential difference ($\approx$50v) with respect to the main high voltage electrodes. The potential applied to the sample electrode draws radicals from the plasma which impinge on the sample and diffuse into the bulk of the material. This method has the advantage that any surface barrier to the penetration of hydrogen can be lowered by the applied potential. The sample is heated to a temperature of approximately 170°C, this is found to be an optimum between the conflicting mechanisms of enhancing the diffusion of hydrogen and thermally limiting the formation of the H-defect complex.

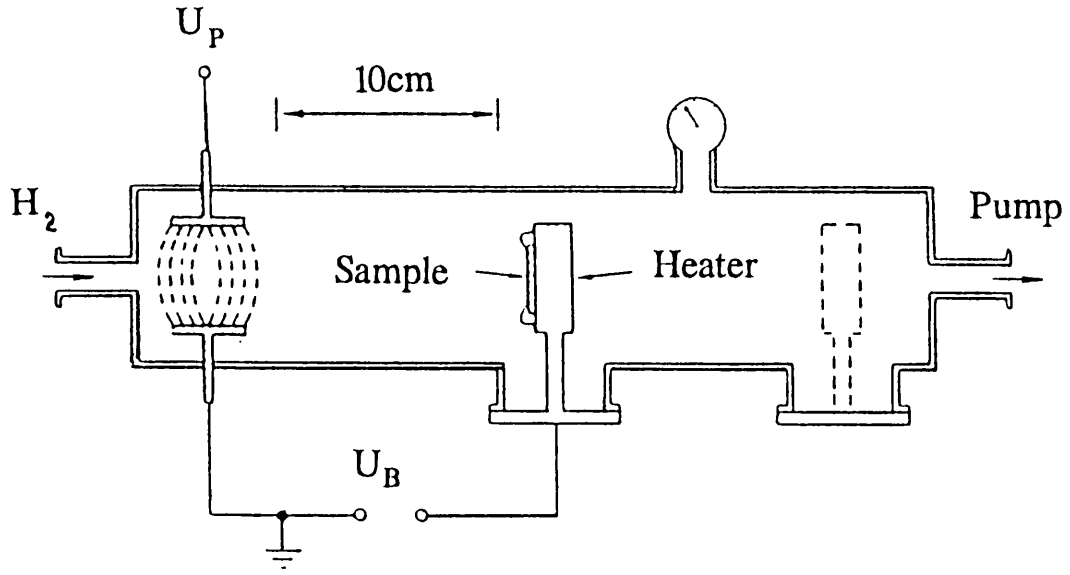

Fig 4.17 Schematic diagram of DC plasma system used for hydrogen passivation of the samples

Fig. 4.18 compares three spectra for the low doped sample. The top curve is for high photon energy excitation showing the single sharp exciton peak, the lower two curves are for low photon energy excitation. The bottom curve is for the sample following treatment in a H plasma for 3hrs. The exciton in this case is found to be at the same photon energy as for the spectra with high energy excitation indicating that the internal field is indeed quenched by the hydrogenation process. The mechanism for the internal field quenching is however ambiguous, it becomes clear that it is not necessary for the surface states to have been passivated, since by passivating the donors we also prevent the loss of charge to the surface and the setting up of an internal field. In either case, however, we confirm the basic charge transfer model.

The halfwidth of the exciton line is also noticeably broader in the passivated case than in the top spectrum. This asymmetric broadening must be associated with a strong localisation of the free exciton. Two mechanisms are possibly responsible for this increased localisation: (i) The H is introduced into the sample by what is effectively a low energy implantation process, this may cause damage to the interface as the H passes through; (ii) a second possible mechanism is that the passivation of the random donor potentials although destroying the bound exciton state leaves a remaining potential fluctuation which is still able to weakly localise the free exciton.

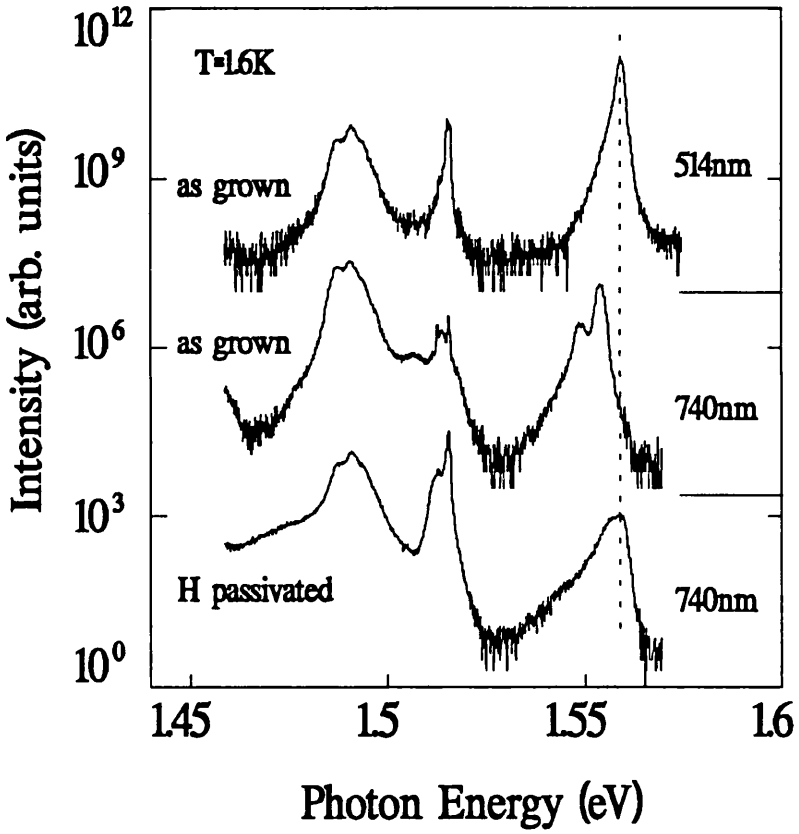

Fig 4.18 PL spectrum for low doped sample before and after H treatment, both excitation conditions are shown.

4.5 Conclusions

The importance of doping in perturbing the local potential in a single quantum well has been demonstrated. Perturbation of the confining potential results from a superposition of the Coulombic field associated with ionized impurities on the band profile. The dopants become ionized due to compensation with background impurities (in particular the carbon acceptor present in MBE growth), or by charge loss to surface states. The observed dependence of the optical spectra upon excitation energy suggest that neutralisation of the ionized impurity occurs when free carriers are photo-generated in the AlGaAs. As expected, the internal-field has an increasingly strong effect as the concentration of dopants is increased. In direct analogy to the case of an externally applied field we observe a reduction in the exciton binding energy and oscillator strength as the field is increased. A simple model is discussed based on the idea of neutralising the ionized donors, which is able to account for the general features observed in the time-resolved spectra. Picosecond time-resolved measurements demonstrate that the capture of excitons at impurities is a realtively strong process at high field strengths. A direct consequence of this result is that at high doping concentrations the perturbation of the band structure coupled with strong capture is able to totally quench the exciton luminescence. If the impurities are neutralised by optical generation and subsequent transfer of free carriers, the exciton is recovered in the luminescence spectra. Dependent on the optical excitation energy we have an effective two state system. Measurements on a ms time scale following a high photon energy pulse have further demonstrated that once the impurities are neutralised they remain neutral at low temperatures for long periods. On the basis of these initial results it is possible to consider applications of this mechanism in a totally optical switching element, using the ability of a high photon energy pulse to flip the

output state of an element and for it to remain in that state for time intervals in the fraction of a second range. Further theoretical work is needed to provide more quantitative support of many of the ideas put forward in this discussion (see future work).

Chapter 5

Photoluminescence studies of highly Si-doped GaAs-AlGaAs quantum wells below and above the metallic limit.

5.1 Introduction.

The properties of semiconductors, both optical and transport related vary substantially as the level of doping is increased. For high doping concentrations a regime is reached in which the material is said to be "degenerate". This threshold corresponds to the onset of overlap of the broadening impurity band with the free-carrier continuum, in turn, representing a transition from insulating to metallic behaviour. The ideas surrounding the Metal to Insulator Transition (MIT) were introduced in chapter 2. The MIT has been studied optically in bulk GaAs for some 30 years [5.1] [5.2], [5.3], [5.4], [5.5], [5.6], [5.7], [5.8]. A detailed understanding of the electronic phase change taking place at high doping concentrations in GaAs has not yet however become clear. At doping levels well below the metallic limit in bulk GaAs (3D) exciton related transitions no longer appear in the optical spectra, even under low intensity excitation conditions; this effect has been associated with the strong screening of the e-h Coulomb interaction by impurities. The typical concentration of impurities in bulk GaAs necessary to completely suppress the exciton (free or bound) is found to be around $10^{16}cm^{-3}$ [5.9]. Optical spectra for higher doping levels are then dominantly band to band and band to impurity related transitions.

The doping level needed to reach the metallic transition has not been accurately determined for bulk GaAs. The difficulty in making a definitive measurement of dopant concentrations [5.10], particularly at high doping levels where compensation effects question the use of methods based on the number of ionized carriers, seem to have excluded to date a systematic study correlated with adequate transport measurements. It is apparent from a survey of optical spectra for n-GaAs obtained by different authors, that the transition occurs at a

doping concentration around $5x10^{17}$ cm^{-3} i.e. a little larger than the theoretical limit calculated from the onset of wavefunction overlap ($\approx$ $2x10^{17}cm^{-3}$) [5.2],[5.3],[5.5],[5.7],[5.8],[5.11]. Above this limit, optical spectra are dominated, for n-GaAs, by transitions from the degenerate electron population in the conduction band to acceptors or valence band states. One issue of continuing debate is whether it is necessary to relax the requirement for momentum conservation in order to account for the observed photoluminescence (PL) line shape [5.7],[5.8],[5.12]. Certainly the scattering that results from a high density of impurities can effectively enhance the contribution from indirect recombination. The observed PL peak position is determined by a combination of two major effects, the shift upwards in photon energy due to band filling up to the Fermi level ('Moss-Burstein' shift) and the counteracting effect of reduction in bandgap due to many-body effects of the interacting carriers (so called bandgap renormalisation). These shifts are of comparable magnitude, but for n-type GaAs the Fermi level shift dominates, leading to an upward shift of the PL peak with increased doping above the metallic limit [5.2],[5.3],[5.5],[5.7],[5.8],[5.11], while in p-type GaAs the reverse situation is true [5.2],[5.3],[5.4],[5.6],[5.8].

In the two-dimensional (2D) case, specifically for GaAs/AlGaAs quantum wells (QW's), there has been relatively little discussion in the literature of the situation where the doping inside the well is increased up to the metallic limit. A major difference between the recombination in 2D and 3D systems is that the excitons are much more important in the optical spectra of the 2D case. The screening of 3D excitons which is already strong at very low doping and carrier densities is not observed in the 2D case. The lowest energy excitons exist simultaneously with free carriers up to sheet carrier densities of about $4x10^{11}cm^{-2}$ [5.13],[5.14],[5.15]. At higher carrier densities, the excitons are quenched due to a combination of many body related effects (carrier screening

due to Coulombic interaction and short range exchange and correlation interactions [5.16],[5.17]), and phase space filling by free carriers. Higher energy exciton states can still be clearly observed in absorption, demonstrating that exciton screening is relatively inefficient [5.18],[5.19],[5.20],[5.21]. The effect of doping in the quantum well itself on the screening and correlation of carriers has received considerably less attention. At low doping the presence of excitons both free and bound, and their dependence on well width and position of the dopant have been extensively studied [5.22]. The properties of highly doped quantum wells ($\approx 10^{12} cm^{-2}$) have previously been discussed in the case of an interesting anomalous polarization of the spectra found for such structures [5.23]. This behaviour has been explained in terms of many-body interactions within the electron Fermi sea [5.17]. No systematic study of the influence of the doping level in the well on the optical spectra of a QW structure however, seems to have so far been presented in the literature.

In this chapter we discuss such a systematic study of the optical properties of n-type Si-doped 100Å QW's, where the doping density has been varied between $2.5x10^8$ and $2.5x10^{12}$ cm^{-2}. The study concentrates on the high doping region, i.e. the transition from exciton to free carrier behaviour in the optical spectra. Steady state PL and PL excitation (PLE) data are complemented with picosecond (ps) transient studies performed with a streak camera unit, in order to reveal the dynamics of the exciton and free carrier systems in the high doping regime. In particular we show that excitons clearly remain in the PL spectra right up to the metallic limit. This result is significant in that it demonstrates that screening of excitons is effective only for free carriers. Even well above the metallic limit broad exciton features are still observed for the higher subbands (n=2).

The chapter is organized in the following way. Section 5.2 presents the experimental data, including both steady state PL and PLE data, and picosecond

time-resolved PL spectra. The development of the optical spectra with doping density is discussed, in particular concentrating on the behaviour just below the metallic limit. A study of samples above the degenerate limit is also presented. The strong non-radiative recombination processes observed at high doping levels are discussed with reference to PL saturation data, ps transient data and temperature dependent PL data. In Section 5.3 we make an extensive discussion of the results making a direct comparison with previous data from the 3D-case (highly doped GaAs) to illustrate the main differences. Finally section 5.4 makes some summary conclusions from this work.

The samples used for this study are again the series of Si doped single quantum wells referred to as set A and as used in the previous chapter.

5.2 Experimental Results

5.2.1 Optical spectra as a function of doping level

The strong dependence of the low temperature PL spectra upon doping concentration in the QW is illustrated in Fig. 5.1,2. The results from samples with doping in the range up to $3x10^{18}$ cm^{-3} ($2.5x10^{12}$ cm^{-2}) are shown. Spectra for both of the excitation energies discussed in the previous chapter are illustrated, above AlGaAs bandgap excitation Fig. 5.1 and below Fig 5.2. In both cases the substrate luminescence has been subtracted for clarity. The data shown in 5.1 correspond to what we believe are near to flat band conditions in the well and are as such a more direct picture of the development of the spectra with doping density. The neutral donor bound exciton is not resolved for any of the samples shown, its presence is indicated by the asymmetric broadening to lower energies of the free exciton peak (this is most clearly seen at a doping density of $2x10^{16}$ cm^{-3}).

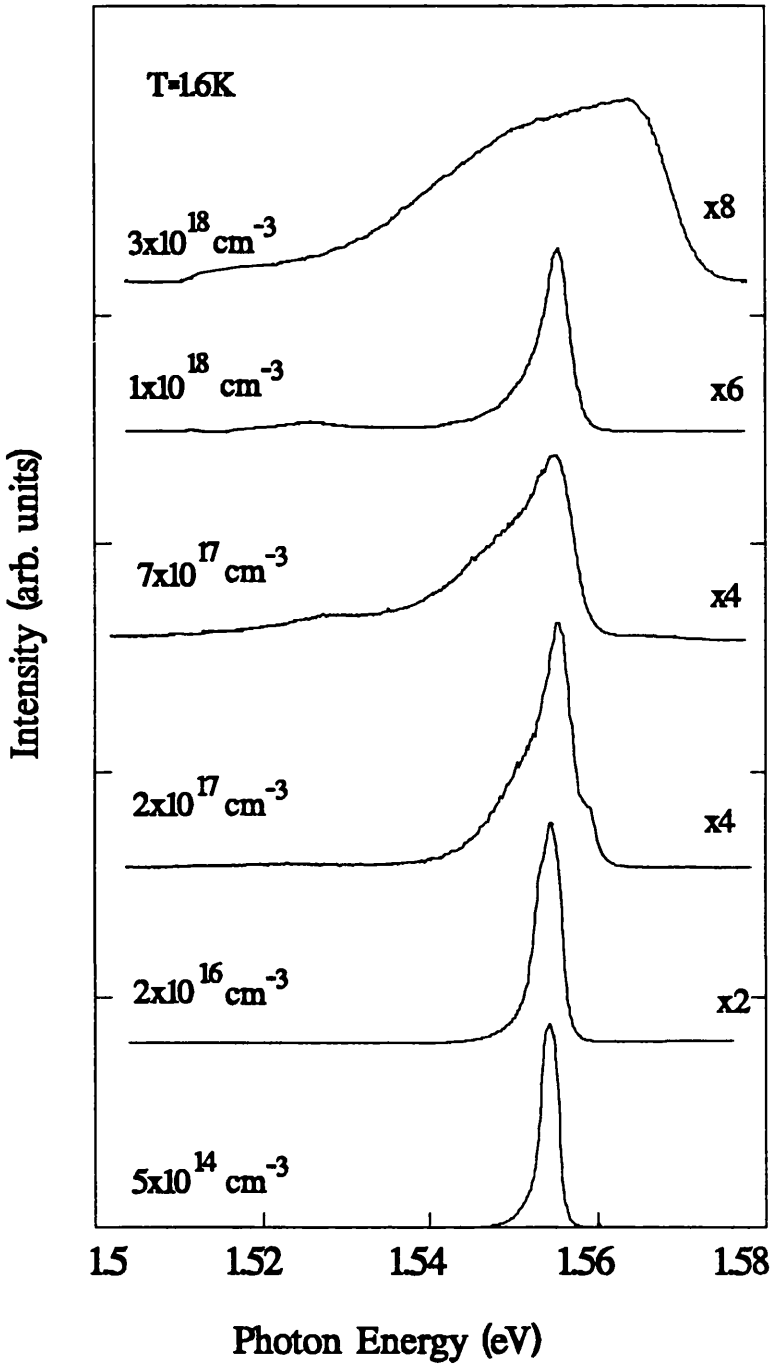

Fig 5.1 Dependence of optical spectra on doping density (5145Å excitation), approximate normalisation terms are indicated.

The linewidth of the exciton transition is found to increase with doping density, in addition, a broad donor to valence band transition appears extending from 1.545eV down to a weak low energy tail as low as 1.45eV.

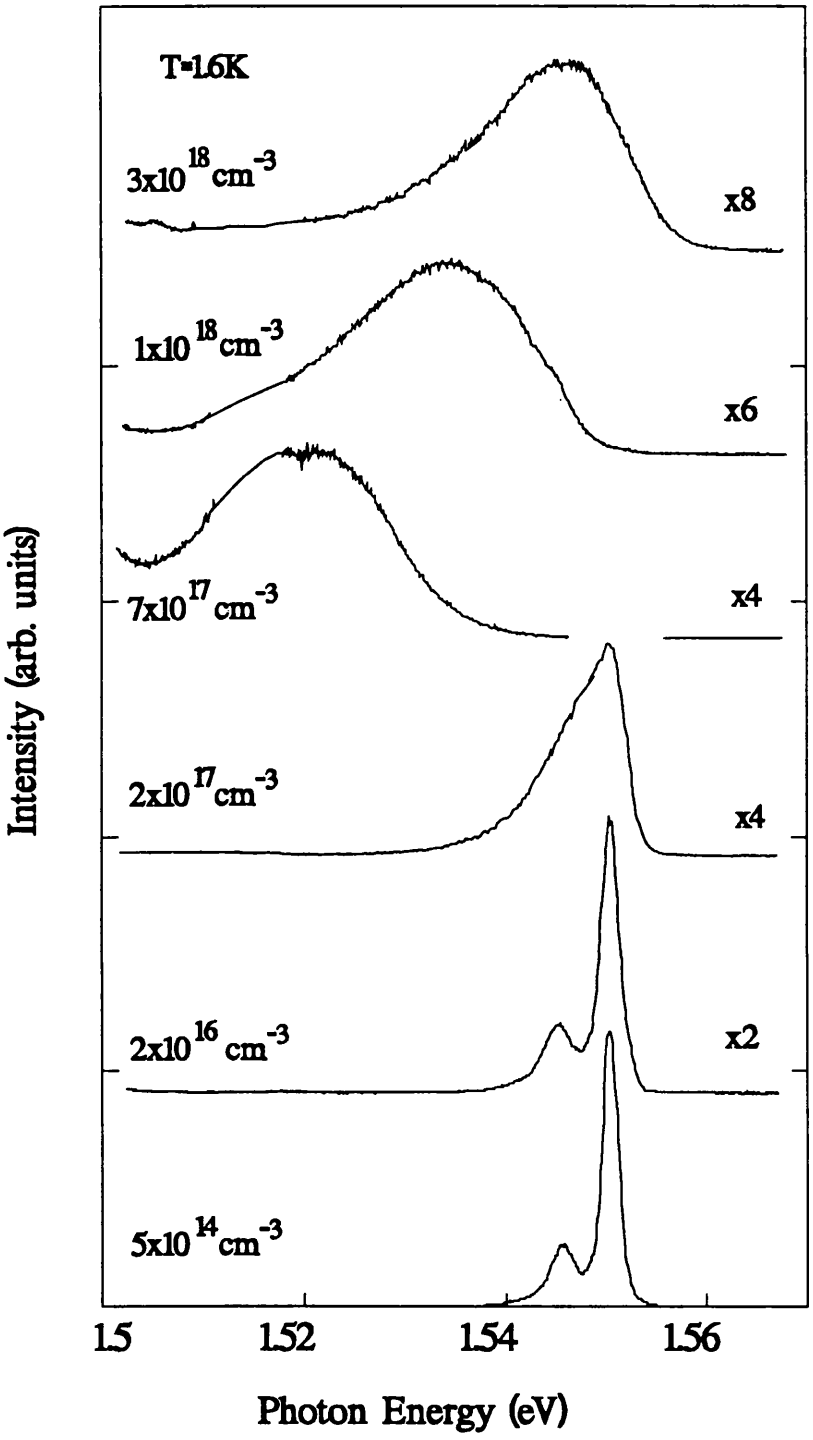

Fig 5.2 Dependence of optical spectra on doping density (7400Å excitation), approximate normalisation terms are indicated.

The broadening low energy tail of the donor to valence band transition can be associated with the strong localisation of the hole. This localisation is again a

consequence of the random potential distribution produced by a high doping density, as described in chapter 2. Compensation, which enhances the potential fluctuations in a material due to the ionisation of acceptors and donors, will play an important role in increasing the localisation in these samples since the Si dopant used is amphoteric and at high densities occupies an increasing fraction of acceptor sites. Between the doping levels of around $7x10^{17}$ cm^{-3} and $1x10^{18}cm^{-3}$ there is a distinct change in the PL spectra, which demonstrates an apparent reverse in the trend of broadening spectra and seems more consistent with a drop in the doping density. Interpreting this effect within the model of localisation in a random potential requires an effective decrease in the size of the potential fluctuations. This is however inconsistent with the increased compensation expected in comparison to the more lightly doped sample. We instead suggest that the spectra can be understood if we assume that this sample is already degenerate, but only marginally above the metallic limit. The presence of a mobile charge smears out the fluctuations in potential due to the random distribution of donors, in turn significantly reducing the localisation. This interpretation also implies that the experimental data show the exciton still remains in the optical spectra even at the degenerate limit. In addition this picture is particularly attractive in that it implies a relatively abrupt transition, as is indeed observed.

The results of experiments with modulation doped structures have demonstrated that the exciton PL is quenched at free electron concentrations greater than $4x10^{11}cm^{-2}$. The degenerate limit proposed here would provide an equivalent sheet carrier concentration of $10^{12}cm^{-2}$, significantly higher than the limit for exciton quenching demonstrated in the modulation doped case. In the present system however, the electrons do not occupy a significant number of subband states, as seen from the absence of a Moss-Burstein shift. The electrons reside mainly in the additional density of states provided by the donors, the current

picture is therefore not inconsistent with the modulation doped limit of $4x10^{11}cm^{-2}$ subband electrons. This same argument applied explains why the problem of phase space filling, which is responsible for the loss of the exciton in the absorption spectra of modulation doped structures, is less severe in the centre doped system due to the donor contributed states. It is in fact not surprising, given the highly doped system, that weak localisation would reduce the effective screening and push up the total carrier limit for which the exciton is ionised.

The uppermost spectrum in Fig. 5.1 clearly demonstrates the shifted emission edge at high energies characteristic of the Moss-Burstein effect due to band filling. At this high density the free exciton transition is finally lost and recombination occurs via band to band transitions.

Excitation at energies below the AlGaAs bandgap is shown in Fig 5.2, as discussed in the previous chapter this corresponds to the situation where a large percentage of the donors are ionised and there exists a strong internal field across the well. Two further consequences of the increased doping are apparent, firstly the internal field becomes very strong at high doping levels, as discussed in chapter 4 this contributes strongly to the quenching of the exciton luminescence. Secondly at high doping levels there is a strong localisation effect, this is due to the random distribution of ionised donor potentials and the increasing localisation of holes at the QW interface with increasing field. The spectra at high doping density ($>2x10^{17}cm^{-3}$) again show an apparent anomaly in the picture of strong localisation. In fact the data provide strong support for the model so far discussed regarding reduced localisation above the degenerate limit. As implied the sample with a doping concentration of $2x10^{17}cm^{-3}$ represents the strongest localisation case, where the random potentials are not smeared out by free carriers. The two higher doped samples demonstrate progressively weaker localisation as the number of free carriers in the well is

increased. In both cases the however there is no band filling present, the loss in exciton luminescence is associated with the Combination of a strong internal field and localisation.

For the low doped samples there are clearly two peaks resolved, these we discussed in chapter 2 as probably resulting from the free exciton and, either an enhanced donor to valence band transition or an exciton bound to an ionised donor.

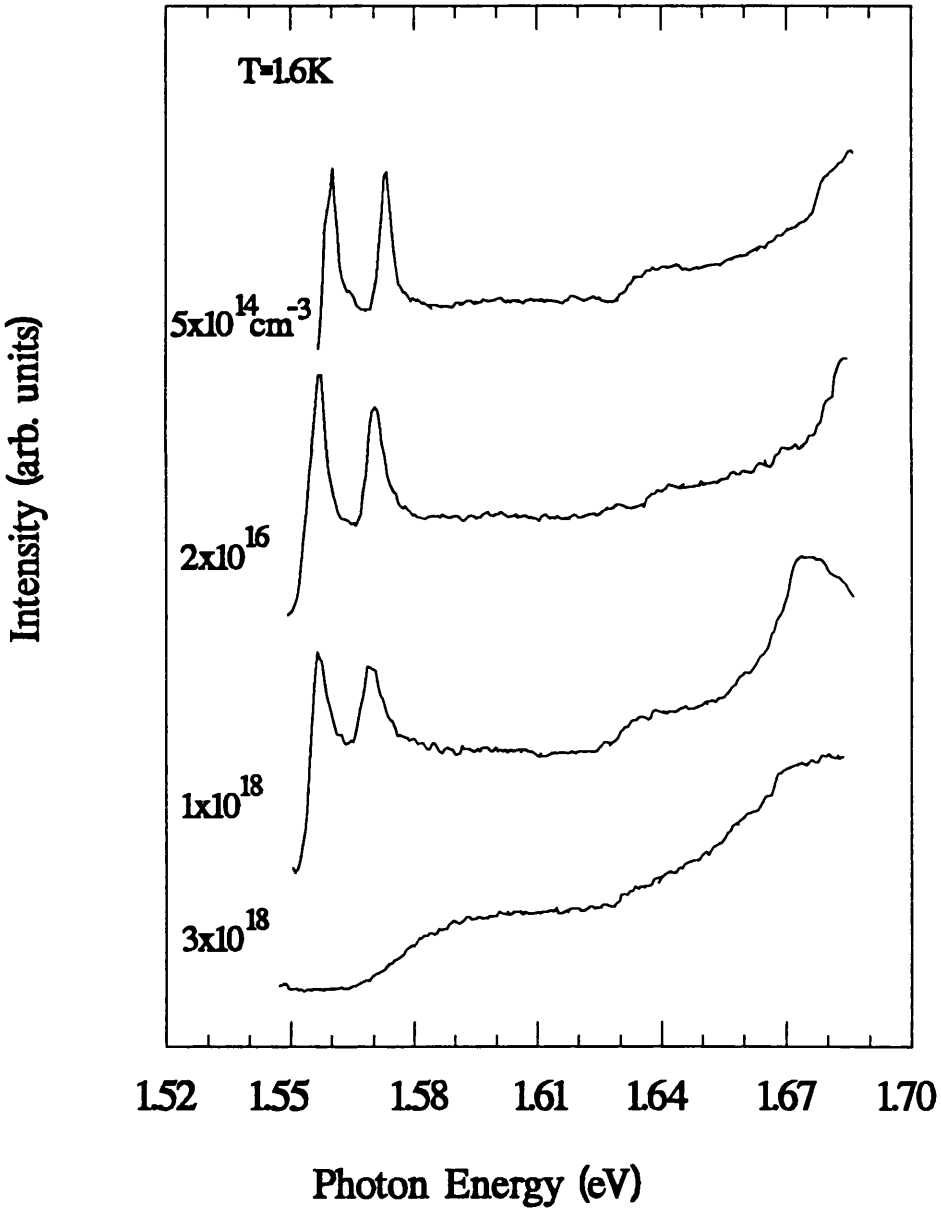

Fig. 5.3 Development in PLE with doping concentration.

Figures 5.3 and 5.4 show the corresponding PLE data for the conditions of Fig. 5.1 and Fig 5.2. Fig. 5.3 is measured with additional low intensity excitation at high photon energy to achieve similar band conditions to those under which PL was measured. The retention of exciton character in the observed transition up to the highest doping level is again illustrated in the PLE data. In fact there is relatively little change in the spectra with doping level other than a slight decrease in the exciton contribution in comparison to the free carrier level.

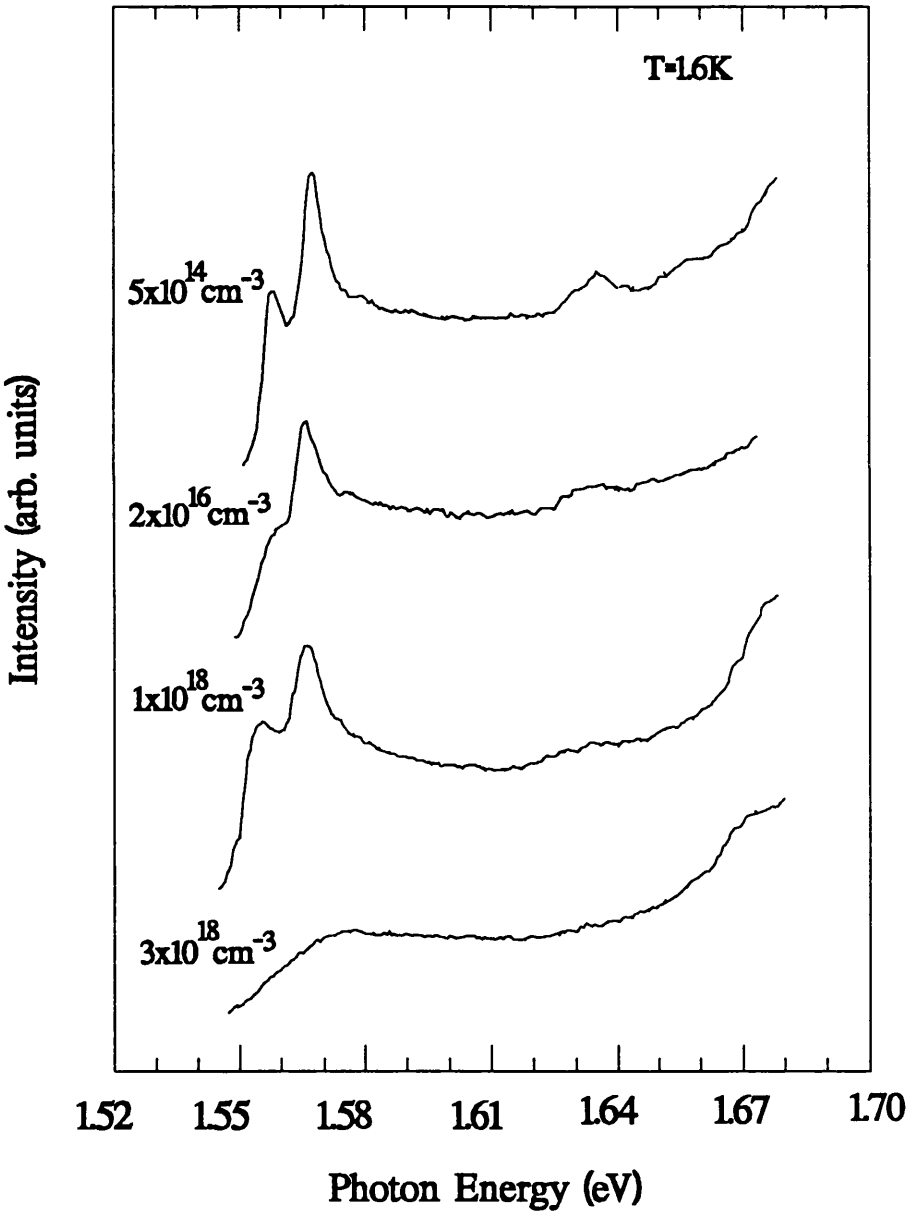

Fig. 5.4 Development in PLE with doping concentration.

The Stokes shift between PL and the heavy hole exciton in PLE is found to increase from less than 1meV at low doping to approximately 3meV at the highest observable level. This is as expected from the increased localisation with doping so far discussed. The data for the highest doped sample does not show any n=1 exciton and is upshifted in energy due to band filling. The low energy absorption tail which corresponds to the position of the electron Fermi level is broadened due to the strong impurity scattering. Fig. 5.4 again makes the contrast with the high internal field case. The heavy hole exciton demonstrates the strongest perturbation for all the doping levels studied. One interesting point to notice is the lower energy absorption threshold for the highest doped sample, this illustrates that there are indeed fewer carriers present in the well and provides further confirmation of the model of chapter 4. The Stokes' shift under these conditions is significantly increased for all the samples to that calculated from Fig. 5.3. This result has in fact already been predicted in chapter 4. The increasing polarisation of the hole distribution towards the QW interface with internal field will inevitably result in a stronger localisation of the exciton and in turn a larger Stokes' shift.

5.2.2 Recombination dynamics at the metallic limit.

The sample with a donor concentration in the well of $1.0 \times 10^{12} cm^{-2}$ represents the limiting case at which the lowest energy n=1 excitons are not observed, due to electron filling in the lowest conduction subband. As shown in Figures 5.1 and 5.3 neither steady state PL nor PLE spectra show any sign of the lowest exciton states, rather the PLE spectrum demonstrates a broadened step-like onset characteristic of a Fermi level above the band edge. The difference in the PL spectra for high doped samples which still exhibit an exciton transition and those for which it is lost can be further studied using time-resolved

photoluminescence. Fig. 5.5 compares the short time development in the PL spectra for two samples, one slightly below the doping limit for which excitons are lost (a) and the second slightly above (b). In both cases excitation is at the a photon energy corresponding to the n=2 exciton. Fig 5.5 (a) can be compared with the data of Fig. 4.15 and illustrates the rapid loss in exciton due to strong localisation and break up of the exciton in the internal field. The continuing relaxation to lower energies of the PL spectra following the loss of the exciton illustrates that further localisation is still taking place. The data above the exciton limit (Fig 5.5 (b)) have in contrast no short lived component but show a relatively weak but continuous localisation. The slower relaxation is again indicative of the weaker localisation potentials present in the strongly degenerate sample.

5.2.3 Nonradiative recombination in the high doping range

The behaviour observed in the PL spectra of highly doped bulk GaAs is a strong reduction of the low temperature PL efficiency of the material with increasing doping level (a factor $\approx 10^3$ at $n \approx 10^{19}$ cm^{-3}) [5.24]. In addition, a similar strong reduction of PL intensity is found with temperature as it is increased in the range 2K-300K (see e.g. Ref.[5.7]). This drop in radiative efficiency has been associated with strong nonradiative recombination processes in the material. We examine here the existence of similar mechanisms for the highly doped QW case. The PL efficiency at the highest doping level ($\approx 3x10^{18}$ cm^{-3}) appears to be reduced by about an order of magnitude as compared to the case of more moderate doping (say 10^{16} cm^{-3}), under conditions of low excitation. An interesting effect is observed for the high doped samples as the excitation density is increased, a superlinear region is typically observed at low temperatures, such that a higher PL efficiency is

obtained at higher power levels (Fig. 5.6).

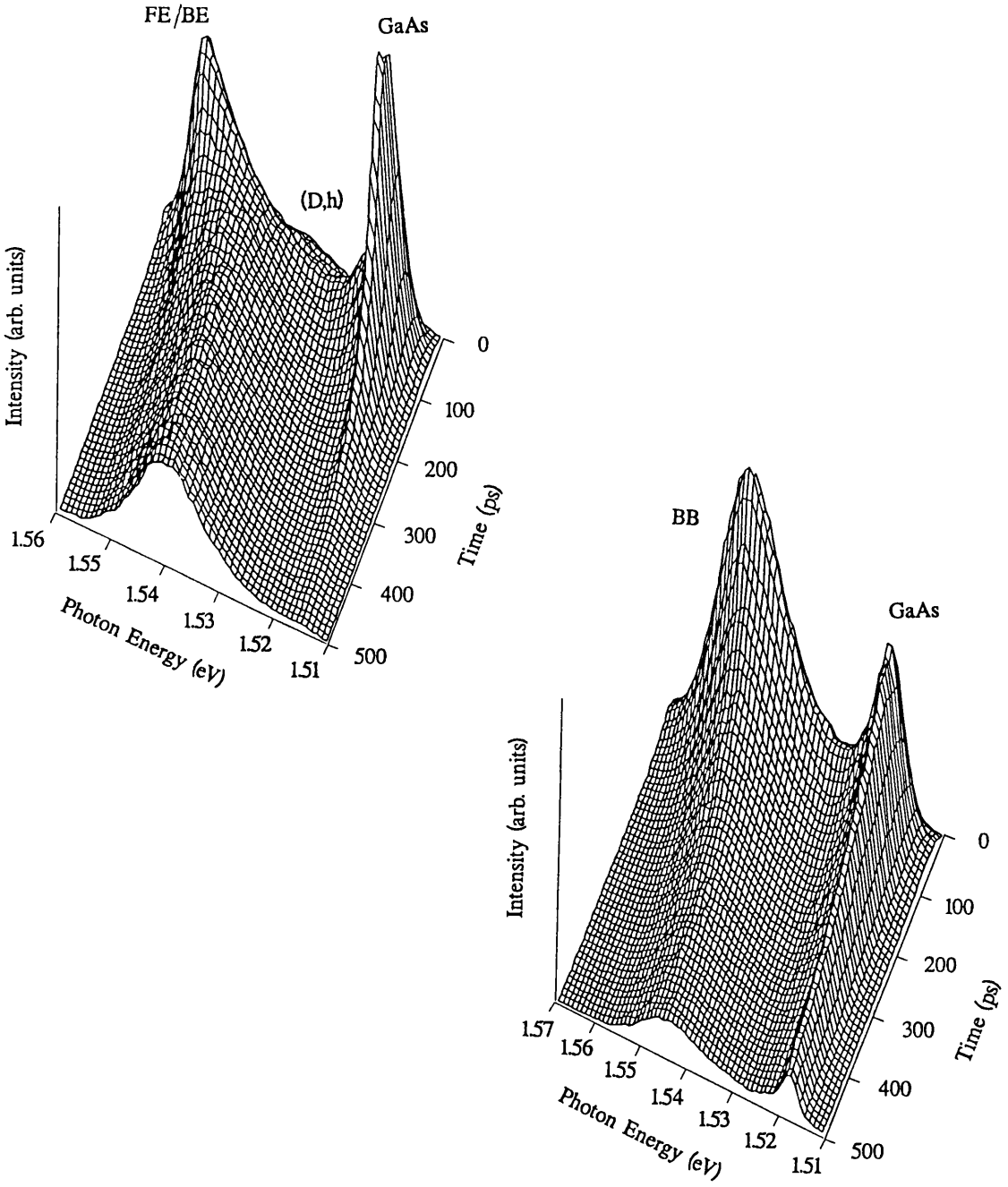

Fig 5.5(a) Time resolved spectra for highly doped sample but for which exciton is still observed in PL. Fig. 5.5 (b) Time resolved PL spectra for sample doped at $3x10^{18}$ cm^{-3}, no exciton is observed in PL under either of the excitation conditions.

This behaviour is, within reason, independent of excitation energy indicating that it is not a dynamics related effect associated with the relaxation in the system. A similar behaviour is in fact observed for all samples even at relatively low doping levels, although generally to a lesser extent. This behaviour is typical of a nonradiative recombination channel that can be saturated at high excitation power. This saturable component however, is certainly not the only non-radiative process involved, since the PL efficiency even at high excitation intensity tends to be substantially reduced compared to the case of an undoped QW. Possible mechanisms for the nonradiative recombination in these samples will be outlined below.

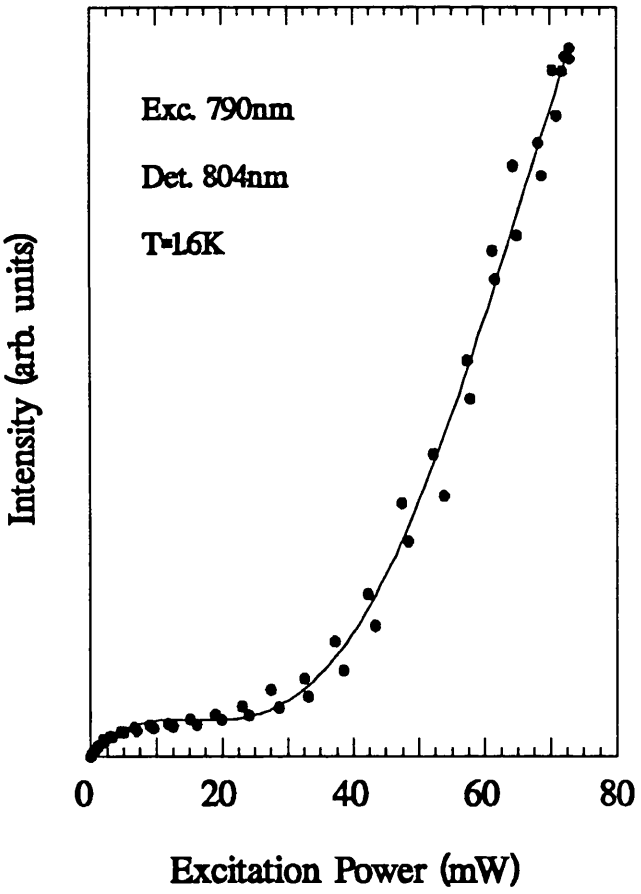

Fig 5.6 Non-linear excitation dependence of intensity, illustrating saturation of non-radiative channel

5.3 Discussion

5.3.1 Comparison of 2D and 3D behaviour at high doping levels

In discussing the results obtained it is useful to compare the properties of highly doped QW's with the corresponding properties of bulk semiconductors in the same doping range. One considerable difference obvious from the results of this work is a higher metallic limit in the QW case, a concentration of about $2.0x10^{18}cm^{-3}$ (corresponding to a sheet density of about $1x10^{12}cm^{-2}$). This is a factor 2-3 times higher than in the 3D case. A simple interpretation for this higher limit in the QW is the considerable difference in donor binding energy between the QW and bulk GaAs. While the shallow donor binding energy in GaAs is about 5.9 meV [5.25], it is increased by a little over a factor of 2 to about 12 meV in a 100Å QW, due to the confinement of the donor wave function [5.26]. There is no evidence to suggest that 'self screening' takes place at higher doping levels, which would reduce the donor binding energy [5.27]. This higher binding energy means that the donor band created at higher doping levels can be broader in energy in the QW, and sustain more donor electrons until the distribution merges into filling the conduction band in the metallic limit [5.1].

Another dramatic difference between bulk and 2D obvious from this work is the behaviour of excitons vs. doping level. In the bulk case excitons are already screened at a donor doping level of a few $10^{16}cm^{-3}$ [5.28]. Above this doping level no excitons are observed, either in PL emission or in absorption. This is very different from the QW case, as already pointed out above. Even at doping levels above the metallic limit i.e. $2.5x10^{12}cm^{-2}$ ($5x10^{18}cm^{-3}$), excitons are still found to exist, as is evident from a broad n=2 peak in the PLE spectra. It is clear that the way in which the excitons are screened is fundamentally different

in the confined system in comparison to bulk material. The argument for the lower screening strength in the low dimensional system follows from the reduced degree of movement available to the carrier. Since screening is basically a many body effect where the carriers arrange themselves to maximise the total Coulombic interaction, and hence minimise the single particle interaction, any restriction on mobility will inhibit their ability to do this. The same qualitative reasoning explains the limited screening due to impurity bound charge. We now apply these arguments to a comparison between impurity screening between the 2D and 3D cases. The increased binding of the centre to the impurity in the low dimensional case naturally implies a reduced contribution to screening in comparison to the 3D. Quantitatively we would probably expect a similar ratio decrease to the increase argued for the degenerate limit i.e. in proportion to the Bohr radius. In addition however the exciton binding energy is also increased, as a result we have two contributions which increase the doping limit at which the exciton is lost due to screening. As a crude estimate we can assume the ideal 2D limit, this gives a factor 2 decrease in the extension of the impurity wavefunction, the increase in the exciton binding energy is a further factor 4. In total then the screening limit for exciton in the 2D system is an estimated factor 8 higher than in the 3D case. Comparing this qualitative argument with our results unfortunately fails to fully account for the difference in critical densities. Additional mechanisms must play a role in sustaining the existence of the exciton at high impurity levels, these are at present not well understood.

The mechanisms of radiative recombination for the high doped sample are also best discussed in comparison with bulk mechanisms. One interesting point is the detailed process of band to band recombination in the presence of a high doping concentration of donors. It is clear from previous studies of BB PL emissions in the case of modulation doping (i.e. nominally undoped wells) that

momentum conservation is obeyed in the radiative recombination process [5.29]. On the other hand, some attempts to fit observed PL lineshapes for highly doped bulk GaAs indicate the absence of momentum conservation in the PL recombination process [5.7,5.8], while other work indicates that momentum conservation still holds [5.12]. From the detailed investigations of the excitation photon energy dependence of the BB and D-bands, it is possible to separately obtain the spectral shapes of these bands in the region of overlap. Fig. 5.8 shows such a spectrum for the BB emission in a strongly degenerate sample, where the spectral shape of the D-band has been subtracted. Apart from the high energy edge, which represents the broadened Fermi level, and the low energy edge, which reflects the band tailing effects on the lowest band edge, a well defined flat region in the spectrum is observed. The observed plateau reflects the 2D step like density of states, as expected in the absence of momentum conservation for radiative recombination in a degenerate population of a single carrier type. Non momentum conserving recombination in a highly excited sample (e-h plasma) would not exhibit this plateau. The mechanism for relaxation of momentum conservation is an impurity assisted scattering process. The carrier scattering leads to effective virtual states through which recombination takes place [5.30] i.e. the impurity site participates in a momentum exchange during the recombination (see Fig 5.8).

The contribution of non-radiative recombination has been shown above to strongly increase at higher doping levels. The characteristic signature of this process in bulk GaAs is the drastic increase in the nonradiative recombination rate for doping concentrations above $10^{18}cm^{-3}$, and also a strong increase with temperature of this process. As the presence of deep levels in sufficient concentrations to explain this behaviour is in general considered unlikely in bulk or epitaxial GaAs, an intrinsic Auger mechanism has been suggested to explain these effects [5.31] [5.24] which is in qualitative agreement with

experimental data for bulk GaAs.

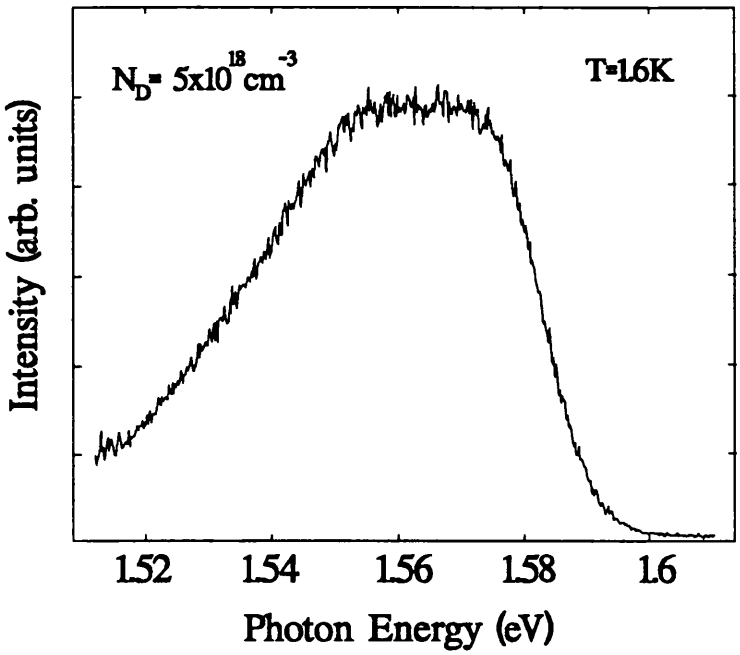

Fig. 5.7 Recombination for highly doped quantum well, broad plateau like shape corresponds to the 2D density of states and indicates the break down in momentum conservation in the radiative transitions.

In the present case we believe there is evidence for two different nonradiative recombination processes. One process is saturable, and believed to be defect related, more specifically related to interface defects known to be present from the conditions of MBE-growth. The role of these interface defects has not yet been characterized in any specific detail in the literature for the AlGaAs-GaAs MBE-grown interface, but would be expected to give rise to strongly localized deep states, which are then natural nonradiative recombination centres. The remaining (nonsaturable) nonradiative process observed for QW's at the very highest doping levels is ascribed to an intrinsic Auger process. In addition to the free carrier Auger processes discussed in the bulk case, excitonic Auger contributions may not be negligible for degenerate QW's, under conditions

where excitons are formed. The mechanism by which Auger processes are enhanced at high doping levels can be understood in terms of the Impurity Band Auger model (IBA) [5.24]. As the donor concentration increases the donor electrons become increasingly delocalised into an impurity band and are thereby more readily available to take part in a three body Auger recombination process. It is however important to recognise that the presence of a large concentration of non-radiative defects caused by the heavy doping of the QW cannot be excluded as a possible recombination channel.

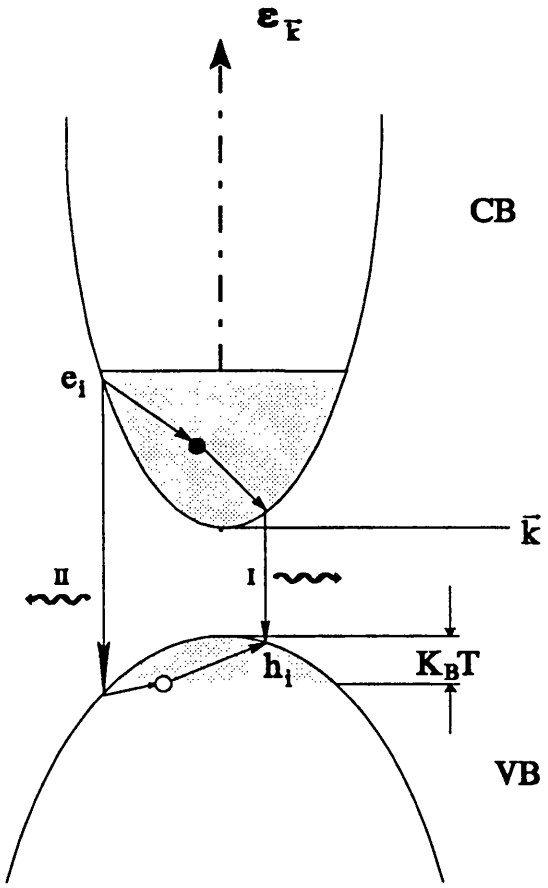

Fig 5.8 Relaxation of momentum conservation via impurity scattering [5.30]. Path I: An electron is scattered into an intermediate state by an impurity and subsequently recombines with the hole. Path II: An electron decays into a virtual hole and is then scattered into the hole by an impurity (open circle). Initial hole and electron states are marked.

5.4 Conclusion

The development of photoluminescence spectra with increasing doping level in a single quantum well is found to be qualitatively very different from the behaviour in bulk material. The exciton dominates the QW luminescence right up to the degenerate doping limit and is not screened by Coulombic interaction with dopants as is the case for bulk material. The metallic limit is reached only at dopant concentrations a factor of approximately 2 to 3 times higher than for bulk GaAs. A simple interpretation of this is the corresponding difference in binding energy of the donor for the confined system. We propose that even at the degenerate limit the exciton is still present in the optical spectra of the QW. A clear reduction in localisation above a certain doping concentration is seen as evidence for the presence of free carriers which smear out the localisation potentials. The exciton is lost only when we begin to fill up subband states. Significantly above the metallic limit where the exciton is no longer observed in PL, the spectrum is made up of free carrier band to band and donor band to valence band recombination. In contrast to recombination from degenerate free carrier populations introduced by modulation doping, momentum conservation is found to be relaxed for the anti-modulation doped case. This process is demonstrated by the observation of a distinct plateau in the PL spectrum, corresponding to the constant 2D density of states in this energy range. Non radiative recombination processes have been discussed and the observation of a saturable non-intrinsic channel reported. The impurity band Auger model has been suggested to interpret the increasing non radiative contribution at higher doping levels.

Chapter 6

Exciton dynamics in doped quantum wells.

6.1 Introduction

6.1.1 Oscillator strength and lifetime of exciton transitions in 3D GaAs and the 2D GaAs/AlGaAs quantum wells.

The predominance of exciton recombination within the radiative emission of quantum wells is well known [6.1]. The strength of this transition is understood in terms of the increased binding energy of the exciton due to confinement. Stronger binding of the exciton also results in the much quoted retention of exciton absorption up to room temperature [6.2]. In addition to the overall prominence of the free exciton recombination it is interesting to note the relatively weaker contribution of the bound exciton in comparison to the bulk GaAs behaviour. The bulk signal is in contrast dominated by the bound exciton component and the polariton-like free exciton is found to be extremely weak in all but the highest purity samples [6.3]. By way of comparison the estimated impurity concentration giving a strong free exciton component for the bulk material is by conservative estimate $\leq 10^{13}$ cm^{-3}. On the other hand the free component in the confined system is the stronger emission up to levels of 10^{16} cm^{-3} and above. This point has not been extensively discussed in the literature, and has been one point in our motivation for the work in this field.

There are a number of important factors which will determine the interaction of free and bound excitons. The enhanced binding energy of the bound state is clearly not the determining factor. In this work we use picosecond time resolved photoluminescence to study the interaction of the free and bound exciton states. In particular the process of capture and thermal emission are looked at and their role in determining the observed luminescence decay time discussed. The whole area of the kinetics of radiative recombination has received considerable interest in the last few years [6.4] [6.5] [6.6] [6.7]. This is in part recognition

that a detailed understanding of the radiative mechanisms in semiconductors can only be achieved by studying the short time scale interactions between free carriers generated in the material. In addition the motivation of using these ultra fast mechanisms in opto-electronic switching devices for future telecommunication applications has guaranteed intense work in this field.

The interaction of photo-excited carriers can be discussed in three basic time regimes [6.4] :

(1) The coherent regime, in which the interaction of a short laser pulse with the electronic states of the semiconductor sets up a coherent macroscopic polarization i.e. the electronic excitation in the semiconductor is in phase with the electric field vector of the exciting light. The decay in coherence is determined by elastic and inelastic scattering (which in turn determines the observed homogeneous linewidth) and is characterised by a time constant T_2, see Fig 6.1.

(2) Cooling, following the loss in coherence the excitons continue to relax as they dissipate excess kinetic energy, typically via phonon emission. Depending on the strength of the carrier interaction either via carrier-carrier or carrier-phonon scattering the distribution can reach a thermal equilibrium at elevated temperature with respect to the lattice. At higher carrier densities the thermalisation process can be extremely rapid, the subsequent cooling from this effective carrier temperature to that of the lattice is referred to as the "cooling curve". Such a relaxation mechanism has been studied for a number of semiconductor systems, both in bulk material and low dimensional confined systems [6.8] [6.9].

(3) Recombination, the third, slowest regime and the one we are primarily interested in this work. The recombination path for an excited system is determined by both the electronic band structure of the material and also by its basic quality in terms of purity and structure. This dependence leads to the

"Spectral Fingerprint" by which a material can be characterised. The different recombination mechanisms which can occur have already been discussed in detail in chapter 2. The three different time regimes for relaxation following photo-excitation are illustrated in Fig. 6.1 for both the 2D and the 3D case [6.4].

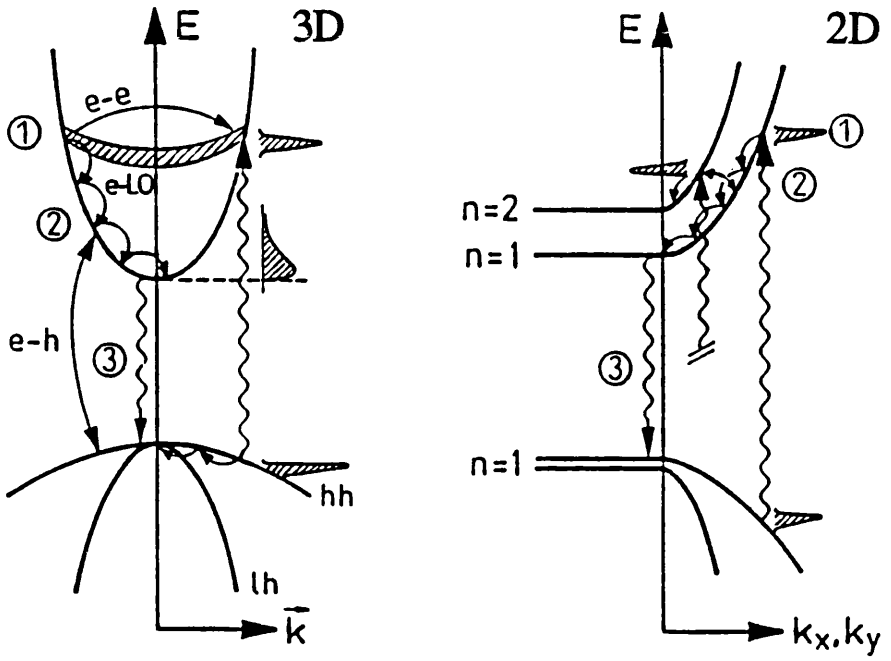

Fig. 6.1 Interaction mechanisms for photo-excited carriers in 2D and 3D systems.

The key to understanding the differences observed in the exciton recombination between the quasi 2D case and bulk GaAs is to be found in discussing the mechanisms occurring on a time scale comparable to the radiative lifetime of these states. This importance justifies a slightly more in depth discussion of the theoretical description for the recombination model. The intrinsic strength of a given recombination is typically described by a single parameter the so-called oscillator strength, which expresses the probability for that transition to occur. We start by looking at a simple argument of the dependence of the oscillator strength upon the dimension of the system.

First considering the free exciton; as a free particle the exciton wavefunction is

made up of the Bloch electron and hole states of the lattice. The probability of finding an electron at any particular lattice site is proportional to the unit cell volume (in 3D α a^3). The probability of finding a coupled hole within the same unit cell is in inverse proportion to the exciton volume i.e. α $(a_{ex})^{-3}$ [6.3], this leads to the cubic ratio $(\frac{a}{a_{ex}})^3$. For bulk GaAs the unit cell length a=5.6 Å and the exciton Bohr radius r_B = 140Å, giving an oscillator strength f $\approx$ 1 x 10^{-4}. The same dimensional arguments applied in the ideal 2D case lead to the quadratic ratio $(\frac{a}{a_{ex}})^2$. In turn this implies the ratio of oscillator strengths between the 2D and 3D exciton should be given by:

$$\frac{f_{2D}}{f_{3D}} = \frac{1}{a}\left[\frac{a_{3Dex}^3}{a_{2Dex}^2}\right] \qquad (6.1)$$

For a_{3Dex}= 140Å and a_{2Dex}= 70Å (strict 2D limit) this gives a value of 100 for the ratio of oscillator strengths. Even such a crude estimation allows a good indication of the relative strength of the 2D transition. It is clear that the dimensionality plays a significant role in promoting the exciton dominance.

The strength of bound exciton recombination in bulk GaAs is surprising if one considers the relative density of FE states in comparison to the number of impurity sites. This anomaly was first explained by Rashba and Gurgenshvili who proposed the concept of a "Giant Oscillator Strength" for bound excitons [6.10]. The transition strength was found to be as a rough estimate related to the free exciton in 3D through the relation [6.11] :

$$f_{BE}=\left[\frac{a_{ex}}{a}\right]3\, f_{FE} \qquad (6.2)$$

which implies for GaAs a value of the order of unity i.e. some 4 orders of

magnitude greater than the free exciton transition. Physically the increased strength of the bound exciton transition can at least in part be understood in terms of the increased overlap of the carrier wavefunctions, due to the fact that both particles are now localised in the vicinity of the impurity. The large spatial extent of the bound exciton however also plays an important role, this is illustrated by the fact that the acceptor bound exciton has a weaker oscillator strength in comparison to the donor despite its greater binding energy. The implication of this result is simply that the overlap of the e-h wavefunctions is dependent upon how the exciton is localised in the vicinity of the impurity, whether at an electron or hole attractive potential [6.12]. In turn then the correlation between particles, which is in fact neglected in the original calculation of Rashba and Gurgenshvili, will also contribute to the transition strength [6.13-6.14]. The two dimensional bound exciton has been studied by Herbert and Rorison [6.14], in which they include the effects of correlation. They conclude that for narrow wells the oscillator strength is in fact decreased in comparison to the bulk value (by a factor of 5 at L_Z=50Å). The giant oscillator strength has also been discussed for localised excitons in quantum wells by Takagahara and Hanumara [6.15] who discuss its implications in enhancing the excitonic optical nonlinearity in the two dimensional system.

We have so far discussed the exciton transition in terms of its oscillator strength; it can equally well be discussed in terms of the radiative lifetime, which is related to the oscillator strength via the equation [6.3] :

$$\tau=\left[\frac{2\pi\varepsilon_o m_o c^3}{\tilde{n}e^2\omega^2 f}\right] \qquad (6.3)$$

where ω is the angular frequency, f the oscillator strength and $\tilde{n}$ is the refractive index, other symbols have their usual definitions. As a result a transition with

large oscillator strength should have a short lifetime. From theoretical calculations the predicted lifetimes for the donor and acceptor bound excitons in bulk GaAs are 0.031 ns and 0.96 ns respectively. In practice values of 0.75 ± 0.15 ns for the DBE and 1.0 ± 0.1 ns for the ABE have been measured [6.16]. The anomalously long lifetime of the DBE has been explained in terms of its large degeneracy due to the existence of rotational states close to the lowest bound exciton state [6.16]. For the free exciton the small oscillator strength implies an extremely long lifetime (40 μs assuming our previously discussed value of $f = 10^{-4}$). Recent measurements on high purity GaAs claim a true lifetime of approximately 3.3 ns for the FE [6.3]. This in turn implies an oscillator strength of order unity, which has led the authors to suggest a giant oscillator strength for the free exciton. This idea is however inconsistent with the oscillator strength as calculated from the total absorption cross section via [6.17]:

$$Nf = \left[\frac{4m_0\varepsilon_0 c\tilde{n}}{e^2 h} \right] \int \alpha(E)\, dE \qquad (6.4)$$

Where ñ is the refractive index, α the absorption coefficient, E is the photon energy, and N is the number of unit cells per volume; m_0 ε_0, c, e and h are fundamental constants with their usual values. Such a calculation gives a value for f of approximately 7×10^{-5} in agreement with the probability deduced earlier. It is however argued that in fact the absorption cross section should be calculated with the number of absorbers N, not equal to the unit cell packing density but instead equal to the maximum density of exciton volumes. Feldman *et al.* have extended this argument to take into account the importance of coherence and discuss the lifetime in terms of the coherence volume of the exciton [6.18]. The argument based on exciton volumes is perhaps reasonable

and would reconcile the differences in oscillator strength between the two calculations. The implication for the bound exciton is that the oscillator strength calculated in this way (per exciton volume) means the strength of the BE absorption is simply an indication of the trapping efficiency at an impurity, that is, proportional to the probability of there being an impurity within the exciton volume [6.19]. It is in fact clear that the term "Giant Oscillator" strength is rather a misleading term. What results from the current understanding is that the oscillator strength for an exciton transition must be considered in terms of the exciton volume occupied by the exciton state whether bound or free.

One further question which is briefly addressed in this chapter is the problem of exciton localisation. The context of localisation has already been discussed to some extent in chapter 5, where the high doping limit was considered. The role of interface roughness i.e. the structural disorder on an atomic scale at the growth surface which becomes the interface will ultimately have a strong influence on the performance of QW devices. For this reason the mechanisms of exciton localisation at interfaces have recently received considerable attention [6.20]. Under standard growth conditions the QW interface probably appears as a large matrix of local steps deviating in height by no more than a few atomic steps. When considering the confinement of the exciton or free particle, a one must consider a value averaged over the local region, the exact distribution being dependent on the growth conditions (Fig. 6.2 (a)). When the growth sequence is interrupted at the interface the surface atoms are sufficiently mobile to form regions where the local monolayer is complete. As a result the interface is made up from a number of relatively large islands that are atomically flat but differ in thickness by single monolayers [6.21] (Fig. 6.2(b)). In fact this picture is somewhat idealistic and recent high resolution measurements using the technique of chemical mapping suggest that even within a well defined monolayer there exists a large degree of roughness due to

single atoms displaced by fractions of an atomic layer [6.22]. Other mechanisms have also been discussed as contributing to interface localisation including alloy disorder (for ternary compounds). Such mechanisms have however been discounted for the GaAs/AlGaAs system [6.23]. The work of Bastard *et al.* [6.24], points in particular to the importance of impurities associated with interface defects in the localisation process, an idea which is taken up in the later discussion.

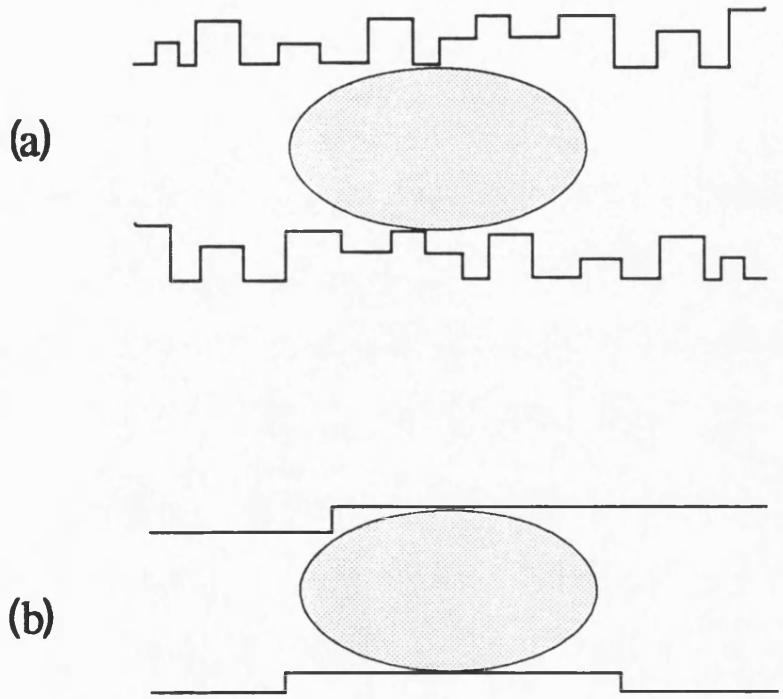

Fig. 6.2 Confinement of exciton in QW with non-interrupted (a) and interrupted (b) growth sequence.

The localisation effect itself is a consequence of the random nature of the potential at the interface. The ability of a random potential to localise a particle wavefunction was first realized by Anderson [6.25] and has subsequently been discussed by a number of authors [6.26]. The contribution of excitons localised in different depth potentials to the total inhomogeneous linewidth has been elegantly studied by Hegarty and Sturge [6.27]. They also discuss the relative

mobility of the localised excitons and the existence of a predicted mobility edge. The former point is looked at in more detail in the current work. In particular the relaxation of mobile excitons by trapping at impurities and furthermore the mobility of bound excitons between weakly localised islands is discussed. Localisation can also result in an enhancement of those transitions involving more than two particles, for example Auger mechanisms [6.28]. This effect can be understood by considering that localisation of the respective wavefunctions necessarily increases their overlap and hence their interaction strength. For the BE recombination this can result in satellite peaks at lower energy, so called Two-Particle Transitions (TPTs). For a neutral donor BE we consider a picture in which the BE recombines simultaneously producing an excitation of a second electron in the BE complex (a two electron transition TET). Similarly, the equivalent mechanism for the neutral acceptor BE results in a two hole transition (THT). This phenomena is sometimes described as a "shake-up" of the electron or hole populations. The observation of TPTs in bulk material has allowed the accurate determination of the binding energies of ground and excited states for many impurities [6.29].

In general shake-up processes are not observed for free excitons due to the small overlap between the exciton and the additional particle wavefunctions. If however the exciton becomes localised along with a second particle then we have the possibility of an analogous TPT to that observed for the true BE state. Such free exciton related transitions have recently been reported for narrow doped quantum wells [6.30]. The observation of various shake-up processes are reported here for a narrow acceptor doped quantum well. Using selective excitation within the localised free exciton envelope we are able to accurately measure both the acceptor bound exciton binding energy and also the first excited state of the acceptor.

In total this chapter studies the interaction of free and bound/localised excitons

in the low-dimensional environment of a quantum well. The work is subdivided into two areas; the first discusses the kinetics of the free-bound exciton interaction which can be studied in a time-resolved set-up; the second considers the interplay of doping density and interface roughness in bringing about exciton localisation. The second section also discusses the observation of a spatial correlation between the localised free exciton and bound exciton populations. This effect is observed using the technique of selective excitation, where the excitation energy is resonant with localised exciton states and a corresponding well defined (in energy) bound exciton population is created. Such a technique also allows an extremely accurate measurement of the acceptor binding energy to be made.

6.2 Exciton Dynamics studied by Picosecond Time-Resolved Photoluminescence

This first experimental section of the chapter deals with the dependence of the short time scale exchange between free and bound exciton populations upon different parameters. In particular the role of capture, emission, and recombination in determining the temporal development of the exciton system is discussed. The interdependence of these mechanisms implies that an analysis can only be made if one takes into account the proper coupled rate equations. Using such a calculation we are able to discuss the relative importance of the different process in determining the overall temporal development.

The photoluminescence spectra observed at short times following pulsed excitation can appear distinctly different from those observed under cw excitation. This difference is due to the fact that we resolve the short time scale interactions, while in a cw experiment the observed signal is an ensemble of

time averaged components. The use of pulsed excitation also allows higher densities to be achieved, frequent use has been made of this to study the intense carrier interaction which occurs for densities at and above the Mott transition. In particular this has allowed the study of a number of many-body related problems [6.31]. Excitation intensity is found to be important for the interaction of excitons even at relatively low densities, this point is discussed in detail in section 6.3.3.

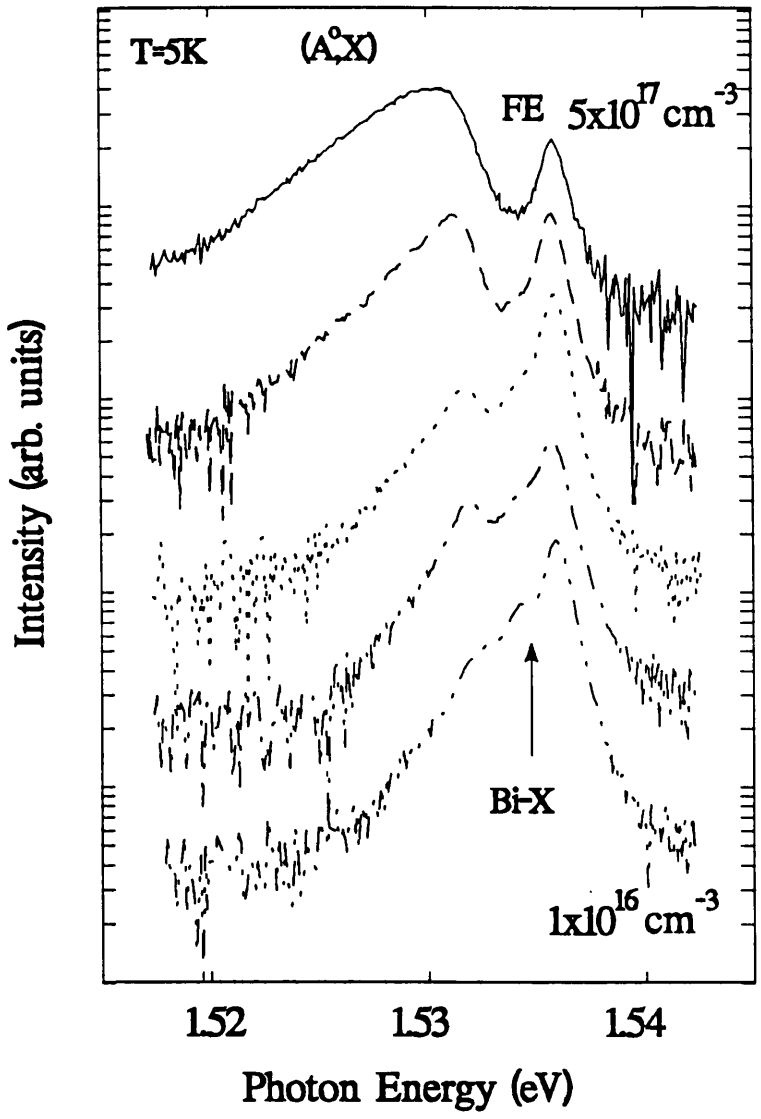

Fig 6.3 Dependence of PL spectra on doping density, spectra shown 36ps seconds after centre of laser pulse.

Fig. 6.3 shows PL spectra taken for a series of 150 Å samples doped with Be acceptors at various concentrations from $3x10^{16}$ to $5x10^{17}$ cm^{-3} (corresponding to a 2D density of approximately $6x10^{9}$ to $1x10^{11}$ cm^{-2}). The spectra are for resonant excitation in the FE and show a time window approximately 36 ps after the centre of the laser pulse. In all cases the luminescence peaks are relatively broad, indicating a relatively strong impurity interaction. The FE is slightly broadened with increasing impurity concentration, although a relatively minor effect, indicating that the line width is probably dominated by interface roughness [6.32]. The BE (A^o, X) on the other hand is strongly affected by the increasing doping concentration and appears as a narrow peak comparable to the FE only at low concentrations. The peak intensity of the BE increases strongly in ratio to the FE with increasing concentration. At higher concentrations the acceptors strongly interact, and the BE recombination becomes extremely broad. This same behaviour has been observed in bulk material and has been discussed in terms of localisation of the exciton in environments of different local impurity concentration. The bound state is found to be able to move between sites via a phonon assisted hopping mechanism and in this case can be observed as a distinct spectral diffusion to lower energies with time (see later discussion). The bound exciton is able to relax via hopping to deeper states typically emitting acoustic phonons in the process. A similar mechanism, due to the cascade emission of LA phonons has been observed in some materials, this results in an "undulation" in the low energy band exciton with a period related to the LA phonon energy [6.33].

The low concentration data also show the presence of a third peak in between the free and bound acceptor exciton transitions. At first sight this is apparently related to residual donors in the system, however from this argument it is not clear why this should be lost at higher acceptor concentrations. The presence of a third peak has not been observed in any of the samples with narrower well

widths, irrespective of dopant concentration, this further indicates a non-extrinsic origin. The intensity dependence of this line appears coupled to that of the free exciton, this is probably a consequence of the thermalisation of the two populations which exists at the 5 K measurement temperature (measurements < 5 K were not possible in the available cryostat). The binding energy of this component relative to the free exciton is also relatively small (1.4meV), we therefore believe the most likely candidate for this transition is the formation of a biexciton. Biexcitons have been observed in quantum wells on a number of occasions [6.34,6.35], although their identification has normally been made solely on the basis of a corresponding binding energy [6.34]. The expected quadratic dependence on excitation density has not been observed. One possible indication of why such a response is not seen is given by the impurity concentration dependence of Fig.6.3. The formation of biexcitons is apparently limited by the preferential capture of free excitons to the bound site. This result is consistent with the non-observation of the biexciton in more strongly confined systems where the stronger impurity binding energy results in stronger capture. Furthermore it suggests that the intensity dependence will be far from quadratic in the presence of any extrinsic element.

Fig. 6.4 goes some way to confirm this assignement by looking at the intensity dependence for the lowest doped sample using cw excitation. As expected the biexciton transition increasinges more strongly in comparison to the free for increasing excitation densities. Fig. 6.5 summarises this point by showing the intensity dependence of the different transitions, as discussed the biexciton is in fact less than quadratic.

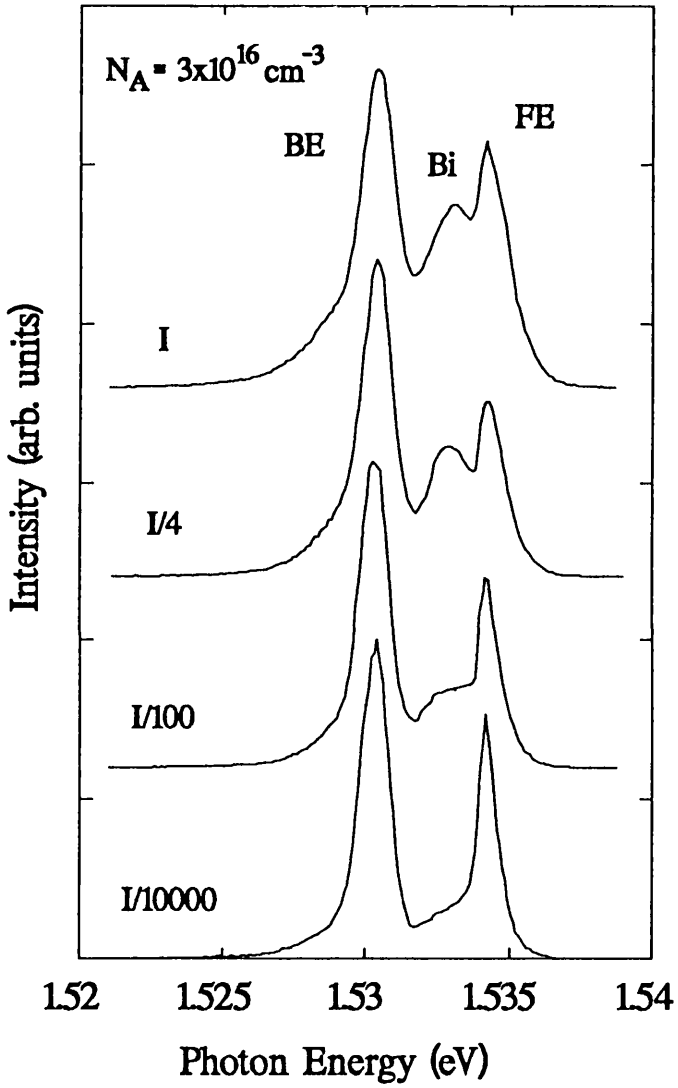

Fig. 6.4 Development of photoluminescence for increasing exciation intensity, illustrating the increasing bi-exciton component.

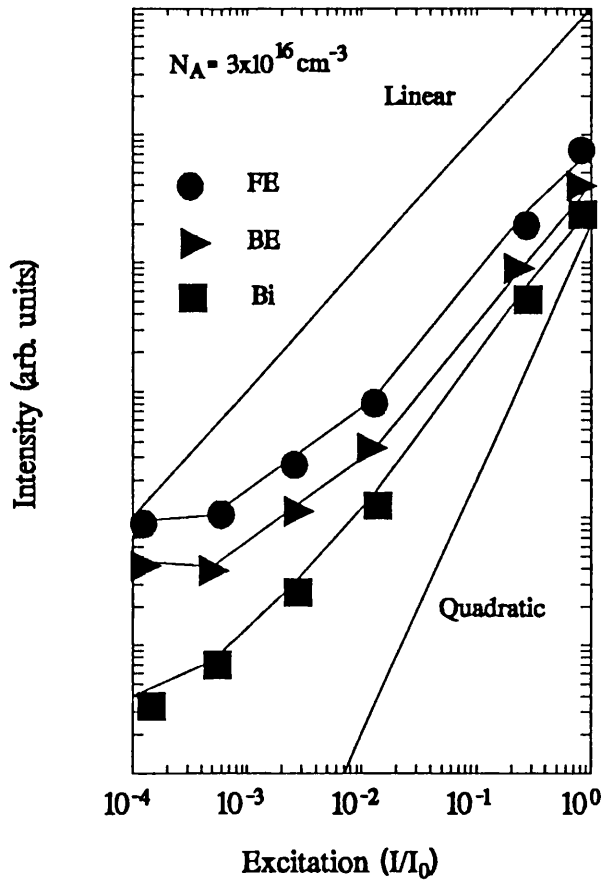

Fig 6.5 Summary of intensity dependence of exciton recombination for 150Å acceptor doped quantum well.

6.2.1 Free-bound exciton exchange (capture vs thermalisation)

The importance of capture strength has already been illustrated in Fig. 6.3. Despite this dependence, capture processes for excitons have in general received relatively little attention, most of which has largely concentrated on Si [6.36]. The process of capture of a free exciton by an impurity site to form a bound exciton can be characterised by a capture cross section. In modelling the capture mechanism it is simplest to consider a single-level system i.e. the particle is either bound or free. The analysis of the decay transient then only requires a single rate equation for the bound state. The predominant capture process is assumed to follow the theory of Lax [6.37] , in which he describes a

cascade capture mechanism as the particle relaxes through the bound excited states via successive phonon emission. In simple terms this model implies that capture will occur only to those bound states that are deeper than the thermal energy k_BT from the free particle continuum. Excitons captured to states below this threshold rapidly relax to the ground state via phonon emission, while those in higher lying states are further ejected. In calculating the total capture cross section appropriate to our single level model we must sum over the cross sections for each level:

$$\sigma_t = \sum_j S_j \sigma_j \qquad (6.5)$$

where S_j is the so-called sticking probability, i.e. the probability that a particle captured in state j reaches the ground state. From the above model this probability is essentially one for states below k_BT and zero above. This simplistic model makes no account of the transition rates for the relaxation process, however this point is unimportant provided the relaxation is rapid in comparison to the observed decay rates and hence that the bound population predominantly resides in the ground state. The occupancy of excited states is important in determining the thermal emission or release from bound to free states, which in turn will represent the temperature dependence of the overall capture mechanism.

The binding energy of a bound exciton state is enhanced by confinement. For the neutral acceptor this varies from approximately 6.5 meV at L_z=50 Å to approximately 3.5 meV at L_z=150 Å. These values are large in comparison to k_BT at 5K, and we therefore expect the thermal emission to be a relatively weak effect. The donor binding energy in comparison is much weaker, and the effect of thermal emission is expected therefore to be correspondingly larger.

Fig. 6.6 illustrates the time dependence of the FE emission for the same set of acceptor samples as Fig.6.3. Again excitation is resonant with the FE and hence the early time response contains no delay due to exciton formation. The use of crossed polarisers allows us to remove the majority of the scattered laser light from the measured signal. The initial rate of decay of the FE peak is found to increase with doping density; in addition the total loss in population is also increased.

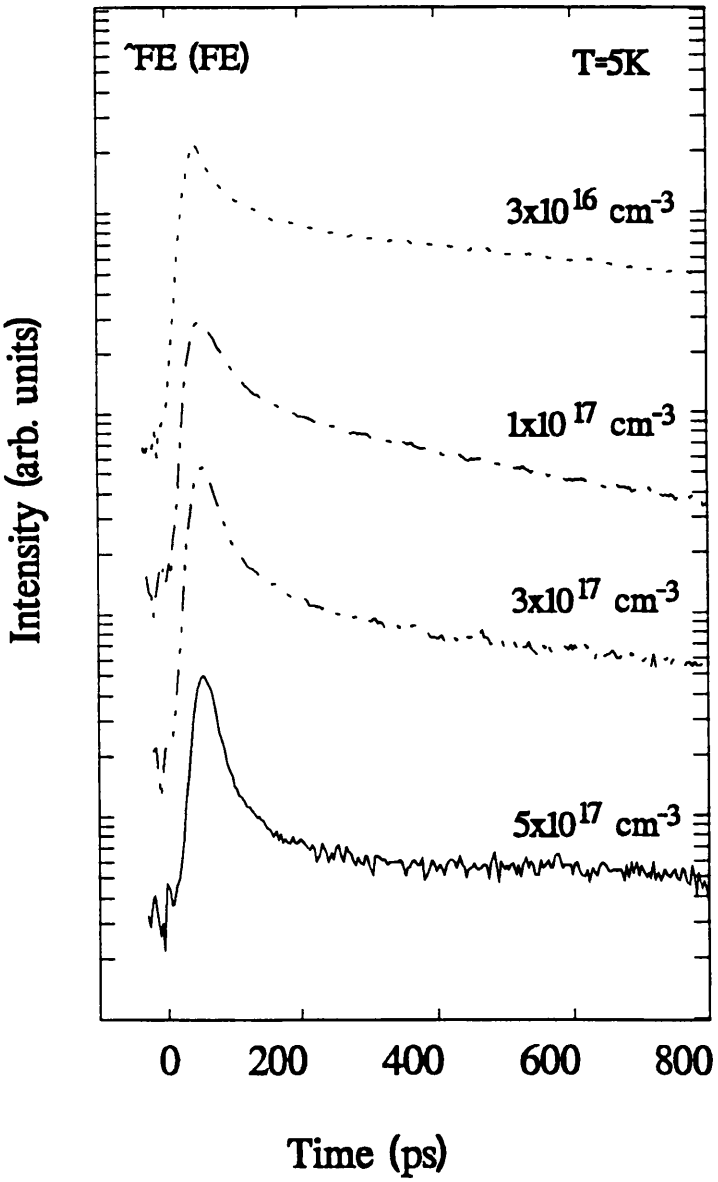

Fig 6.6 Dependence of radiative decay of FE on acceptor doping density

It is apparent that this initial decay is associated with the capture of free excitons at the acceptor state, the rate of capture being proportional to the concentration of available sites:

$$\frac{dN_{BE}}{dt} = \eta_C [N_{FE}].[A_o - N_{BE}] \qquad (6.6)$$

where η_C is the capture rate, A_o the total acceptor concentration, and N_{FE}, N_{BE} the concentrations of free and bound excitons respectively. It is also interesting to note that the apparent lifetime at long times t > 400 ps is also dependent upon doping concentration but that this dependence is the reverse of the time dependence of the capture stage i.e. the decay rate is faster for the low doped samples. The relatively low density of free excitons excited ($\approx 10^9$ cm^{-2}) suggests that this effect is not due to saturation of the bound sites. The response of the BE (to be discussed next) also indicates that there is essentially no back transfer due to thermalisation from bound to free which might determine this observed decay. One important mechanism that will determine the FE response is the thermalisation of the resonantly created excitons (with $K \approx 0$, i.e. corresponding to a temperature of approximately 1K [6.38]) to the actual lattice temperature, whereby most of these excitons are scattered up to sufficiently large K values that they are no longer radiative. The balance between those scattered and those captured will determine the long term radiative decay of the free exciton. Fig 6.7 shows the equivalent dependence on doping for excitation resonant with the bound exciton. In contrast to the FE, the decay is not significantly changed by the increasing doping level. The onset shows a rapid population of the bound exciton state during the laser pulse. The subsequent decay is a well defined exponential as is expected for a system where the rate of decay is simply proportional to the remaining population.

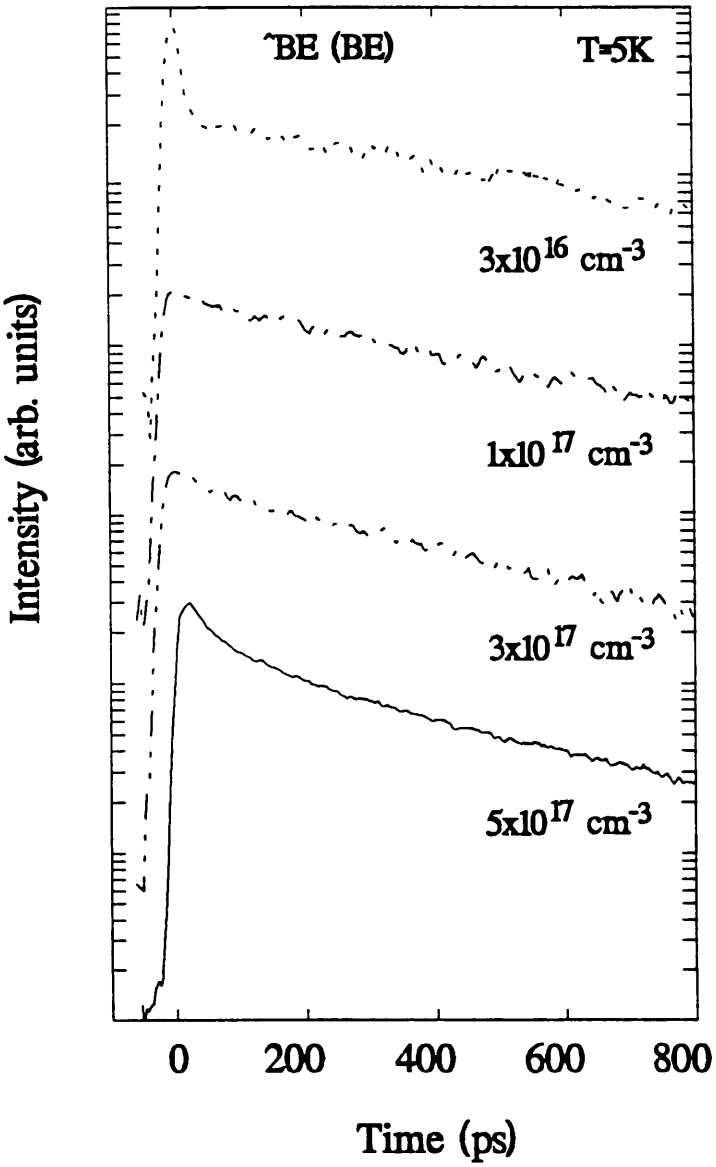

Fig. 6.7 Doping dependence of BE decay following resonant excitation in BE.

Such behaviour indicates that the BE system is essentially decoupled from the free i.e. no thermalisation occurs and that there is a fixed recombination channel. Two further comments to this series; the highest doped sample shows a slightly faster rate of decay than the more lightly doped. This relatively minor effect may well be due to the enhancement of non-radiative recombination which is found to occur with increased localisation at the high doping densities, in particular Auger mechanisms are enhanced by the localisation (see chapter 2). The lowest density result shows a sharp spike at the onset of the decay. This

is certainly in part the remainder of the scattered laser light which is difficult to remove for such a weak signal. Since the width is significantly broader than the laser there is apparently an additional contribution, this term is not, as originally thought, a short lived coherent excitation (due for example to Rayleigh scattering) and can be excluded by using a polarisation experiment. This additional short time spike is at present not totally understood.

The temperature dependence of the exciton decay is illustrated in Fig 6.8. Again excitation resonant in both the free and bound excitons is shown. The sample is in this case a 100Å MQW centre-doped at the 10^{16} level with Be. At 5K the FE decay is dominated by capture at the bound site as shown in Fig. 6.6. As the temperature is increased the long time behaviour is dramatically altered. The FE population is sustained by the thermal release of bound excitons. The processes of capture and emission therefore begin to balance at higher temperatures and the populations of free and bound excitons are effectively coupled. The relation between capture and emission rates can be expressed using the principle of detailed balance. This is a statistical idea which states that for a system in equilibrium the rate of a process and its inverse are equal [6.39]. Assuming non-degenerate statistics we obtain the result [6.40] :

$$\frac{\eta_R}{\eta_C} = \left[\frac{4\pi m^* k_B T}{h^2}\right] \frac{g_{FE}}{g_{BE}} e^{-E_{BE}/k_B T} \qquad (6.7)$$

where η_R and η_C are the rates corresponding to the release and capture processes respectively, g_{FE} and g_{BE} are the degeneracy ratio of the free and bound exciton (g_{FE}=4, g_{BE}=2) and E_{BE} is the binding energy of the exciton to the acceptor. This result is used later to estimate the parameters required to model the exchange of excitons in a series of coupled differential equations (see section 6.4).

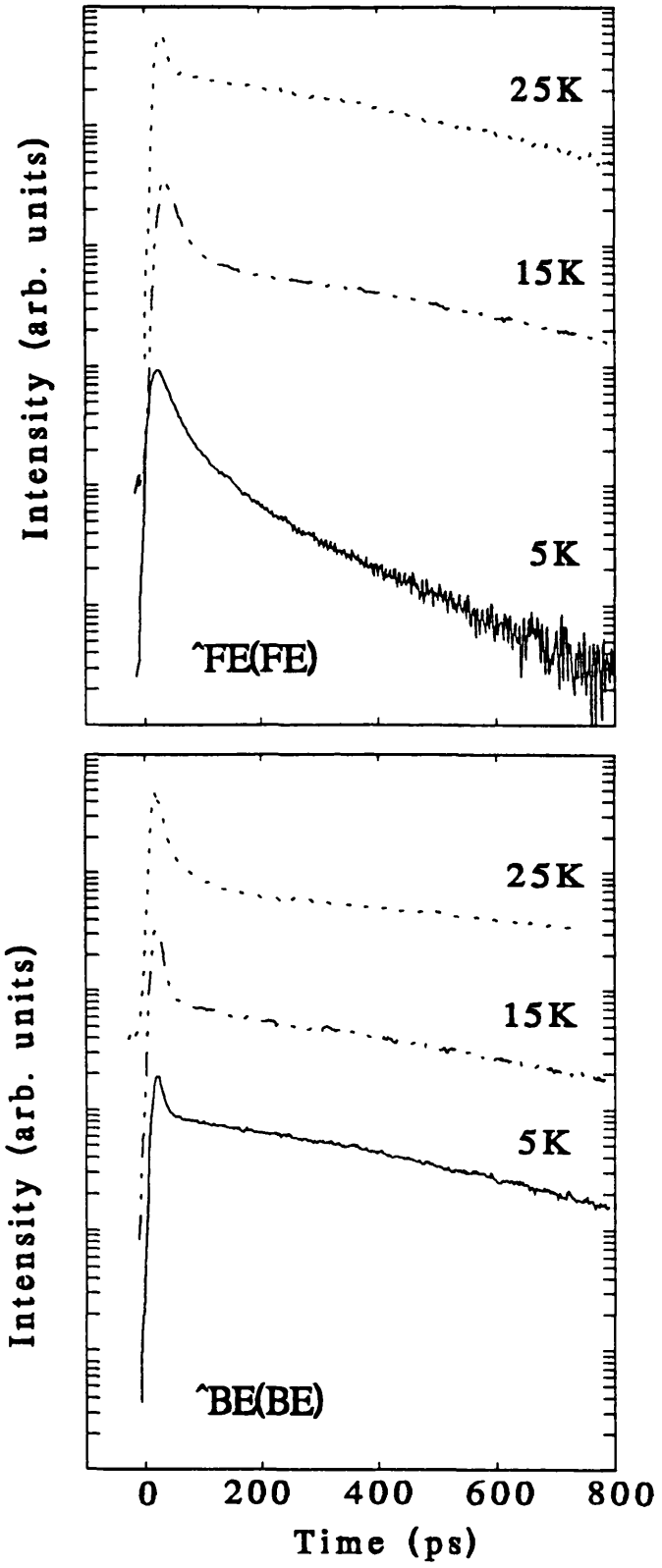

Fig 6.8 Temperature dependence of the radiative decay of FE and BE.

The observed lifetime at 15K and 25K is larger than that measured at 5K. This effect has been explained in terms of the increased scattering of excitons away from K=0 as previously discussed [6.38]. The BE result clearly follows the interpretation of that for the FE. At higher temperatures the lifetime couples with that of the FE and at 25K they have a common decay. The initial rapid decay of the BE is consistent with that observed for low doping in the previous figure (Fig 6.7), the rate in fact is apparently increased for increasing temperature. The short time scale of this mechanism is comparable to the scattering of the FE as it thermalises to the lattice temperature. Since the bound exciton is created cold i.e. in it's ground state it is possible that this population is subsequently distributed amongst excited states. Given that these excited states have a marginally longer recombination time then we can understand the initial rapid decay as simply a depopulation of the ground state. Note that for a bound state conservation of momentum in the radiative transition is achieved via interaction with the bound site i.e. excess momentum can be passed to the impurity, and hence is not a restriction to recombination. Such a model is consistent with the experimental results, however requires further work to be supported.

Fig 6.9 illustrates the dependence on well width of the FE recombination. It in many ways confirms the ideas presented so far upon the dependence of the thermalisation/ capture process upon the binding energy. The binding energy of the exciton to the acceptor is increased for decreasing well width. As a result we would expect the contribution of thermal release from the bound exciton to decrease with well width, exactly this behaviour is observed in Fig. 6.9. For the 150Å sample the coupling is quite strong and the long-time decay rate is correspondingly slow. For the 50Å sample the capture is very strong and the BE is by far the dominant recombination channel once this capture has occurred.

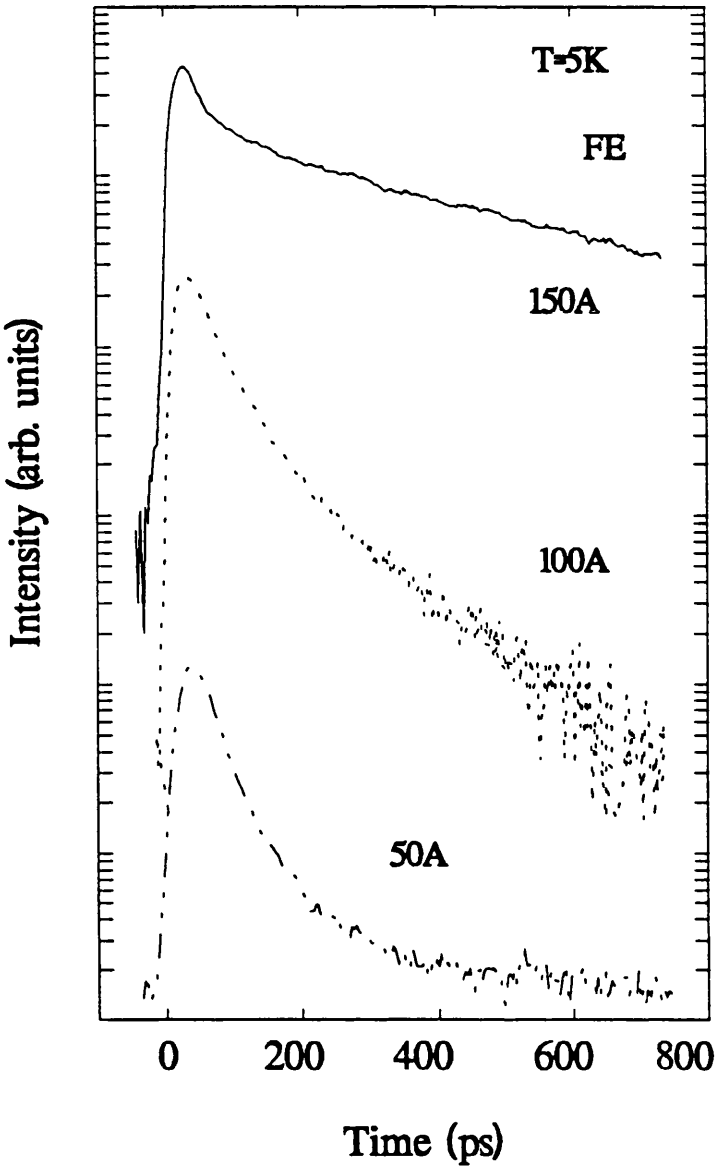

Fig 6.9 Dependence of FE recombination upon width of acceptor doped well

6.2.2 Comparison with donor doped samples

The binding energy of the donor bound exciton complex is significantly smaller than that of the acceptor, approximately 2.2meV for L_Z=100Å in comparison to 4.5meV for the acceptor. As a result the kinetics will be significantly different

for the donor interaction and the free and bound populations are strongly thermalised even at 5K. A direct comparison of the decay transients for 100Å QWs with acceptor or donor doping is shown in Fig. 6.10. Excitation is resonant with the free exciton for (a) and (b) and with the bound exciton in (c). In each case the differences observed are consistent with the difference in binding energy.

Fig 6.10 (a) illustrates the maintained population of the free exciton via thermal emission from the bound exciton. The acceptor doped sample in contrast shows a free exciton dominated by the capture process. The opposite picture is clear from 6.10 (c), where for resonant excitation in the bound exciton it is essentially uncoupled from the free and demonstrates an exponential decay at long times. On the other hand, the donor result illustrates the strong loss in population due to thermal release to the free exciton. The results for detection in the bound exciton while exciting in the free exciton (Fig 6.10 (b)) are perhaps less clear, since here we have the coupled effects of capture at and emission from the bound site. As expected the long time decay can be compared to case (a) for the donor and to case (c) for the acceptor.

Fig. 6.11 illustrates the temperature dependence of the BE decay for resonant excitation, again for the same 100Å donor doped sample as shown in Fig. 6.10. The results can be contrasted with Fig. 6.8 for an acceptor doped sample of the same well width. As expected, the thermalisation process is dramatically increased with temperature. The increase in lifetime of the FE with temperature as discussed earlier is reflected in the now strongly coupled BE. Despite the drop in capture rate with temperature the BE population is still dominated by the FE. This behaviour is a consequence of the fact that capture can result from all FE states while radiative recombination occurs only from only those states around K=0. The total exciton population reaches an effective three state equilibrium, that of bound - free - scattered free. With increasing temperature

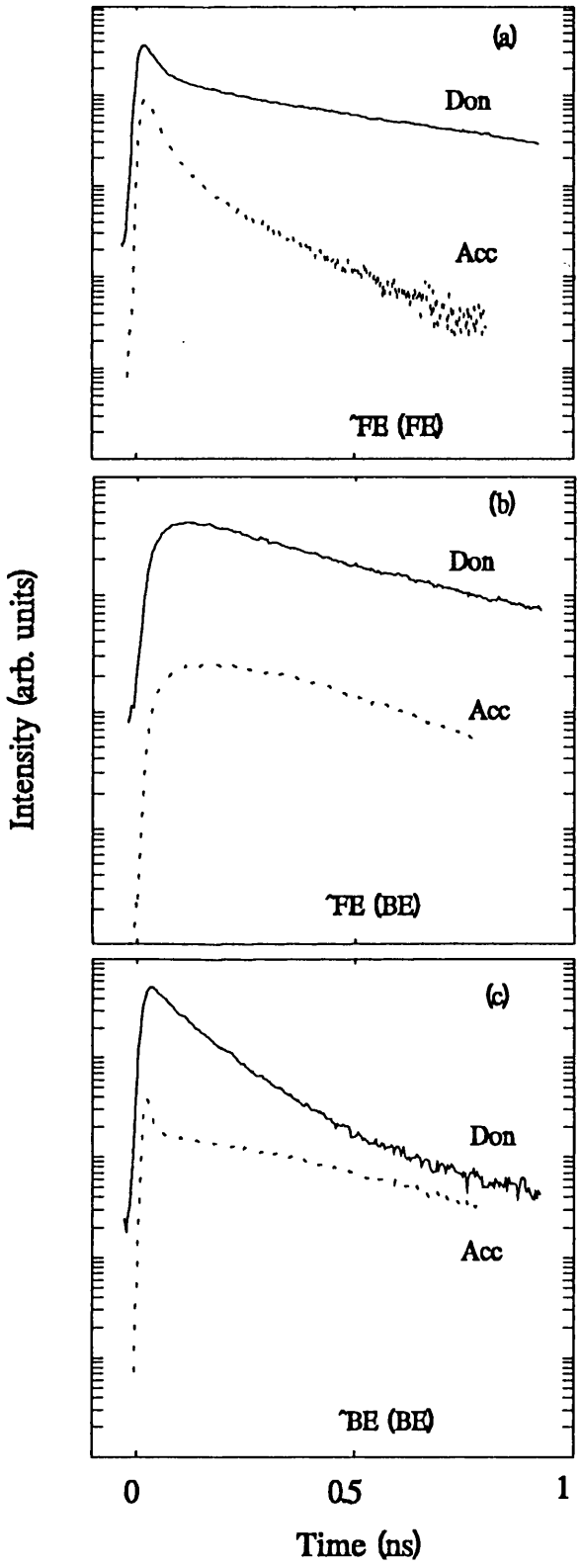

Fig 6.10 Comparison of transients for donor and acceptor bound excitons for samples with comparable well widths and doping concentrations.

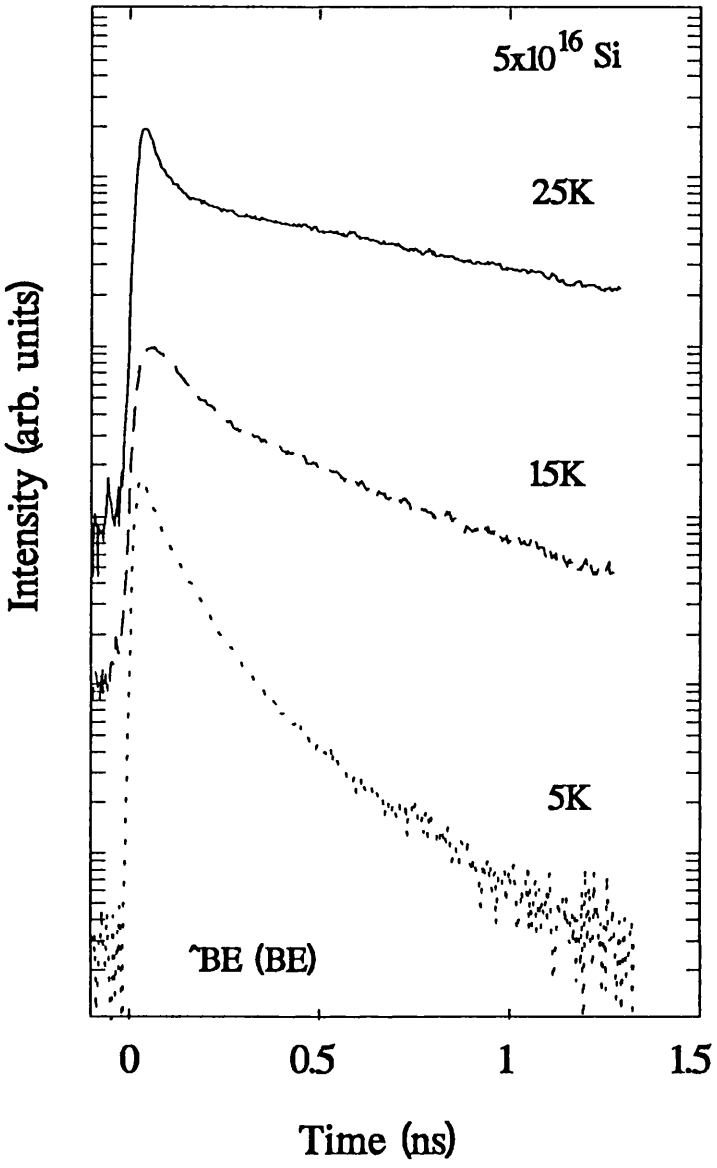

Fig 6.11 Temperature dependence of donor bound exciton recombination.

the equilibrium is pushed to the right towards the non recombining channel, which hence increases the effective lifetime. In the next section we discuss an additional mechanism which is again able to couple the three states described above and in turn determines the equilibrium set up between them at short times; this process is one of high density exciton-exciton scattering.

6.2.3 Exciton-exciton scattering in doped QWs.

Radiative decay of excitons in a direct-gap semiconductor can be classified into essentially three different regimes according to the excited exciton density: (i) radiative recombination of excitons in a weakly interacting dilute boson gas, the limit so far discussed, (ii) recombination in a dense interacting exciton gas which is dominated by scattering mechanisms, and (iii) an electron hole plasma where the density exceeds the screening limit for ionisation of the excitons. The majority of studies to date have considered either of the two limits, the dilute exciton gas or the degenerate electron-hole plasma as appropriate for the study of many-body interactions [6.41] [6.42]. In this work we have studied how the interaction between the bound and free exciton states is enhanced by increasing excitation density. By employing resonant excitation we restrict our discussion to predominantly scattering mechanisms between free and bound excitons, it is however clear that as a result of inelastic scattering we will inevitably produce a significant number of free electrons and holes. The scattering of excitons with free carriers, although a highly efficient mechanism is we believe of relatively secondary importance in the measurements discussed. Experiments have again been carried out for both donor and acceptor doped samples, the stronger effects are observed for the donor doped samples and hence we concentrate our discussion primarily on these results.

Fig 6.12 shows a series of radiative decays for both the free and bound excitons for excitation resonant with the free at various excitation densities. The FE decay 6.12 (a) shows relatively little change with increasing density even over the three orders of magnitude shown here. The clearest effects occur at short times where the initial decay appears to become shorter. In fact a very similar result was observed for increasing temperature, although in this case it is less dramatic. By analogy with the temperature effect it seems reasonable to

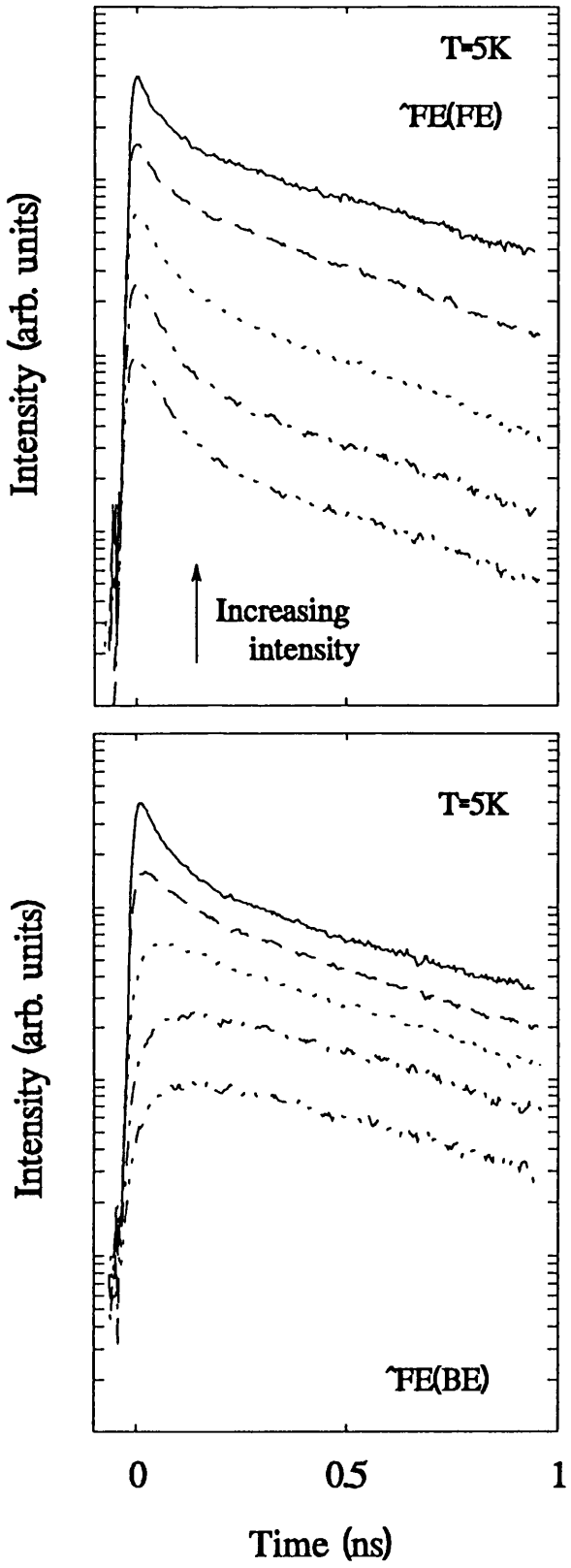

Fig 6.12 Series of radiative decays for free exciton (a) and bound exciton (b) illustrating dependence on excitation intensity.

suppose that we are observing a relaxation of excitons initially scattered away from K=0. It is clear however, that the long-time radiative decay shows a relatively minor change. Unlike the temperature mechanism, the scattering of excitons to higher K-values is a short lived effect in this case; we propose that this scattering occurs via the interaction of excitons at high densities producing inelastic exciton-exciton scattering. One immediate difficulty with this model is the simple requirement for conservation of energy, since we excite an exciton population essentially "cold" i.e. around K=0 and hence with essentially no kinetic energy. As we are looking at a relatively high purity direct gap material we can neglect direct Auger mechanisms which would allow for the transfer of kinetic energy to one free exciton via the recombination of a second. Strong localisation effects can also be excluded since we are using a relatively wide QW with low doping. Instead we propose that there exists a three body process which allows the scattering event between two free excitons to result in one free exciton being captured at a bound site while the energy gained is transferred as kinetic energy to the second (see Fig. 6.13). The scattered exciton therefore has an initial well defined energy and an associated k-vector which excludes direct recombination. As a consequence of this mechanism we have a direct population of the bound exciton on a time scale equivalent to the exciton-exciton scattering event. This extremely rapid transfer is dramatically illustrated in the results of Fig 6.12 (b). As the excitation density is increased so the effective capture rate contains an increasingly dominant component which is essentially coincident with the laser pulse. The effect of a capture mechanism dominated by the free exciton interaction is that as the density is increased so the bound exciton decay more closely follows that of the free. The development with intensity of the data illustrated in 6.12 gives convincing support for these arguments.

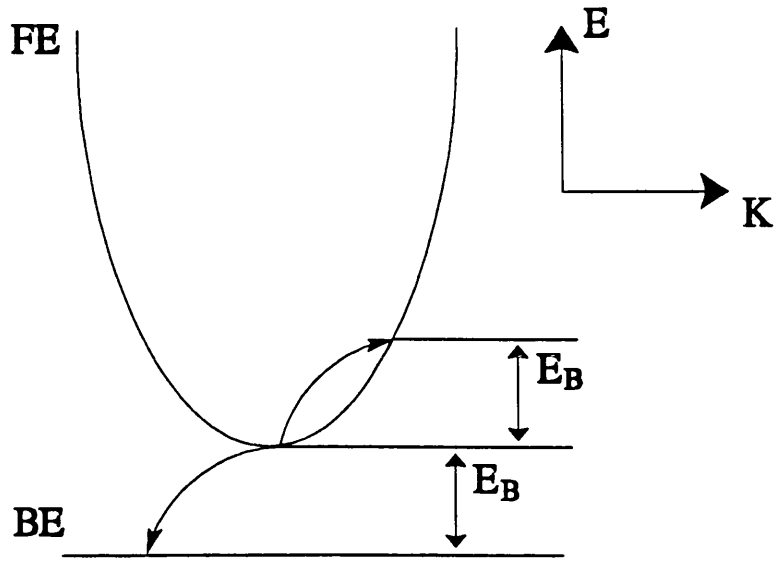

Fig. 6.13 Model for exciton-exciton scattering leading to an enhanced capture rate at the BE

So far we have discussed the short time dependence of the spectra on excitation density, the long time exponential like decay also shows a clear dependence on intensity. Fig 6.14 illustrates the development in the lifetime derived assuming an exponential fit to the radiative decay at long times. The fitted curves are 3rd order polynomials which are intended as a guide to the eye. Two points are immediately apparent (i) the lifetime is strongly dependent on intensity even at relatively low exciton densities where exciton-exciton interaction is assumed to be negligible, and (ii) the true radiative lifetime in a doped quantum well system is not obtainable from a simple exponential fit to the data despite a decay which in general is well described by such. In the next section we discuss how the exciton system can be accurately modelled using a series of coupled differential equations which include terms describing the interaction mechanisms considered above.

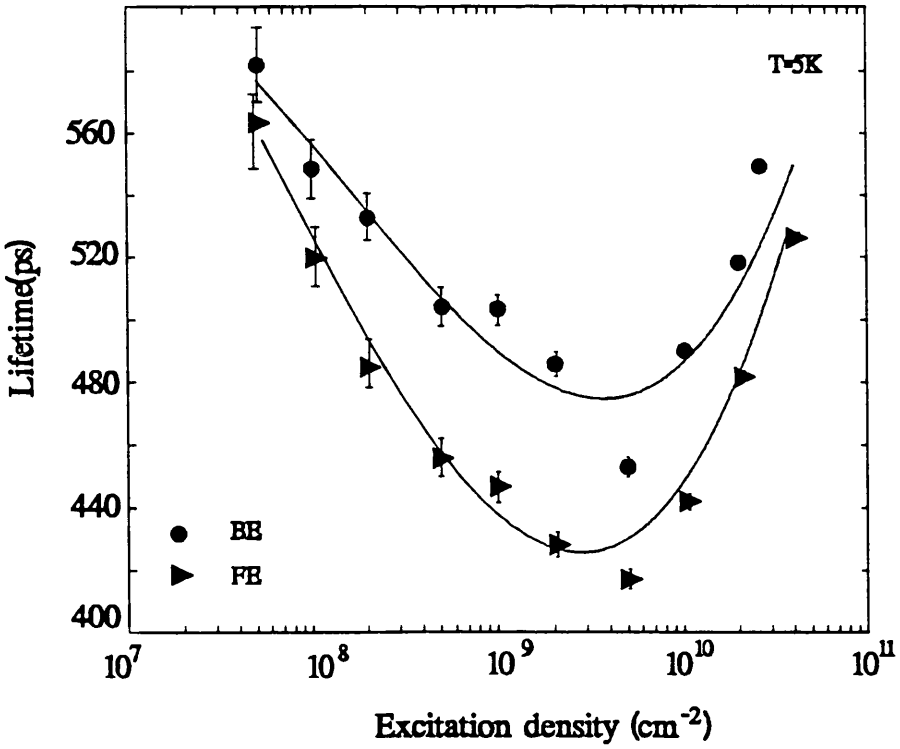

Fig 6.14 Dependence of lifetime on excitation density assuming exponential fit to long time decay rate.

6.2.4 Modelling of free-bound exciton exchange

The discussion of the proceeding sections has highlighted the complexity of the interaction between free and bound excitons and the difficulty in deriving even the simplest lifetime parameters. In this section we consider how the kinetics can be modelled using a series of coupled rate equations, and from a simple fitting procedure the component parameters can be found. The numerical solution to these equations has been carried out using a computer and allows fairly complex expressions to be analysed with a high degree of accuracy. In order to have a manageable number of terms we make a number of basic assumptions regarding the interaction mechanisms, in particular for the low intensity data we restrict the terms to those describing simple capture and

emission and the effective lifetime for each channel. This gives for the case of free exciton resonant excitation:

$$\frac{dN_{FE}}{dt} = G(t) - \frac{N_{FE}}{\tau_{FE}} - \eta_C N_{FE} (N_i^0 - N_{BE}) + \eta_R N_{BE} \qquad (6.8)$$

$$\frac{dN_{BE}}{dt} = -\frac{N_{BE}}{\tau_{BE}} + \eta_C N_{FE} (N_i^0 - N_{BE}) - \eta_R N_{BE} \qquad (6.9)$$

where G(t) is the generation rate of free excitons during the short laser pulse. N_{FE}, N_{BE} are the number of free and bound excitons respectively and τ_{FE}, τ_{BE} are the associated lifetimes. η_C is the capture rate for a free exciton to a bound site, η_R is the reverse process of release from the bound site to become a free exciton. As discussed earlier the capture and release terms can be related when in thermal equilibrium through the principle of detailed balance (eq 6.7), this places some restriction on our choice of parameters, in particular at low temperatures the exciton system is clearly not in thermal equilibrium and the emission rate will be relatively low in comparison to a value calculated from detailed balance. As an initial estimate of the lifetimes for free and bound excitons a value taken from the long time slope of the decay is used. Given these starting conditions the fitting procedure is a simple iterative process of trial and error. For the simplest model this is simply the four parameters (τ_{FE}, τ_{BE}, η_R, η_C) are to be determined. Note that since we take no account of phonon interaction the lifetimes derived are those thermalised to the lattice temperature i.e. >5K). Fig 6.15 illustrates the near to perfect fit achieved for the lowest intensity data for the donor doped sample described above, the parameters derived are summarised in Table 6.1.

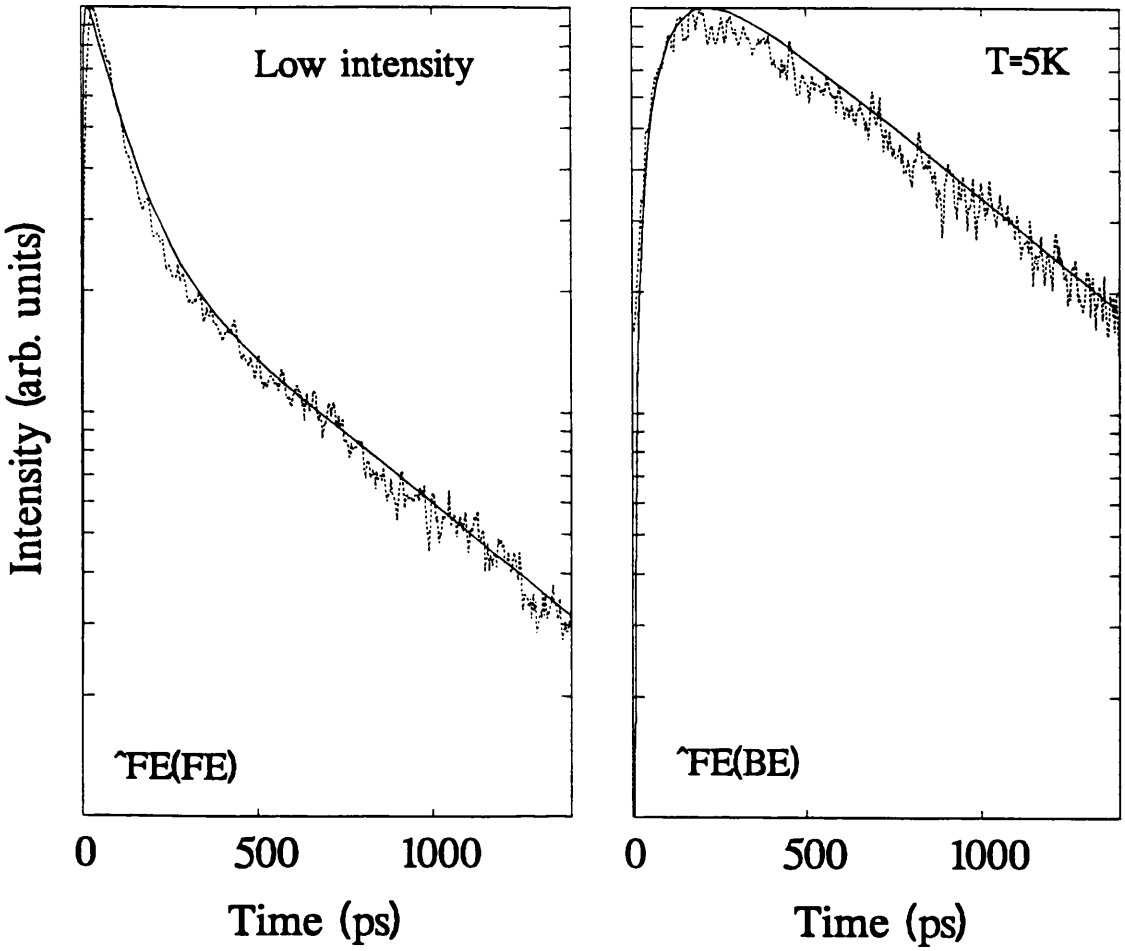

Fig 6.15 Fit to low intensity data using simulation of decay based on series of coupled diffferential equations.

	τ_{BE}	τ_{FE}	η_R	η_C
Value	620ps	650ps	2.5×10^9	0.35

Table 6.1 Parameters for simple fit to low intensity data.

As the intensity is increased the simple model is no longer adequate to describe the determining physical processes. The possible mechanisms which come into play in addition to capture and release are potentially extremely diverse. It is clear that no realistic model can hope to include all possible terms and maintain

any value in the parameters derived. Instead we make a qualitative discussion here of a model including a subset of terms we believe to be important in the analysis so far carried out.

As discussed in the previous section 6.2.3, there is strong evidence to suggest the importance of exciton-exciton scattering. For both donors and acceptors the effective rate of capture is enhanced with increasing excitation density, so that at high densities, the initial population of the BE is essentially coincident with that of the FE. This constraint determines the strength of the scattering parameter. The second observation is that, again at high densities, the BE decay appears thermalised with that of the FE i.e. the two decays follow each other during the initial stage of the decay. This would indicate a greater effective carrier temperature than that of the lattice or in other terms a higher local phonon density. In fact this is an attractive interpretation since a clear consequence of the exciton scattering and the strong capture process is a large phonon emission. The excess phonons generated couple to both free and bound excitons. In general the phonon energies available are not large enough to release a bound exciton from the ground state, the dominant effect is instead a strong reduction in the capture rate. The total sticking probability becomes smaller as the probability for re-emission from higher excited states is increased.

From the point of modelling this interaction using our coupled rate equations we require a number of substantial approximations to be made. Unlike the exciton population which we have treated as two discrete sets of equivalent particles the total number of phonons is described by a continuous distribution. Such a distribution which is at all times dynamic, is extremely difficult to couple to a system of rate equations. Instead we assign an additional rate equation which describes the change in absolute population of phonons. The coupling terms to this phonon population then contain a factor which accounts

for the fraction of the population which are able to take part in the interaction. For example for the bound exciton we derive the terms:

$$\frac{dN_{BE}}{dt} = -\gamma_{BE}(N_{BE} \cdot N_p) \qquad (6.10)$$

$$\frac{dN_p}{dt} = -\gamma_{BE}(N_{BE} \cdot N_p) \qquad (6.11)$$

For the free exciton a similar coupling will occur such that excitons are scatttered away from K=0 and are no longer radiative. Finally we require a fourth channel which totals the scattered excitons in the system which are in excess to those thermalised by the lattice.

In total the additional parameters required for a system of equations which take into account the phonon assisted interaction can be listed:

(i) γ_{FE}, γ_{BE}, phonon coupling to free and bound exciton (equivalent dimensions to capture rate: $[\text{density}]^{-1} \cdot [s]^{-1}$).

(ii) τ_R relaxation rate for scattered exciton back to K=0, this term can be intensity dependent due a bottle-neck effect as a high density of excitons attempt to relax simultaneously [6.43].

(iii) A Phonon cooling term τ_C, which describes the contribution of two physical mechanisms which occur; the phonon distribution relaxes with time such that there are a progressively larger number of phonons at lower energy, below a certain threshold energy these no longer contribute to the mechanisms described above. Secondly this phonon cooling can be impurity assisted via absorption and re-emission, and as a result can be a relatively fast process.

Fig. 6.16 illustrates a series of transients for a given set of parameters (see Table 6.2) for different excitation densities. The trend for the BE decay demonstrated in Fig. 6.12 is relatively well reproduced. Given the simplicity of

the model this is a good indication that a phonon mechanism might well produce the observed behaviour.

	γ_{BE}	γ_{FE}	τ_R	τ_C
Value	0.28	0.28	50ps	150ps

Table 6.2 Additional parameters for fit to high intensity data (terms are defined in the text).

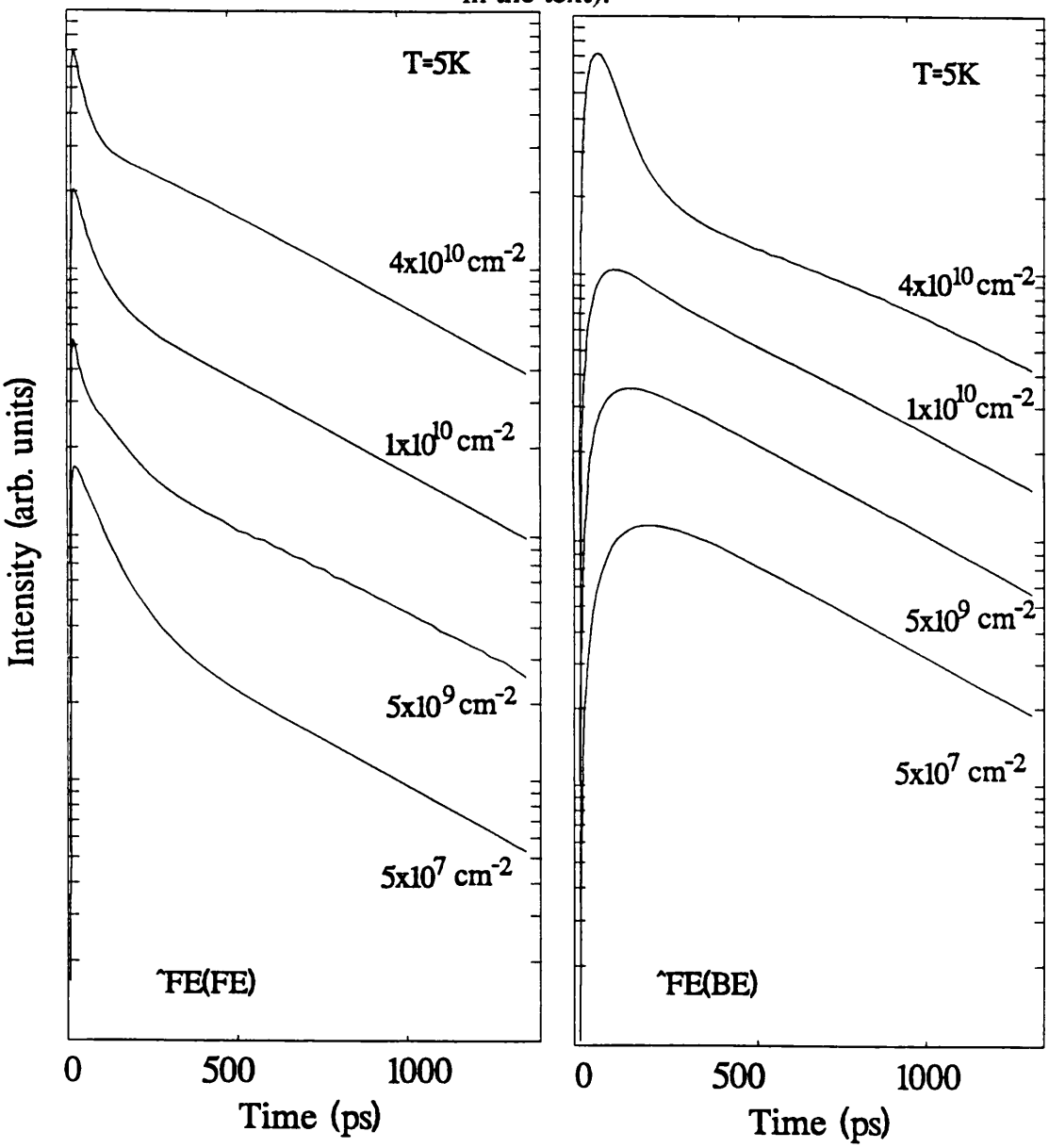

Fig 6.16 Series of transients calculated using different assumed excitation densities within differential equation model.

Fig. 6.17 however, puts the model more into perspective and compares the results with actual data. The BE transient is reproduced in general trend, however the quality of the fit is poor in comparison to the low intensity data. Although the parameters can undoubtedly be further optimised to slightly improve this fit we have perhaps already obtained as much information as is reasonable to deduce from such a treatment. There are certainly alternative mechanisms which may play an additional role, even a dominant one, in the observed decay but are not included in this example. This particular piece of work is on-going, here we have discussed a single system to illustrate the complexity of the interactions occurring and their analysis using a modeling technique.

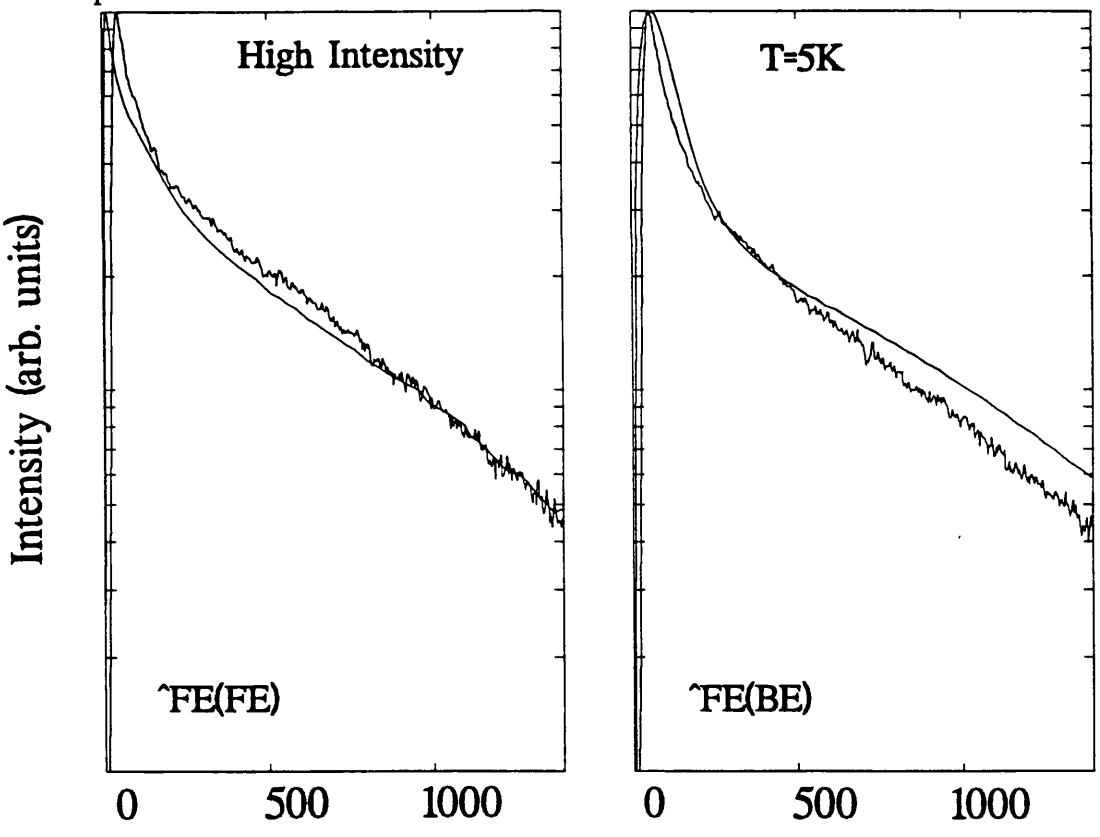

Fig 6.17 Fit to high intensity data, although the general trend is reproduced the fit is poor in comparison to Fig 6.15.

6.3 Exciton localisation in narrow doped QWs

The effect of localisation of excitons on the optical spectra of high quality QWs has received considerable interest and is frequently discussed in terms of the exciton linewidth and the observed Stoke's shift between emission and absorption spectra [6.44] [6.45]. In general this localisation has been associated with fluctuations in the interface between GaAs and the AlGaAs barrier. The extent of this interface roughness is found to be strongly dependent on the growth conditions used, in particular the use of interrupted growth at the interface has been shown to produce extended islands (typically 1μm diameter) which differ in thickness by a single monolayer (see Fig. 6.2 and earlier discussion). Relatively little work has been carried out on the interaction between the interface localisation and the impurity related potentials. In this section we consider such an interaction for a narrow 50Å QW acceptor doped in the centre to a level of $3x10^{10}$ cm^{-2}. The narrow QW implies that the interfaces interact strongly with the exciton and the optical spectra as a result demonstrate an extremely large linewidth. This linewidth can in fact be considered as an envelope over a large number of transitions corresponding to localisation of the exciton in different depth potentials. We show here that it is in fact possible to resonantly excite excitons within these local potentials. In this way we create a well defined exciton population and are able to study the subsequent capture at a correlated impurity potential. In addition this leads to an effective spatial correlation between the resonantly excited localised exciton and those impurities which are then able to capture the exciton. Using a selective excitation technique we are thus able to make an extremely accurate measurement of the acceptor bound exciton binding energy. Furthermore as a consequence of the localisation of the bound exciton this sample is also particularly suitable for the study of the shakeup processes discussed earlier,

namely the two hole transition (THT). Two different experiments are presented which have allowed us to study the phenomena discussed above. Time integrated PL spectra have been measured at 2K using a tunable Ti-sapphire laser for excitation and a photon counting detection technique. Time-resolved data were again obtained using a streak camera, with tunable excitation form a synchronously pumped Dye laser giving pulses of approximately 5ps duration. The latter technique illustrates the transfer from localised to bound excitons and the subsequent relaxation to lower energies.

6.3.1 Experimental Results

A series of spectra illustrating the development in PL spectra as the excitation energy is tuned through the exciton envelope is shown in Fig. 6.18. The top curve shows the broad exciton transition typically seen for non- resonant excitation. For excitation resonant with the high energy tail of the emission there is relatively little change in the observed spectra. Since this energy corresponds to only weakly localised or even mobile excitons it is clear that inter-diffusion will result in population of all states at lower energy and hence not alter the observed lineshape. Excitons are able to migrate between localised islands towards the lower energy sites by emitting acoustic phonons. In fact the results as a whole illustrate the relative mobility of the localised excitons. Although not well defined one might distinguish the so-called mobility edge as existing within the high energy tail at around 1.6158eV i.e. the point at which a BE peak becomes resolved. As the excitation energy is decreased a sharp BE peak appears, this BE population corresponds to those directly correlated with the localised exciton excited i.e. the exciton is trapped at an acceptor within the same localisation volume. We can distinguish the signal as PL and not a resonant scattering process due to the rather slow rise time observed in a time

resolved measurement (around 100ps). In addition to the sharp peak there is an associated low energy tail, from those BEs populated via inter-diffusion between different localised islands.

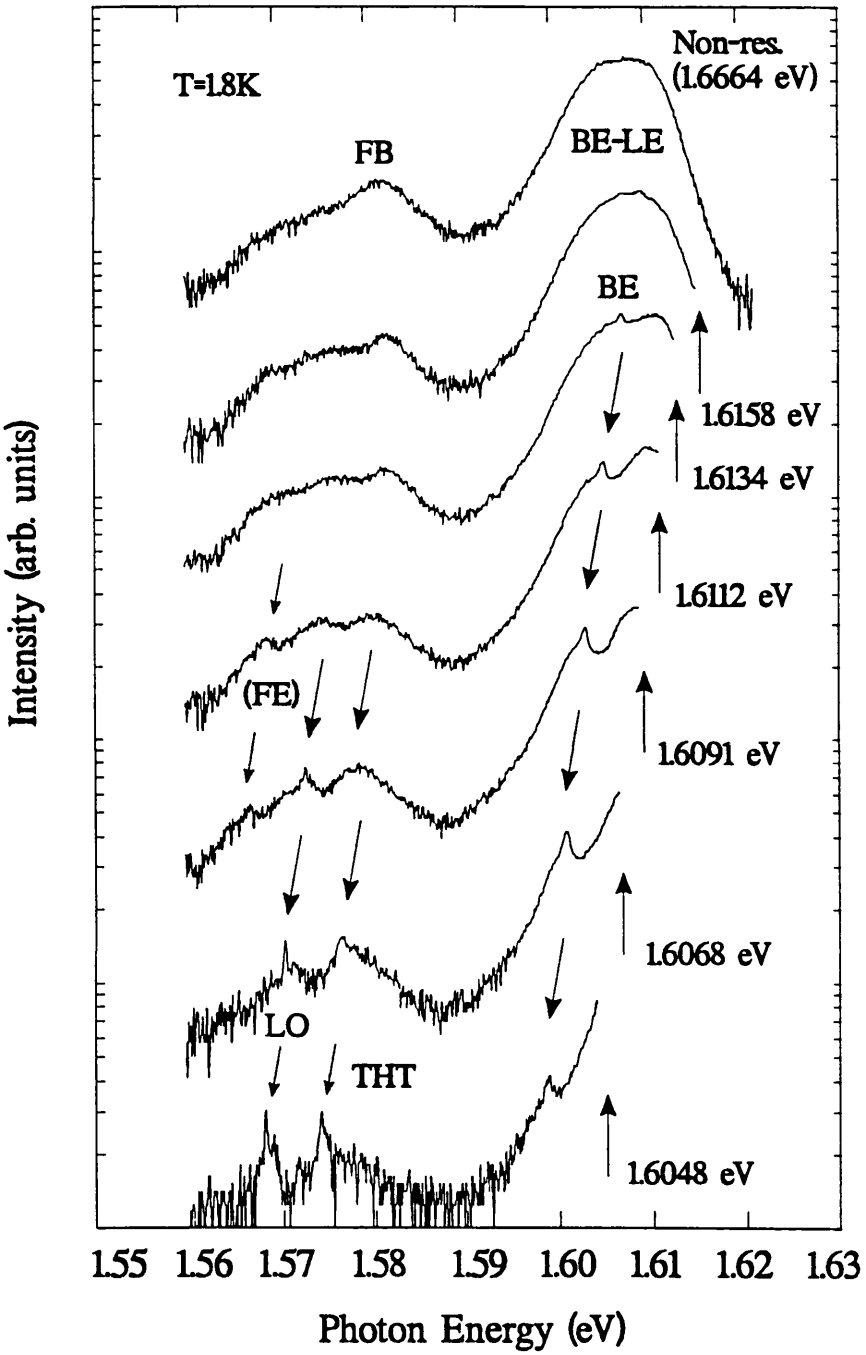

Fig 6.18 Summary of spectra obtained for excitation resonant at different energies within the broad exciton envelope of a 50Å quantum well.

As the localisation energy is increased i.e. excitation at lower energies, the sharp BE peak increasingly dominates over this low energy tail. This is again as expected assuming that the transfer between localised regions follows a thermally activated hopping mechanism. Indeed at higher temperatures the excitation energy at which a BE peak can be resolved is correspondingly decreased. In addition to the spatially correlated BE further satellite transitions at lower energy are also observed. For excitation in the high energy tail the free to bound transition (FB) corresponding to the recombination of a free electron with an acceptor bound hole is resolved. Excitation resonant with the exciton has been shown to enhance the FB transition [6.46], although associated with free carrier and not exciton recombination. An Auger type mechanism has been proposed to account for this behaviour. As the excitation energy is decreased, further structure is resolved in the PL spectra.

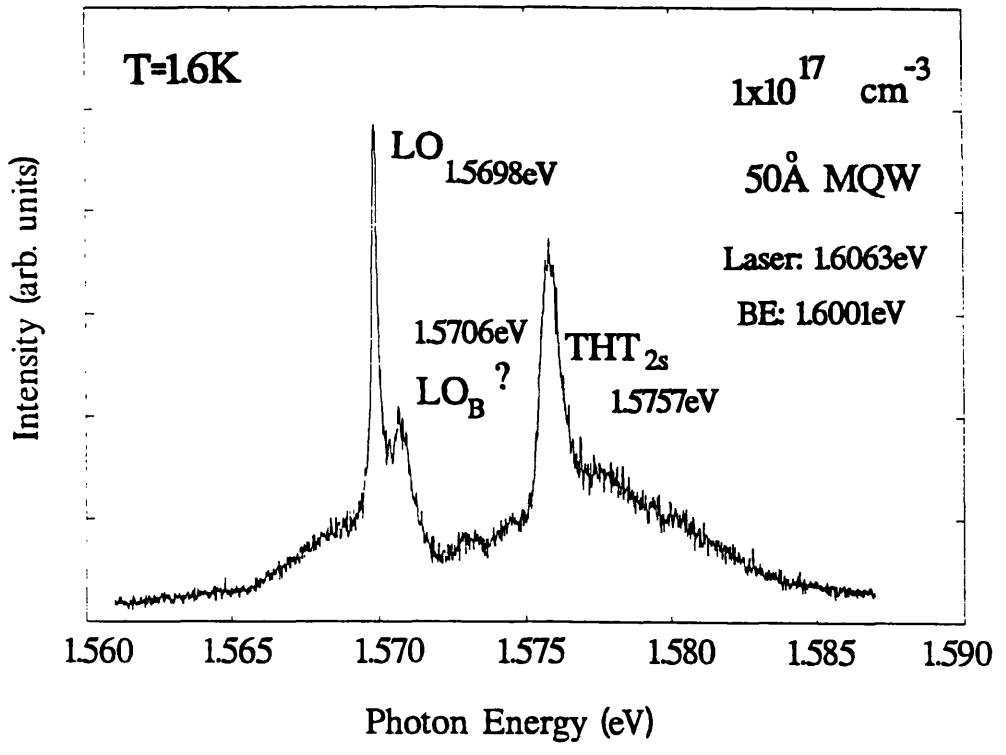

Fig 6.19 High resolution section of spectra showing region around THT.

Fig 6.19 shows a high resolution section covering these low energy transitions. A sharp peak at around 30.5meV from the laser line corresponds to the THT associated with the resonantly excited bound exciton recombination, leaving the neutral acceptor in a 2s excited state. Neighbouring transitions at lower energy but in this figure only weakly observed are possibly due to further excited states. The sharp replica observed at 36.6 meV below the laser line is the LO-phonon Raman scattering process. A neighbouring peak at slightly higher energy (approximately 0.8meV) is possibly due to an impurity bound LO phonon replica [6.47], such transitions have been observed in bulk material [6.48], [6.49], however it is clear that no definitive assignment can be made and other mechanisms such as shake up processes involving excited FE states cannot be excluded. One final peak which is seen at slightly higher photon energy excitation (curves in middle of Fig. 6.18.) but at even deeper energy shift from the laser line, about 42meV, is interpreted as a shake up process related to the localised FE. As discussed earlier a localised exciton can interact with, in this case, a localised hole such that when the exciton recombines the hole is excited into a higher subband (n=2).

The transfer from localised free exciton to bound exciton is also well illustrated by ps transient measurements using the streak camera. Fig 6.20 illustrates the development of the PL spectra in the near bandgap exciton region. The streak camera is unfortunately not sensitive enough to allow measurements in the low energy satellite region. The figure illustrates excitation in the upper tail of the LE band, the spectrum demonstrates a considerable down shift in energy as the free excitons are increasingly strongly localised and at the same time trapping to bound impurity sites occurs. At long times ($\approx$ 1ns) only the bound exciton channel is observed, which continues to slowly shift to lower energies. For excitation at a lower energy within the localised exciton band the emission does not shift appreciably with time and the bound exciton is only weakly populated,

in contrast to the results shown. Capture to the bound exciton is apparently significant only within the first 100ps and does not dominate the long time recombination as was the case for high energy excitation. The spectral diffusion illustrated in Fig. 6.20 strongly supports the model of hopping of weakly localised excitons as a means of relaxation and capture of excitons at impurity sites spatially correlated with the localisation.

In summary selective excitation can provide detailed information regarding the electronic states of the exciton-acceptor complex. The observation of a spatially correlated BE transition allows the accurate determination of the bound exciton binding energy in a system where the overlap of the bound and localised exciton transitions would normally prevent the determination of this value. The rich spectra of satellite peaks at low energy offer further detailed information as to the excited states of the acceptor. Overall the system provides a clear illustration of the possible interaction between weakly localised islands and the Coulombic potential of an impurity.

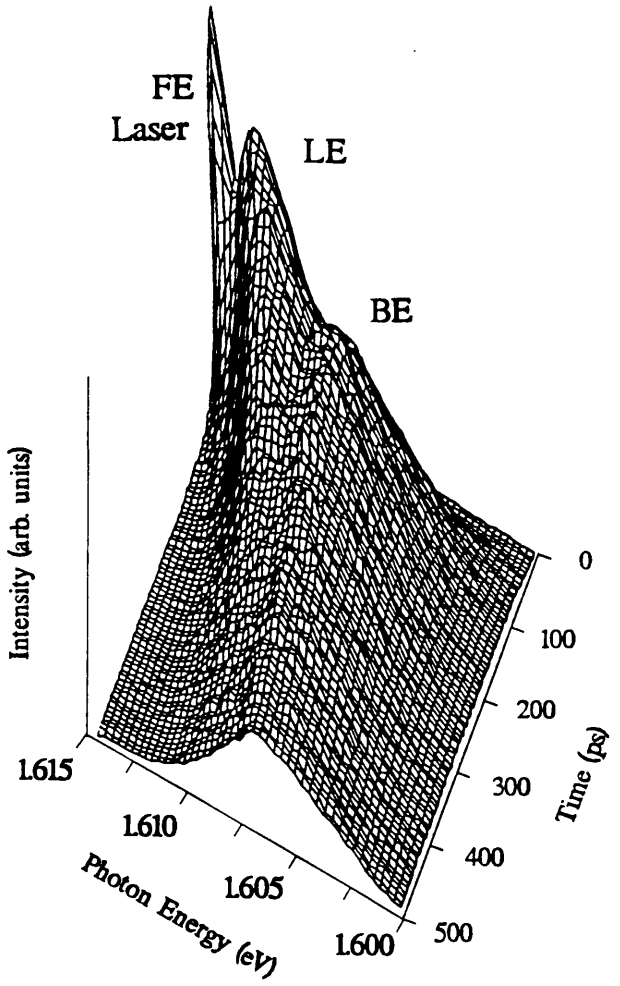

Fig 6.20 Picosecond time resolved spectra for excitation at the high energy side of the localised exciton.

Chapter 7

Correlation Effects in Degenerately Centre-Doped Quantum Wells.

7.1 Introduction

The importance of exciton recombination in the observed luminescence of quantum wells has been emphasised in the preceeding chapters of this thesis. In this chapter we consider how the presence of free carriers in the well affects the Coulomb interaction of the electron-hole pair in forming the exciton. This problem has received considerable attention in the case where an equilibrium population of free carriers is introduced by modulation doping [7.1]. The present work looks at a single quantum well doped n type to a concentration above the degenerate limit so that the system contains a large population of free carriers. As a result of the large electron population there is a large degree of interaction between the carriers, the properties of the system therefore reflect the total collective interaction of the charge. A clear understanding of the observed behaviour is only possible if one takes this into account, the system therefore requires an analysis within a many-body framework [7.2]. The convenient structure of modulation doped systems for the study of many body related effects has lead to a wealth of both experimental and theoretical work in this area. A lengthy review of this material is not attempted here, a number of detailed accounts however exist in the literature (see for example [7.3]) and only that material which is directly relevant to the work presented is discussed in any detail. As a starting point we consider the screening of the electron-hole Coulomb interaction which leads to an reduction in the binding energy of the hydrogen-like exciton state.

The single particle correlation between electron and hole (the conventional exciton) which exists at low densities is found to have a many-body counterpart at high densities. Although the single particle binding energy is lost (see chapter 5), the hole is still able to form a correlated state via it's

Coulomb interaction with the total Fermi-electron sea. Such a state is then considered bound with respect to the Fermi level. Because the bound state is so close to the Fermi energy, scattering effects reduce the lifetime and lead to broadening of the observed transition. As a result this "exciton" state gradually disappears in the extreme high density limit. This correlated exciton-like state is the so called "Mahan" exciton or "Fermi-Edge Singularity" (FES) [7.4].

7.2 The Fermi Edge Singularity

The possibility of enhanced oscillator strength for transitions in the vicinity of the Fermi-level was first realised for a degenerately doped semiconductor in the early work of Mahan (hence "Mahan" exciton) [7.5]. This initial work followed on from what is an analogous effect observed in the X-ray spectra of metals, and referred to as the "X-ray edge singularity" [7.6]. Here an X-ray excites a core electron from its inner shell leaving behind a tightly bound "core" hole. This strongly localised hole acts as a strong scattering site for electrons. The low energy threshold for electron scattering is dictated by the exclusion principle, since electrons can only scatter into empty states (Fig. 7.1). The Fermi-level E_F hence provides an abrupt limit above which multiple electron scattering can occur, resulting in an enhancement in the recombination between the electrons and the strongly localised hole. The enhancement is then specifically associated with transitions at the Fermi-edge energy, hence its common reference as the "Fermi-Edge" Singularity.

The first calculations of Mahan were concerned with degenerately doped direct band-gap material. The development of this work towards the 2D case has been considered by a number of groups, in particular for modulation doped systems by Ruckenstein *et al* [7.7]. and by Rorison [7.8], and for the

undoped case under high intensity excitation (e-h plasma) by Schmitt-Rink *et al* [7.4]. At present the agreement between the theoretical and experimental values of the relative enhancement factors is fairly poor, but recent work which takes account of the non-ideal geometry of the quantum well giving only a quasi 2D system, has made some improvement in this direction [7.9]. The remaining discrepancy might be associated with the neglect of homogeneous broadening terms in the calculations [7.10].

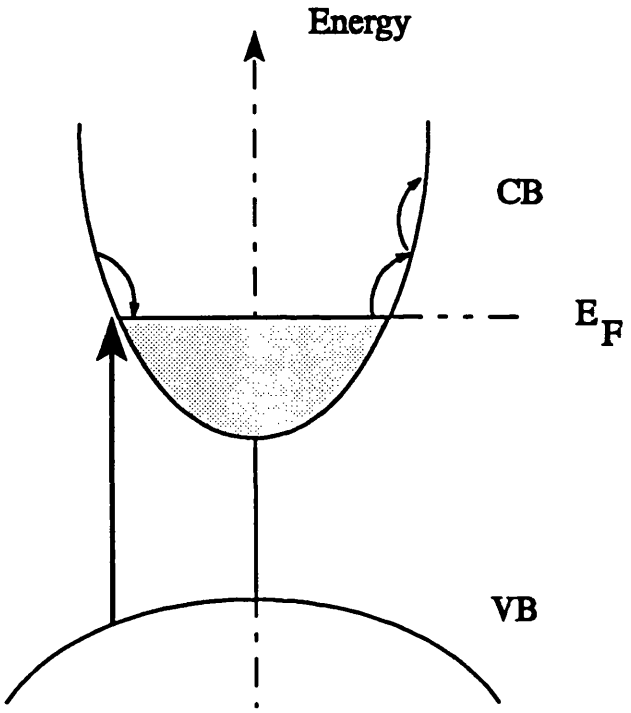

Fig 7.1 Illustration of scattering of electrons occurring only at and above the Fermi-level

7.3 The FES in Modulation Doped Structures

The FES was first observed for a low dimensional semiconductor in the work of Skolnick et al. for the InGaAs/InP system [7.11]. Using an n-type modulation doped structure they were able to demonstrate, at low temperatures and relatively low excitation conditions, an enhanced

recombination for transitions in the vicinity of the electron Fermi-level. For recombination to be observed at the Fermi-level a significant number of holes with wave vector k corresponding to that of the Fermi-level are required. This restriction is fulfilled in the above system due to localisation of the holes, providing a sufficient spread of values in k-space (from the uncertainty principle) for the transition to occur. The enhancement observed results from a correlation between the hole and electron populations as they rearrange according to the Coulombic interaction between them i.e. the electrons adopt an equilibrium arrangement around the hole dictated by their mutual interaction. The correlation mechanism proceeds via multiple scattering of electrons at the Fermi-level allowing the hole to be accommodated at a minimum screening site from which it recombines. As pointed out above this is observed only when the hole has an appropriate wavevector. The situation for which the hole is localised can then be seen to be directly analogous to the effect in metals described above.

Momentum conservation is guaranteed in an absorption process, as a result it was possible to observe the Fermi-Edge enhancement for systems in which no significant hole localisation occurs, for example in the GaAs/AlGaAs system, using either a direct absorption measurement [7.3, 7.12] or by photoluminescence excitation spectroscopy [7.10]. These techniques are equivalent only in the case when the relaxation from excited to detection energies is independent of the excitation process itself (see Chapter 3 and later discussion).

The experimental observations are now briefly discussed for the modulation doped structure, to provide a basis for comparison with the results of the current work. The figures shown are taken from Ref. [7.10] which shows results obtained with the same experimental system as has been used in the new work to be presented here, allowing a direct comparison. Fig 7.2

illustrates the temperature dependence of photoluminescence excitation spectra for a GaAs/AlGaAs modulation doped structure. At low temperatures we observe a large increase in the recombination intensity for excitation at the low energy absorption edge. This enhancement is gradually quenched as the temperature is increased.

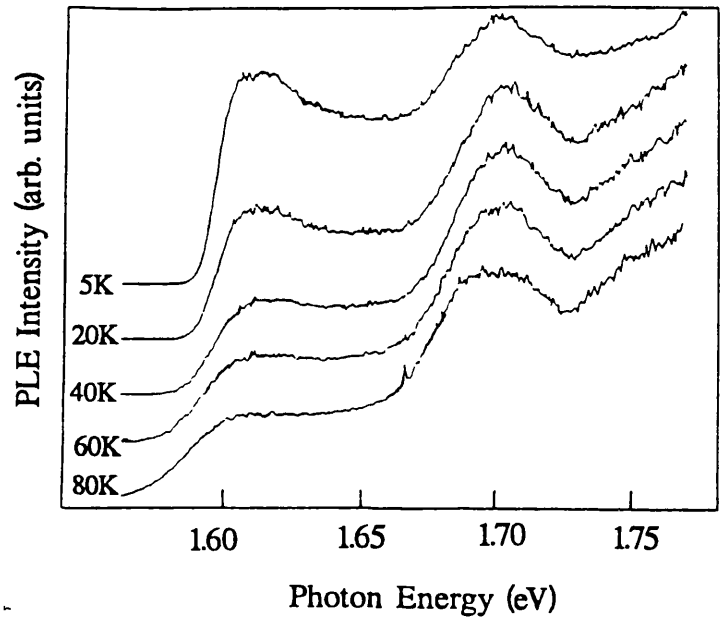

Fig 7.2 Dependence of enhanced absorption on temperature for Modulation doped structure

Fig. 7.3 shows the sample under increasing excitation intensity, again a consistent quenching of the enhancement effect is observed as the intensity is increased. It is interesting to note that the observed enhancement at the n=2 subband edge (approx. 1.72eV) shows an entirely different character to the low energy edge and is not reduced by the above change in external conditions. This behaviour of the n=2 peak is typical for the normal band-edge exciton resonance. The dependence on temperature shown in Fig. 7.2 is in qualitative agreement with that theoretically predicted. The density dependence illustrated in Fig 7.2. is however not predicted by current theoretical treatments.

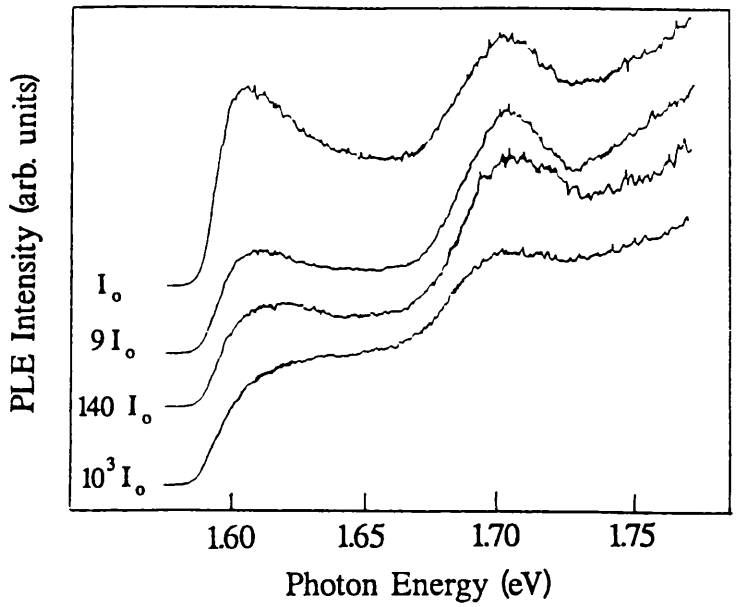

Fig 7.3 Quenching of Fermi edge enhancement with increasing excitation

A decrease in the Fermi-exciton resonance is predicted at large electron densities [7.7], however the overall increase in density following excitation is, in the case of these measurements, a small fraction of the total electron population and should have no effect on the enhancement. Instead it is believed that the density dependence is indicative of the influence of the increasing hole population which in contrast represents an order of magnitude change [7.10].

7.4 Correlation in Anti-Modulation Doped Structures.

The picture of the FES so far discussed gives us a suitable background from which to now argue the similarities observed in the degenerately centre doped structure. Correlation effects in such structures leading to enhanced recombination have not been extensively discussed in the literature to date [7.13]. The free carrier many body system is additionally complicated in the case of centre doped structures by the presence of a fixed array of charged

sites due to the ionised impurities. In considering the observed behaviour one needs to take account of three distinct charged species; the free electron, whether intrinsic or photo-excited, the photo-excited hole and the fixed positive centre due to the ionised donor. The dynamic interaction between all three is found to be a determining parameter in the correlation process.
The following discussion of the current work starts with a brief discussion of the experimental setup and then presents results which allow a direct comparison to be made with the modulation doped case described above.

7.4.1 Experimental Details

The sample studied is again part of the series A described in the earlier chapters of this work. The doping concentration is degenerate so that at low temperatures there is an equilibrium population of free carriers in the well. As discussed in the earlier chapters of this thesis the exact structure has important consequences for the internal band structure of the system. The close proximity of the well to the surface implies that in the absence of a heavily doped compensating capping layer, a depletion region associated with the high density of surface traps extends through the quantum well [7.14], [7.15]. The implication in this case is that the degenerate population of electrons is significantly reduced, leaving an excess of fixed positive charge in the well. Re-balancing the charge distribution is possible by making use of the band bending in the structure. Free electrons photo-excited in the AlGaAs barrier using above bandgap excitation, are swept into the well giving us a direct control of the electron population in proportion to the above bandgap excitation intensity. This effect is made use of in examining the influence of the electron density on the observed enhancement.
Measurements have been carried out using the time resolved equipment

previously described. The use of a pulsed laser system allows us to use higher excitation densities than are otherwise achievable with cw. The spectra are however detected using a standard photon counting technique, time integrated to give quasi-stationary conditions. Photoluminescence excitation spectra have been measured in the range 720 to 805nm at temperatures from 5K up to room temperature.

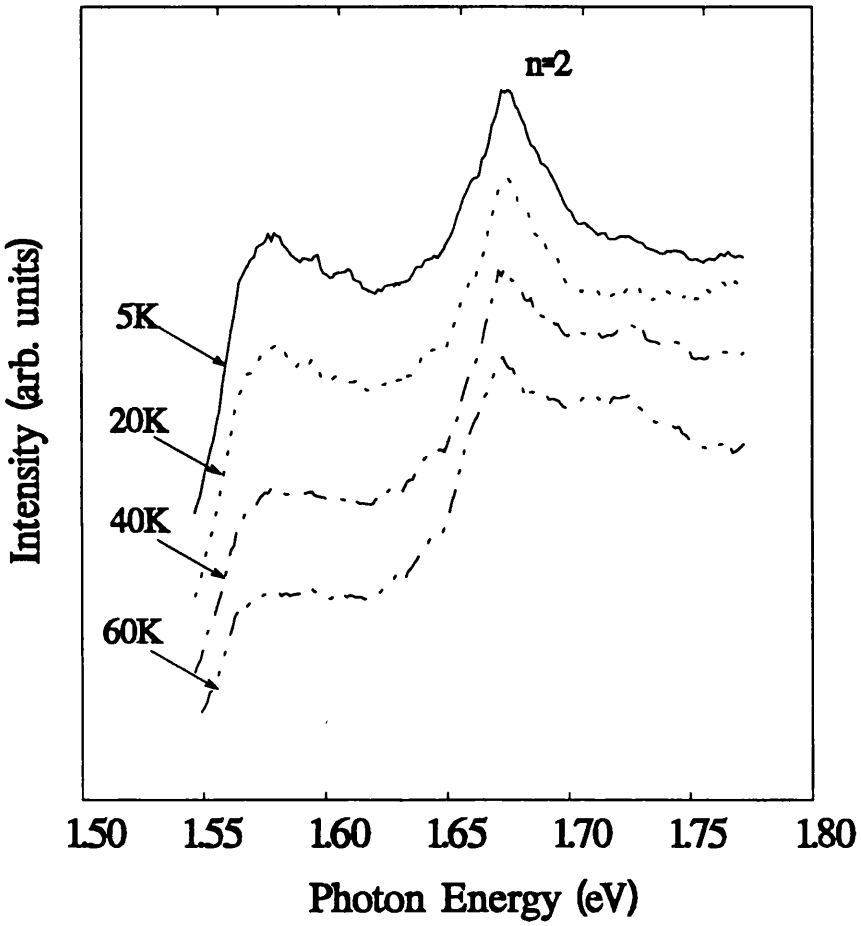

Fig 7.4 Dependence of PLE on temperature for centre doped structure

7.4.2 Results

The dependence of photoluminescence excitation spectra on temperature is illustrated in Fig. 7.4. The signal is detected at the low energy side of the broad PL emission. At low temperatures a strong enhancement in

recombination is observed for excitation at the low energy absorption edge which corresponds to the electron Fermi level. This enhancement is gradually quenched as the temperature is increased to 60K. The peak at higher energies corresponding to the n=2 band edge exciton is however affected relatively little by the increase in temperature. It is also interesting to note that there is some apparent enhancement extending to considerably higher energies above the n=1 band edge (approx. 1.62eV). This temperature dependent behaviour can be exactly compared with the modulation doped case (Fig. 7.1).

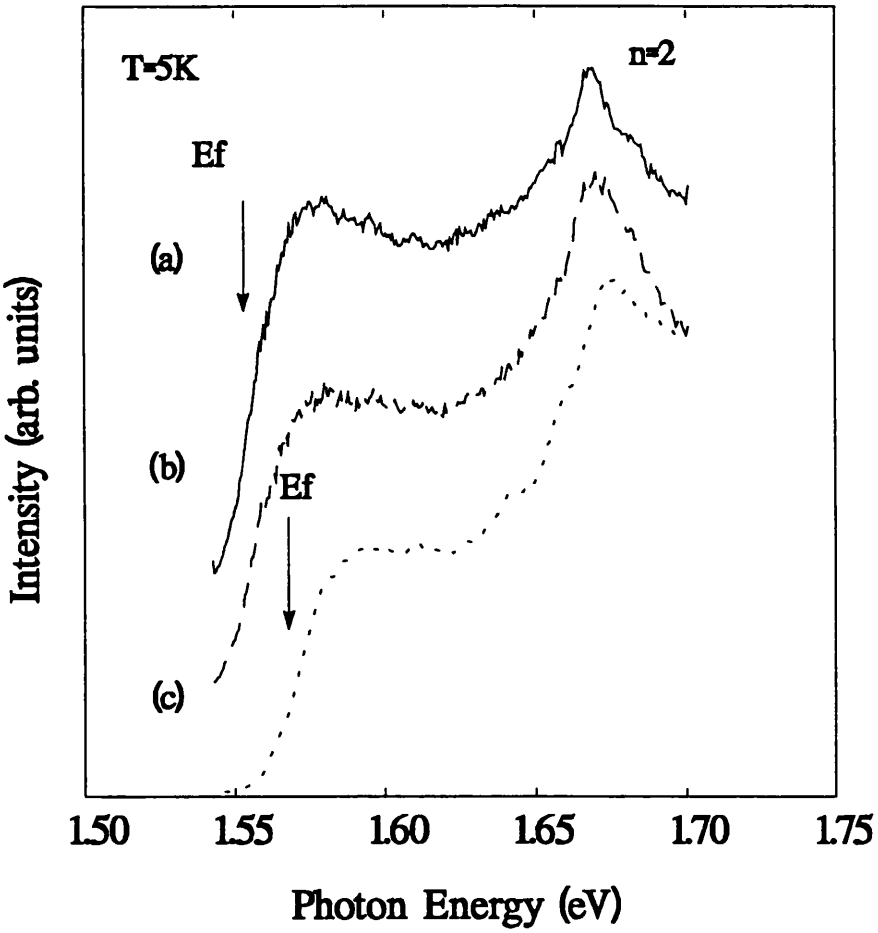

Fig 7.5 Dependence of PLE on excitation density

The same analogous behaviour can be seen in the excitation dependence shown in Fig 7.5. At high densities, curve (a) in comparison to curve (b), the

enhancement is strongly reduced. This effect is equivalent to that observed in Fig. 7.3, however as pointed out it is in contrast to that theoretically expected and is perhaps again indicative of the importance of the hole density in this case. The final curve of Fig. 7.5, (c) illustrates the effect of the additional excitation which increases the electron population and hence neutralises a proportion of the ionised donors. The result is again to quench the enhancement. This is an important effect in that it indicates the importance of the excess proportion of positively ionised donor potentials in the mechanism responsible for enhancement.

So far we have drawn the parallels that exist between the traditional FES picture and the current work. On the basis of these results we can identify the observed effects as due to many-body interactions. We now show why the fundamental differences in the structure under investigation require a different interpretation of the effect to that forwarded in the modulation doped case. In particular the presence of the ionised donors complicates the picture of correlation between the photo-excited hole and the Fermi electron sea. Enhancement is in fact only observed under conditions for which the positive ionised donors represent the majority charge population. Screening must therefore be considered with respect to the most favourable site for the electron and not the hole to recombine. In the conventional FES model, the mobility of the Fermi-electron sea allows the accommodation of a hole at a screening minima. The excess positive charge is in contrast in the present case fixed and unable to participate in a rearrangement (scattering) process. The dynamics of the screening process are therefore fundamentally different in this case. The dependence of correlation upon the ionised donor population implies that the observed phenomena should also show distinct differences to the modulation doped case. Fig 7.6(a,b,c) show time-resolved measurements for different photon energy excitation. The spectra have been measured using a synchroscan streak camera giving a possible time

resolution of approximately 10ps. The sample is excited using the same tunable dye laser as above pumped to give pulses of typically 5ps duration. Fig. 7.6(a) illustrates excitation in the n=1 subband, under these conditions the peak luminescence intensity shifts relatively rapidly to lower energies (about 10meV in the first 1ns). The results for the same photon energy excitation but with additional excitation to increase the electron population are shown in Fig 7.6(b), in this case there is essentially no shift in the luminescence spectrum. For excitation at a photon energy corresponding to the n=2 subband (Fig 7.6(c)), the luminescence again relaxes to lower energies with time, the response is however significantly slower than for the n=1 level excitation.

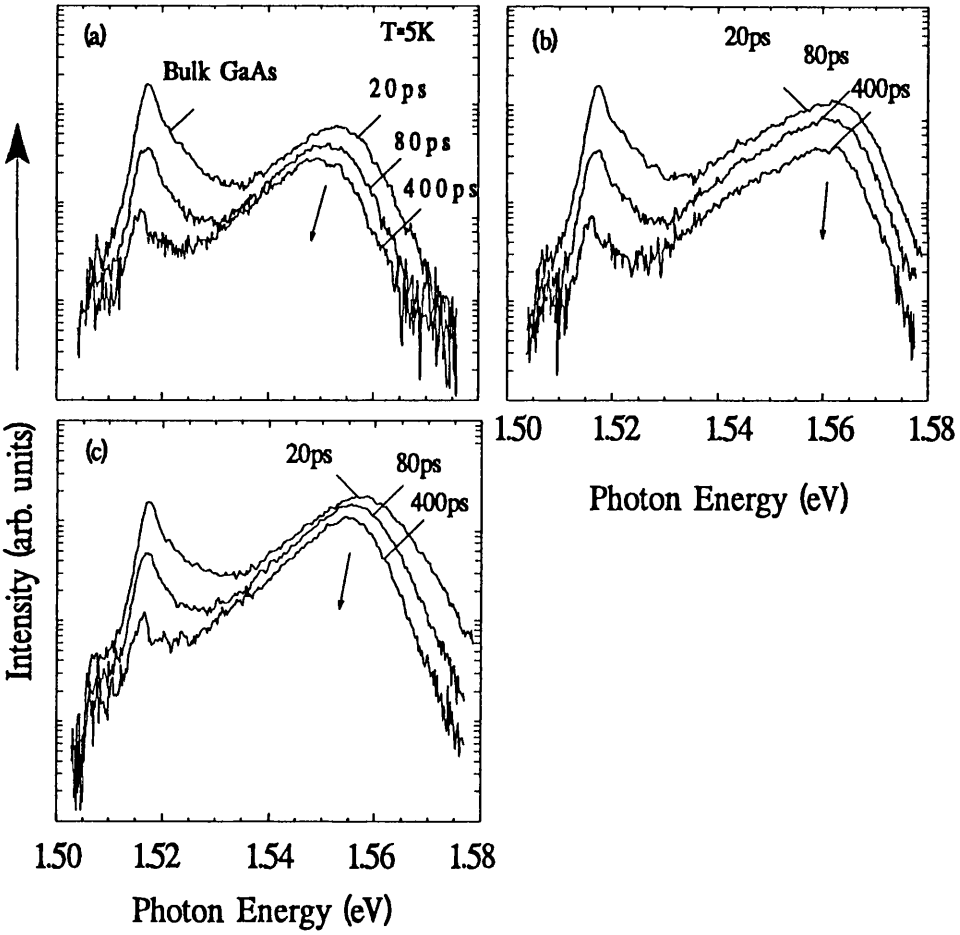

Fig 7.6 Time resolved measurements illustrating dependence of relaxation on photon energy of excitation

It is clear from these transient results that recombination at different energies within the total luminescence emission shows both a different behaviour in time, and also a different excitation energy dependence. This second point is highlighted in Fig. 7.7 by the dramatic difference in excitation spectra for detection at different recombination energies. The high energy tail of the luminescence is only strongly observed for the higher excitation densities corresponding to the n=2 subband level.

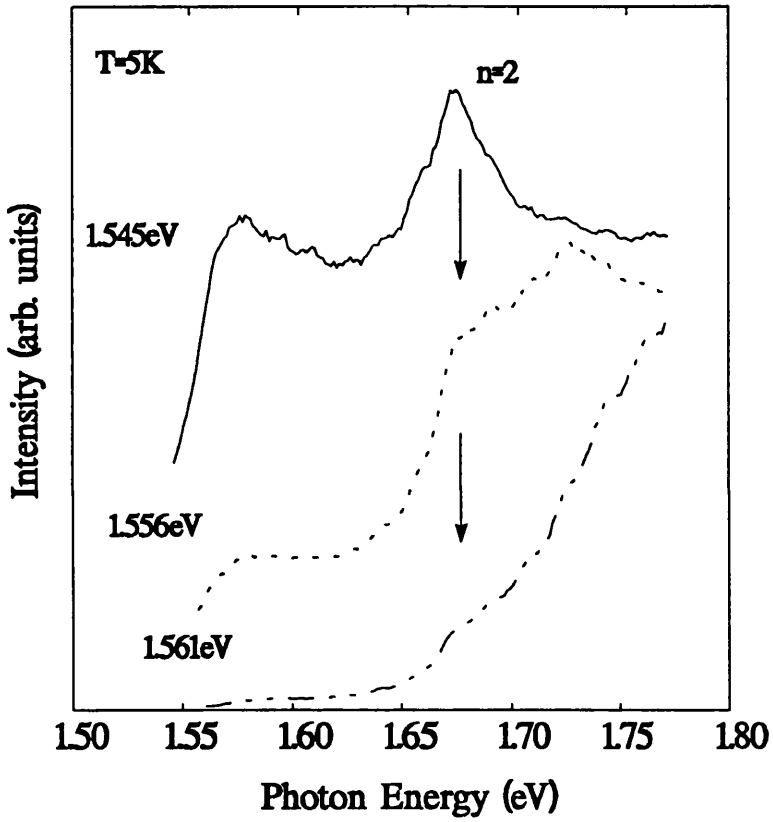

Fig 7.7 Dependence of PLE on detection energy

7.5 Discussion

The photoluminescence excitation spectra presented in Figs. 7.4 and 7.5 clearly illustrate the enhancement dependence which has previously been discussed in terms of the Fermi-Edge Singularity as observed in modulation-doped quantum wells. It is however, at the same time clear that the results of

Figs. 7.6 and 7.7 do not follow the same interpretation. As already discussed a good indication of the important factors in this new mechanism, comes from the dependence of enhancement on the density of ionised donor potentials. The enhancement factor can be related to the scattering strength of these potentials. This fact is a total contradiction to what is normally considered as the ground for the non-observation of the Fermi-edge resonance in highly doped bulk semiconductors i.e. "strong scattering of carriers by the random impurity potentials" [7.3]. We must consider then a correlation mechanism which is strongest in the positive environment of a majority population of ionised donors. The photo-excited electron is created in what is an overall positive background charge. The donors are however fixed and therefore unable to react to the presence of the electron by scattering to accommodate it, as would be the analogy of the FES. An important dynamic role is therefore still played by the electrons. The interaction of the photo-excited electron with the positive background is determined by the screening ability of the total electron population. The predominant component of this is the dynamic screening of those electrons at and above the Fermi-level. This point is worth stressing since the density of excited electrons in a typical experiment is a small fraction of the existing population, it is only the fact that these electrons make a dynamic contribution to the screening which makes them significant. Once the excited electrons relax to the Fermi-edge their additional contribution to screening is lost. The relaxation proceeds via two basic mechanisms; an extremely rapid thermalisation with the existing electron population due to electron-electron scattering (see Fig. 7.8) and secondly a less rapid cooling of the total electron population via acoustic phonon emission. The former takes place on a time scale of a few ps, while the second mechanism requires typically 100ps [7.16]. The efficiency of electron-electron scattering in establishing a new

thermal equilibrium between the intrinsic electron population and those photo-excited, would account for the strong broadening of the Fermi edge resonance and the absence of significant enhancement at energies well above the Fermi level (the Uncertainty principle dictates the spectral width for such short lived states). This in itself allows us to conclude that the relaxation observed in the time resolved results of Fig. 7.6 is not due to a change in screening, since from the above arguments we believe the electron system to be totally relaxed in terms of the screening after only 100ps. The luminescence peak however continues to shift rapidly to lower energies for times up to 1ns. In addition to a change in the dynamic screening there is also a simple reduction in the electron concentration with time due to recombination. The change in electron population, which in turn results in a small change in local potential, is however not significant in altering the subband energy levels and correspondingly shifting the luminescence spectrum. To understand the temporal development we need to go back and consider the minority carrier in this system, the photo-excited hole.

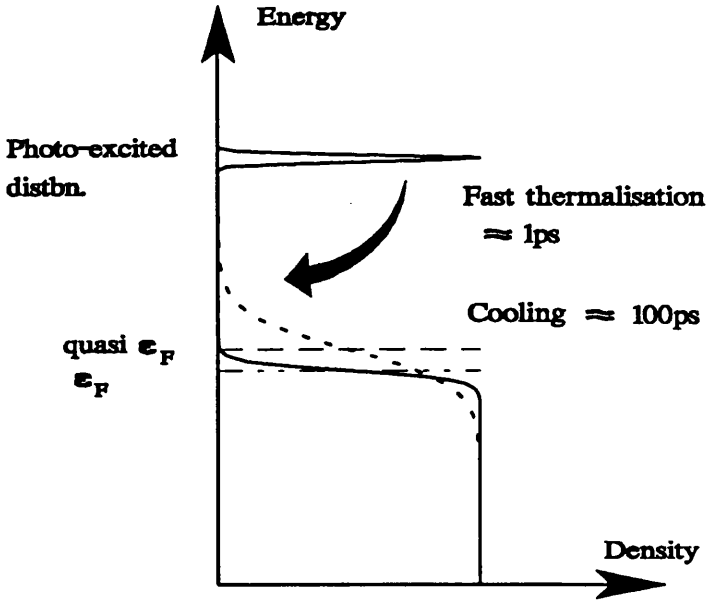

Fig 7.8 Thermalisation of photo-excited electron distribution

The hole is generated in a system of random positive potentials surrounded by a smaller number of electrons. In such an environment the hole represents a mobile charged species to which the electrons will react via their coulomb interaction. It is therefore possible to consider that the hole is able to move to provide a favourable recombination site for the electron in an overall positive background. This picture is at first sight unrealistic since the photo-excited hole is repelled by the positive donor potential and will move away from such centres, losing the possibility for enhancing electron interaction. The random nature of the donor potentials, however has the effect that holes in scattering between these potentials become effectively localised (Anderson type localisation, see chapter 2) [7.17]. Localisation of this kind is in particular enhanced in a strongly compensated system, which is almost certainly the case for this sample. Since the Si dopant is amphoteric, a significant amount of the Si atoms will be present at high doping levels as acceptors on the As site. Typically this fraction is around 10% [7.18]. Separate evidence for such localisation is obtained from studies of the low energy tail in PL spectra of centre doped QWs [7.19].

So far we have argued that the movement of the hole will determine the recombination site with the electron and that at the same time the hole becomes localised. The time scale over which such processes occur is again a key to the role they play in the overall effect. The relaxation of a photoexcited hole is found to be considerably faster than that of an electron [7.20]. The mechanisms described above for the hole are therefore active in an environment which is strongly screened by a large excess of high energy electrons. As a result the final distribution of relaxed holes is determined by the initial screening, which in turn is dependent on both the excited electron energy and also the total density. Following this argument through we propose that the observed differences in recombination are simply the result

of the dependence of the hole distribution on the screening ability of the excited electron population. The slower time development of the PL spectra follows from the relative difference in recombination rates for holes in different states. Briefly, our model predicts that each recombination channel will show a dependence on excitation which reflects the occupation of the hole state. Exactly this behaviour is observed in Fig. 7.4. The enhancement in the vicinity of the Fermi-level is a function of the relative screening efficiency of these electrons. This effect is strongest for the low energy recombination where the hole occupancy is less density dependent. The high energy recombination is only observed for high excitation densities, while in contrast the low energy transitions are observed for all excitation levels but the relative radiative efficiency and recombination rate is screening dependent.

7.6 Conclusion

A correlation effect has been demonstrated for degenerately centre doped structures which is analogous to that observed for the Fermi-Edge singularity in modulation doping. A qualitative model is proposed which accounts for both the time integrated and the temporal development of the photoluminescence emission. The dynamics of the recombination process in a many-body correlated system are highlighted as being vital to the correct understanding of the role of the different carrier types in correlation. In particular the relative time scale of the electron and hole relaxation implies that the effects observed are probably unique to n-type samples. The corresponding effect in p-type material it is believed would not be observed due to the loss of the additional screening before the electron population relaxes. The important question of why it is at all possible to observe such a

correlation given the problems of strong scattering by the random impurity potentials is not entirely resolved. The mechanism discussed in the text could in concept also apply to bulk material. Perhaps one indication of why it has been observed first here in the confined case is the idea that in 2 dimensions one only requires an arbitrarily weak potential to support a bound state, and therefore weak localisation in a degenerate system can in this case play a more significant role.

Chapter 8

Summary and future work

The work prepared in this thesis falls naturally into two categories describing different aspects of the problem of impurities in low dimensional semiconductor structures. The first of these points can be simply stated as the influence of the electrical potential associated with an impurity on the two dimensional confinement itself. The band offset between different materials, which defines the simple square well problem used to analyze these structures, can be dramatically distorted by the Coulombic potential associated with an ionised impurity. This idea has been extensively studied in chapter 4. A number of interesting consequences have been demonstrated for a bandstructure perturbed in this way. As a result of the dependence of the distortion on the charge state of the impurity a novel charge transfer effect can be demonstrated. This charge transfer is the redistribution of photo-excited charge to compensate the potential produced by ionised impurities. Such a mechanism has previously been recognized in modulation doped structures where the dopant impurities are naturally intentionally ionized. In the current work the ionization of the impurities is a consequence of depletion by surface related states. In both cases there exists a well defined threshold energy for charge transfer which corresponds to the AlGaAs band gap and the resulting generation of free carriers in this material. This dependence suggests that it may be possible to design novel optical switches based on such ideas. In any case, the utilisation of the charge state of an impurity is an additional parameter open to the design of quantum devices and implies enormous scope for future work in this area. Work is in progress to look at the charge transfer mechanisms in a more

controlled manner. This is achieved by using acceptors placed in the barrier to intentionally ionise donors in the well. By adjusting the separation between acceptor and donor populations we aim to be able to control the lifetime of the neutral state (Fig.8.1)

Chapter 5 has focused on the development of the optical properties of a single quantum well with doping level. Again one aspect of these results has been to demonstrate the dependence on doping density of the quantum well distortion discussed above. In addition the opposite viewpoint, that of the effect of confinement on the impurity states, is also discussed. Two important results coming from this work are the difference in the dependence on doping of the degenerate limit and of the ionisation of excitons due to screening when comparing the 2 and 3 dimensional cases. Both increased limits can be understood in terms of the simple confinement of the particles within the 2 dimensional layer. This restriction reduces the overlap and hence the interaction between carriers, in addition their reduced freedom of movement implies a less effective screening action.

The use of an amphoteric dopant such as Si results in strong compensation effects at high doping levels. The strong potential fluctuations in a compensated system produce correspondingly strong localisation of free carriers and excitons. The smearing out of these random potentials due to a mobile charge population has been shown in chapter 5 to dramatically reduce the localisation and produce a novel line-narrowing of the exciton transition at the degenerate limit. This effect has not been discussed for bulk material although a survey of optical spectra appearing in the literature suggest that similar line narrowing effects are present in the observed band transitions.

The ideas of localisation and exciton interaction are expanded in chapter 6, which makes an extensive study of the dynamics of free exciton and bound exciton interaction over a wide range of doping levels and for different applied

conditions. The mechanisms via which a resonantly excited exciton interacts with impurities and with the lattice before recombining occur on a picosecond time scale. These dynamic processes have been studied using a time-resolved technique allowing the recombination of both free and bound exciton to be measured in parallel. One important result which is clear from this work is that the observed recombination rates are often determined by the coupling between channels due to capture and thermal emission. The concept of a radiative lifetime as an intrinsic measure of a particular recombination efficiency is therefore of limited value for a doped system under typical low temperature conditions.

For narrow well widths localisation at interface states dominates the observed photoluminescence (PL) spectra. In such a system, it is not possible to measure the binding energy of an impurity directly from the PL spectra. Using the technique of selective excitation we are able to restrict the excited population to a well defined localisation energy. In turn the bound states occupied are those occurring in the same localisation volume, referred to in the text as "spatially correlated." Depending on the relative mobility of the states excited the bound exciton recombination appears as a sharp well resolved peak, separated from the laser by exactly the exciton-impurity binding energy. Such a technique allows an extremely accurate measure of the binding energy to be made. Work is in progress now to study the enhancement in binding energy of the impurity according to the size of the localisation volume in which it appears.

Correlation is again the topic of Chapter 7. As discussed above, at high doping densities the exciton is ionised due to screening in the electron sea. In this case, it is possible to form a bound state between a single hole (in n-type material) and the total electron sea. This mutli-particle excitation has been observed on a number of occasions in modulation doped structures and is referred to as the Fermi-Edge Singularity (FES) or the "Mahan" exciton. A related effect in

strictly centre doped structures is reported here for the first time. The determining effect in this phenomenon is found to be the energy dependence of the screening efficiency of electrons. Electrons with energy around the Fermi-level are found to be most effective in screening. As a result it is these electrons which most effectively correlate with a hole in the conventional FES picture. This same argument applied in the case of the strong localisation present in a highly doped structure implies that the degree of electron screening determines the localisation occurring in the system. The distribution of states occupied and in turn the observed recombination will follow from the exact energy of the carriers excited. The dependence of the hole distribution on the screening of electrons implies that their exists sensitive balance within which the change in electron concentration, or the effect of dynamic screening will have a measurable effect for a particular state. As a result the measurement is fairly difficult to carry out and the exact degree of enhancement not consistently reproduced! The mechanism is however an interesting one and further more detailed measurements are planned to study how the state occupation is influenced by the carriers in the system.

In making an overall conclusion to the work presented in this thesis the obvious statements are perhaps the ones that best describe the situation. A number of different properties and ideas have been discussed which highlight the diversity of effects that an impurity can promote in a quantum confined structure. It is without question that there remains a vast amount of work to be done in this field, indeed it is more than 10 years since the first theoretical confined impurity calculation of Bastard and we are still very much in the infancy of the subject. Some of the more important topics for future work areas follows: (i) Localisation. As discussed extensively in this work localisation is particularly important in a 2D system. The presence of interfaces which remain rough on an atomic scale inevitably results in localisation to some degree. This

localisation will for example influence the interaction of carriers and hence determines the observed properties of the system. The mechanisms of interface localisation are at present not well understood. Recent interesting results looking at the problem in AlGaAs-GaAs structures have, as an example, proposed that the interface between the binary compound GaAs and the ternary AlGaAs is inevitably poorer than the interface between two binary alloys GaAs and AlAs [1]. By growing a single monolayer of AlAs at the interface between GaAs and AlGaAs remarkable improvements in exciton linewidths have been demonstrated indicating a smoother interface. (ii) Deep states and non-radiative recombination. Deep states tend to be ignored in 2D since they are not observed optically, however as non-radiative channels they can potentially be of great importance. Again relating to the previous point, many of the defect states associated with the interface can be expected to be relatively deep. A good indication of this is found if one compares the radiative linewidth with the decrease in radiative efficiency with increasing temperature. Although not a general correlation, a broader linewidth typically indicates a more dramatic drop in radiative recombination with temperature.

The use of externally applied perturbations to the quantum well has not been discussed in this work. Among those techniques which will certainly be of particular importance are the use of hydrostatic pressure and magnetic fields. As an example of this first method there has been quite extensive work carried out to look at how the band offsets between well and barrier change with increasing pressure. The different pressure coefficients of the bulk bands (Γ,X,L) results in a crossover in which of the valleys forms the conduction band minima. This crossover is different in the AlGaAs barrier when compared with the GaAs well. As a result it is possible to achieve a transition from what is called a type I structure (both carrier types are confined in the same material) to a type II structure(carriers confined in different materials). As a parallel to

this we can ask the question what happens to an impurity under the transition from a type I to type II bandstructure? For example an impurity present in the well becomes ionised and loses its charge to the barrier as the conduction band minima in the barrier becomes lower than that in the well. Work we have so far carried out indicates that this crossover is not easily observed since the spatially indirect transition (well to barrier) is not seen and only a dramatic drop in the direct transition is apparent.

Finally a brief comment about magnetic field measurements which is by far the most extensively applied of the two techniques. In this work it has been used to look at the transitions observed in the low doped quantum well under the two excitation conditions discussed in chapter 4. Using a Faraday geometry (excitation parallel to magnetic field) with the field perpendicular to the 2D plane we observe strong quenching of the low energy transition while at the same time a corresponding enhancement of the free exciton. We interpret this as evidence to support the assignment of the low energy transition as due to the ionised donor bound exciton. The application of a magnetic field to the higher doped samples is perhaps one of the more interesting experiments that should be carried out in the future to look further at the mechanisms discussed in this work.

References

Chapter 1

[1.1] H.-J.Queisser: The Conquest of the Microchip. Harvard University Press, 1988.

[1.2] A.J.R. de Kock in: Handbook on Semiconductors **3**, Vol.Ed. S.P. Keller, Ser.Ed. T.S. Moss. North Holland, Amsterdam 1980, 247.

[1.3] M. Razeghi: The MOCVD Challenge. Adam Hilger, Bristol 1989.

[1.4] A.Y. Cho, Appl. Phys. Lett. **19**, 467 (1971) and A.C. Gossard, IEEE J.Quantum.Electron. **22**, 1649 (1986).

[1.5] L. Esaki review in IEEE J.Quantum Electron. **22**, 1, (1986).

[1.6] L. Esaki and R. Tsu, IBM J. Res. Dev. **14**, 61, (1970).

[1.7] K. von Klitzing in: Physics and Applications of Quantum Wells and Superlattices, Eds. E.E. Mendez, K. von Klitzting. NATO ASI Ser.**170**. Plenum Press, New York, London 1988, 179 and 229, and D.C. Tsui, H.C. Störmer and A.C. Gossard, Phys. Rev. Lett. **48**, 1559 (1982).

[1.8] J.M. Baranowski, M. Grynberg and S. Paravski in: Handbook on Semiconductors **1**, Vol.Ed. W. Paul., Ser.Ed. T.S. Moss. North Holland, Amsterdam 1982, 323..

Chapter 2

[2.1] G. Bastard, Phys.Rev. **B24**, 5693 (1981).

[2.2] N.W. Ashcroft and N.D. Mermin: Solid State Physics. Holt, Rinehart and Winston, New York 1976.

[2.3] The ideas for this analysis are based on an original program by Dr. G. Brunthaler, Johannes Kepler University, Linz, Austria.

[2.4] G. Bastard: Wave Mechanics Applied to Heterostuctures. Les Editions de Physique, Les Ulis 1988.

[2.5] M. Guzzi and J.L. Staehli, Solid State Phenomena **10**, 25 (1989).

[2.6] J.C. Phillips: Bonds and Bands in Semiconductors. Academic Press, London 1973.

[2.7] W. Kohn in: Solid State Physics **5**, Eds. F. Seitz, D. Turnbull. Academic Press, New York 1957, 257.

[2.8] M. Jaros: Deep Levels in Semiconductors. Adam Hilger, Bristol 1982.

[2.9] S.T. Pantelides, Rev.Mod.Phys. **50**, 797 (1978).

[2.10] W. Kohn and J.M. Luttinger, Phys. Rev. **97**, 869 (1955).

[2.11] G. Bastard, Phys. Rev. **B24**, 4714 (1981).

[2.12] R.L. Greene and K.K. Bajaj, Solid State Commun. **45**, 825 (1983).

[2.13] C. Mailhiot, Y.-C. Chang and T.C.McGill, J.Vac.Sci.Technology **21**, 519 (1982) and also Phys. Rev. **B26**, 4449 (1982).

[2.14] S. Chadhuri and K.K. Bajaj, Phys. Rev. **B29**, 1803 (1984).

[2.15] K.Tanaka, M. Nagaoka and T. Yamabe, Phys. Rev. **B28**, 7068 (1983).

[2.16] S. Chadhuri, Phys. Rev. **B28**, 4480 (1983).

[2.17] R.L. Greene and K.K. Bajaj, Phys. Rev. **B31**, 913 (1985).

[2.18] W.T. Masselink, Y.-C. Chang and H. Morkoc, Phys.Rev. **B32**, 5190 (1985).

[2.19] J.A. Brum, C. Priester and C. Allan, Phys. Rev. **B32**, 2378 (1985).

[2.20] W.T. Masselink, Y.-C. Chang and H.Morkoc, Phys.Rev. **B28**, 7373 (1983).

[2.21] D.C. Reynolds, K.K. Bajaj, C.W. Litton, P.W. Yu, W.T. Masselink, R.Fischer and H. Markoc, Phys. Rev. **B29**, 7038 (1984).

[2.22] W.T. Masselink, Y.-C. Chang and H. Morkoc, J.Vac.Sci.Technology **B2**, 376 (1984).

[2.23] B.V. Shanabrook, J. Comas, T.A. Perry and R. Mermin, Phys.Rev. **B29**, 7096 (1984).

[2.24] S. Chadhuri and K.K. Bajaj, Solid State Commun. **52**, 967 (1984).

[2.25] The terms moderately and lightly doped are material dependent.

[2.26] G.E.Stillman and C.M. Wolfe, Thin Solid Films **31**, 69 (1976).

[2.27] N.F.Mott and W.D. Twose, Advances in Physics **10**, 107 (1961).

[2.28] N.F.Mott: The Metal Insulator Transition. Taylor and Francis, London 1974.

[2.29] M.N. Alexander and D.F. Holcomb, Rev. Mod. Phys. **40**, 815 (1968) and N.F. Mott, M. Pepper, S. Pollet, R.H. Wallis and C.J. Adkins, Proc. Royal Soc. London **A345**, 169 (1975) and T. Ando, A.B. Fowler and F. Stern, Rev.Mod.Phys. **54**, 437 (1982).

[2.30] N.F. Mott, Philos.Mag. **6**, 287 (1961) and N.F.Mott, Contemp.Phys. **14**, 401 (1973).

[2.31] J. Basiniski and R. Oliver, Can. J. Phys. **45**, 119 (1967).

[2.32] B.I. Shklovski and A.L. Efros: Electronic Properties of Doped Semiconductors. Spinger Series in Solid-State Sciences **45**. Springer-Verlag , Berlin 1984, 32.

[2.33] H. Sigg, K. von Klitzing, M. Hauser and K. Ploog in: Shallow Impurities in Semiconductors 1988, Ed. B. Monemar. Inst.Phys.Conf.Ser. **95**. Institute of Physics, Bristol and Philadephia 1989, 11.

[2.34] P.W. Anderson, Phys.Rev. **109**, 1492 (1958).

[2.35] N.F. Mott , Advances in Physics **16**, 49 (1967).

[2.36] I.D. Voronova: Localisation in compensated Gallium Arsenide, PhD thesis P.N. Lebedev Institute, Moscow.

[2.37] J.I. Pankove: Optical Properties of Semiconductors. Dover Publ., New York 1971.

[2.38] W.J. Rappel, L.F. Feiner and M.F.H. Schurmans in: Excitons in Confined Systems., Eds. R. Del Sole, A. D'Andrea, A. Lapiccirella. Springer Verlag, Berlin 1988, 63 and C. Weisbuch and R. Ulbrich, Phys.Rev.Lett. **39**, 654 (1977).

[2.39] I. Broser and R. Broser, J.Lumin. **12/13**, 201 (1976) and C. Benoit à la Guillaume, A. Bonnot and J.M. Debever, Phys.Rev.Lett. **24**, 1235 (1970).

[2.40] L.C. Andreani and F. Bassani, Phys. Rev. **B41**, 7536, (1990).

[2.41] M.Kohl, D. Heitman, P.Grambow and K. Ploog, Phys.Rev. **B42**, 2941 (1990).

[2.42] J.C.M. Henning in: Excited State Spectroscopy in Solids, Eds. U.M. Grassano, M.Terzi. Proc. of the Int. School of Physics "Enrico Fermi". Course **96**, North Holland, Amsterdam 1987, 167.

[2.43] J.J. Hopfield, R.G. Thomas and R.T. Lynch , Phys.Rev.Lett. **17**, 312 (1966) and D.G. Thomas and J.J. Hopfield, Phys. Rev. **128**, 2135 (1962) and J.J. Hopfield and D.G. Thomas, Phys. Rev. **122**, 35 (1961).

[2.44] M. Voos, R.F. Leheny and J. Shah in: Handbook on Semiconductors **2**, Vol.Ed. M. Balkanski, Ser.Ed. T.S. Moss. North Holland, Amsterdam 1980, 329.

[2.45] P.J. Dean and D.C. Herbert in: Excitons, Ed. K. Cho. Topics in Current Physics **14**. Springer Verlag, Berlin 1979, 55.

[2.46] B. Monemar, U. Lindefelt and W.M.Chen, Physica **B146** , 256 (1987).

Chapter 3

[3.1] B. Henderson and G.F. Imbush: Optical Spectroscopy of Inorganic Solids. Monographs in Physics and Chemistry. Oxford Science Publications 1989, gives a good discussion of modern developments in doped crystals as tunable laser sources.

[3.2] M.D. Lumb: Luminescence Spectroscopy. Academic Press, London 1978.

[3.3] R.L. Fork, C.H. Bruto Cruz, P.C. Becker and C.V. Shank, Optics Lett. **12**, 483 (1987).

[3.4] W. Demtröder: Laser Spectroscopy. Springer Series in Chemical Physics **5**. Springer Verlag , Berlin 1982.

[3.5] P.M. Rentzepis, Science , **164**, 239 (1970).

[3.6] P.M.Rentzepis and W. Struve in: Spectroscopy, Ed. D.A. Ramsey. International Review of Science Phys.Chem.Ser.**3**. Butterworths, London 1976, 263.

[3.7] E. Hartfield and B.J. Thompson in: Handbook of Optics, Eds. W. Driscall, W. Vaughan. McGraw Hill, New York 1974, Sect.17.

[3.8] A. Yariv, Optical Electronics, CBS College Publishing 1985.

[3.9] F.O.Neill, Opt. Commun. **6**, 360 (1972) .

[3.10] J. Kuhl, H. Klingenberg, D. von der Linde, Appl. Phys. **18**, 279 (1979).

[3.11] N.H. Schiller and R.R. Alfano, Laser Focus **18**, 43 (1982).

Chapter 4

[4.1] N. Holonyak, Jr, B.A. Voyak, H. Morkoc, T.J. Drummond and K. Hess, Appl. Phys. Lett. **40**, 658 (1982).

[4.2] A.M. Vasil'ev, P.S. Kop'ev, M.Yu. Nadtochil and V.M. Ustinov, Sov. Phys. Semicond. **23**,1320 (1989).

[4.3] A. Zrenner and F. Koch in: Shallow Impurities in Semiconductors 1988, Ed. B. Monemar. Inst.Phys.Conf.Ser. **95**. Insitute of Physics, Bristol and Philadephia 1989, 1.

[4.4] A.S. Chaves, A.F.S. Penna, J.M. Worlock, G. Weimann, and W. Schlapp, Surf. Sci. **170**, 618 (1986).

[4.5] C. Delalande, J. Orgonasi, M.H. Meynadier, J.A. Brum, G. Bastard, G. Weimann and W. Schlapp, Solid State Commun. **59**, 613 (1986).

[4.6] A.S. Plaut, I.V. Kukushkin, K. von Klitzing and K. Ploog, Phys. Rev **B2**, 5744 (1990).

[4.7] H. Yoshimura, G.E.W. Bauer and H. Sakaki, Phys. Rev. **B38**, 10791 (1988).

[4.8] C. Delalande, J. Orgonasi, J.A. Brum, G. Bastard, M. Voos, G. Weimann and W. Schlapp, Appl. Phys. Lett. **51**, 1346 (1987).

[4.9] A. Chandra, C.E.C. Wood, D.W. Woodward and L.F. Eastman, Solid State Electron. **22**, 645 (1979).

[4.10] E.F. Shubert, J.M. Kuo, R.F. Kopf, A.S. Jordan, H.S. Luftman and L.C. Hopkins, Phys. Rev. **B42**, 1364 (1990).

[4.11] T.S. Moss, Proc.Royal Soc. London **B76**, 775 (1984) and E. Burstein, Phys. Rev. **93**, 632 (1954).

[4.12] J.A. Brum and G. Bastard, Phys. Rev. **B31**, 3893 (1985).

[4.13] E.E. Mendez, G. Bastard, L.L. Chang, L. Esaki, H. Morkoc and R. Fischer, Phys. Rev. **B26**, 7101 (1982).

[4.14] T.H. Wood, C.A. Burrus, D.A.B. Miller, D.S. Chemla, T.C. Damen, A.C. Gossard and W. Wiegmann, Appl. Phys. Lett. **44**, 16 (1984).

[4.15] L.V. Keldysh, Soviet Physics JETP **7**, 788 (1958) and W. Franz, Z. Naturforsch. **13a**, 484 (1958).

[4.16] D.S. Chemla, T.C. Damen, D.A.B. Miller, A.C. Gossard and W. Wiegmann, Appl. Phys. Lett. **42**, 864 (1983).

[4.17] M. Stopa and S. DasSarma, Phys. Rev . **B40**, 8466 (1989).

[4.18] M.H. Meynadier, J.A. Brum, C. Delalande, M. Voos, F. Alexandre and J.L. Lievin, J. Appl. Phys. **58**, 4307 (1985).

[4.19] Jia-Lin Zhu, Dao-Hua Tang and Jia-Jiong Xiong, Phys.Rev. **B39**, 8609 (1989).

[4.20] D.C. Reynolds, C.E. Leak, K.K. Bajaj, E.E. Stuty, R.L. Jones, K.R. Evans, P.W. Yu and W.M. Theis, Phys. Rev. **B40**, 4156 (1989).

[4.21] L. Pavesi and P. Giannozzi, Phys.Rev. **B43**, 2446 (1991).

[4.22] J. Weber, S.J. Pearton and W.C. Dautremont-Smith, Appl.Phys.Lett. **49**, 1181 (1989).

Chapter 5

[5.1] N.F. Mott: Metal-Insulator Transitions. Taylor and Francis, London 1974.

[5.2] D.A. Cusano, Solid State Commun. **2**, 353 (1964).

[5.3] D.E. Hill, Phys.Rev. **133**, 866 (1964).

[5.4] J.I. Pankove, J. Appl. Phys. **39**, 5368 (1968).

[5.5] H.C. Casey and F. Stern, J. Appl. Phys. **47**, 631 (1976).

[5.6] D. Olego and M. Cardona, Phys. Rev. **B22**, 886 (1980).

[5.7] Jiang De-Sheng, Y. Makita, K. Ploog and H.J. Queisser, J. Appl. Phys. **53**, 999 (1982).

[5.8] G. Borghs, K. Bhattacharyya, K. Deneffe, P. Van Mieghem and R. Mertens, J. Appl. Phys. **66**, 4381 (1989).

[5.9] J. Shah, R.F. Leheny and W. Wiegmann, Phys. Rev. **B16**, 1577 (1977).

[5.10] G.E. Stillman and C.M. Wolfe, Thin Solid Films **31**, 69 (1976).

[5.11] T. Lideikis and G. Treideris, Semicond. Sci. Technol. **4**, 938 (1989).

[5.12] B.E.Sernelius, Phys. Rev **B34**, 5610 (1986) and **34**, 8696 (1986).

[5.13] S. Schmitt-Rink, D.S. Chemla, and D.A.B. Miller, Advances in Physics **38**, 89 (1989).

[5.14] D.A. Kleinman, Phys. Rev. **B32**, 3766 (1985).

[5.15] A.E. Ruckenstein and S. Schmitt-Rink, Phys.Rev. **B35**, 7551 (1987).

[5.16] A.Pinczuk, S.Schmitt-Rink, G.Daman, J.P.Valladares, L.N. Pfeiffer and K .W. West, Phys. Rev. Lett. **63**, 1633 (1989) .

[5.17] A.E. Ruckenstein, S. Schmitt-Rink and R.C. Miller, Phys.Rev.Lett. **56**, 504 (1985).

[5.18] H. Yoshimura, G.E.W. Bauer and H. Sakaki, Phys.Rev. **B38**, 10791 (1988).

[5.19] D. Huang, H.Y. Chen, Y.C. Chang, R. Houdré and H. Morkoc, Phys. Rev. **B38**, 1246 (1988).

[5.20] G. Tränkle, E. Lach, M.Walther, A. Forchel and G. Weimann, Surface Science **196**, 584 (1988).

[5.21] D.Huang, J.I.Chyi and H.Morkoc, Phys. Rev. **B42**, 5147 (1990).

[5.22] R. Stepniewski, S. Huant, G. Martinez and B. Etienne, Phys.Rev. **B40**, 9772 (1989).

[5.23] R.C. Miller and A.C. Gossard, Phys. Rev. **B28**, 3645 (1983).

[5.24] J.C. Tsang, P.J. Dean and P.T. Landsberg , Phys. Rev. **173**, 814 (1968).

[5.25] C.J. Armistead, P. Knowles, S.P. Najda, and R.A. Stradling, J.Phys. **C17**, 6415 (1984).

[5.26] W.T. Masselink, Y.-C. Chang, H. Morkoc, D.C. Reynolds, C.W. Litton, K.K. Bajaj and P.W. Yu, Solid State Electon. **29**, 205 (1986) .

[5.27] J.A.Brum, G.Bastard and C.Guillemot, Phys. Rev. **B30**, 905 (1984).

[5.28] E. Hanamura, J.Phys.Soc.Japan **28**, 120 (1970).

[5.29] A. Pinczuk, J. Shah, H.L. Störmer, R.C. Miller, A.C. Gossard and W. Wiegmann, Surface Science **142**, 492 (1984).

[5.30] S.K.Lyo and E.D.Jones, Phys. Rev. **B38**, 4113 (1988).

[5.31] M. Takeshima, Phys. Rev. **B25**, 5390 (1982).

Chapter 6

[6.1] R. Dingle, W. Wiegmann and C.H. Henry, Phys. Rev. **B33**, 827 (1974).

[6.2] This result also requires that phonon coupling is not enhanced by confinement, D.A.B. Miller, D.S. Chemla, D.J. Eilenberger, P.W. Smith, A.C. Gossard and T.W. Tsang, Appl. Phys. Lett. **41**, 679 (1982).

[6.3] G.W. t'Hooft, W.A.J.A. van der Poel, L.W. Molenkamp and C.T. Foxon, Phys. Rev. B **35**, 8281 (1987).

[6.4] E.O. Göbel, Festkörperprobleme **30**, 269 (1990).

[6.5] J. Kuhl, A. Honold, L. Schultheis and C.W. Tu, Festkörperprobleme **29**, 157 (1989).

[6.6] L. Schultheis, J. Kuhl, A. Honold and C.W. Tu in: Excitons in Confined Systems, Eds. R. Del Sole, A. D'Andrea, A. Lapiccirella. Springer, Berlin 1988, 50.

[6.7] E.O. Göbel, J. Kuhl and R. Höger, J.Luminescence **30**, 541 (1985).

[6.8] H. Saito and E.O. Göbel, Phys.Rev. **B31**, 2360 (1985).

[6.9] K. Kash, J. Shah, D. Block and A.C. Gossard, Physica **B134**, 189 (1985).

[6.10] E.I. Rashba and G.E. Gurgeneshvili, Sov. Phys. Solid State **4**, 759 (1962) [Fiz. Tver. Tela **4**,1029 (1962)].

[6.11] C.H. Henry and K. Nassau, Phys. Rev. **B1**, 1628 (1970).

[6.12] B. Monemar, U. Lindefelt and W.M. Chen, Physica **B146**, 256 (1987).

[6.13] G.D. Sanders and Y.C. Chang, Phys. Rev. **B28**, 5887 (1983).

[6.14] D.C. Herbert and J.M. Rorison, Solid State Commun. **54**, 343 (1985).

[6.15] T. Takaghara and E. Hanumara, Phys. Rev. Lett. **56**, 2533 (1986).

[6.16] E. Finkman, M.D. Sturge and R. Bhat, J. Lumin. **35**, 235 (1986).

[6.17] D.L. Dexter in: Advances in Solid State Physics **6**, Eds. F. Seitz and D.Turnbull .Academic Press, New York 1958, 251.

[6.18] J. Feldmann , G. Peter, E.O. Göbel, P. Dawson, K. Moore, C.T. Foxon and R.J. Elliot, Phys.Rev.Lett. **59**, 2337 (1987).

[6.19] K. Cho Ed.: Excitons. Topics in Current Physics **14**. Springer Verlag, Berlin 1979.

[6.20] J. Christen, Festkörperprobleme **30**, 239 (1990).

[6.21] B. Deveaud, A. Regreny, J-Y. Emery, and A. Chomette, J. Appl. Phys. **59**, 1633 (1986).

[6.22] A. Ourmazd, D.W. Taylor, J. Cunningham and C.W. Tu, Phys.Rev.Lett. **62**, 933 (1989).

[6.23] H.X. Jiang, L.Q. Zu, J.Y. Lin, Phys. Rev. **B42**, 7284 (1990).

[6.24] G. Bastard, C. Deladande, M.H. Meynadier, P.M. Frijlink and M. Voos, Phys.Rev. **B29**, 7042 (1984).

[6.25] P.W. Anderson, Phys. Rev. **109**, 1492 (1958).

[6.26] D.J. Thouless, J.Phys. **C3**, 1559 (1970) and E.N. Economou and M.H.Chen, Mater.Res.Bull. **5**, 807 (1972) and R.Abouchara, D.J. Thouless and P.W. Anderson, J.Phys. C **6**, 1734 (1973).

[6.27] J. Hegarty and M.D. Sturge, Surface Science **196**, 555 (1988).

[6.28] J.C.Tsang, P.J. Dean and P.T. Landsberg, Phys. Rev. **173**, 814 (1968).

[6.29] P.J. Dean and D.C. Herbert in: Excitons, Ed. K. Cho. Topics in Current Physics **14**. Springer Verlag, Berlin 1979, 55.

[6.30] P.O. Holtz, H.P. Hjalmarson, M. Sundaram, J.L. Merz and A.C. Gossard, Superlattices and Microstructures **9**, 407 (1991).

[6.31] G. Tränkle, H. Leier, A. Forchel, H. Haug, C. Ell and G.Weimann, Phys.Rev.Lett. **58**, 419 (1987) and S. DasSarma, R. Jalabert and S.-R. Eric Yang, Phys.Rev. **B41**, 8288 (1990).

[6.32] C. Weisbuch, R. Dingle, A.C. Gossard and W. Wiegmann, Solid State Commun. **38**, 709 (1981).

[6.33] B. Monemar, N. Magnea and P.O. Holtz, Phys. Rev. **B33**, 7375 (1986).

[6.34] R.C. Miller, D.A. Kleinman, A.C. Gossard and O. Munteanu, Phys. Rev. **B25**, 6545 (1982).

[6.35] S. Charbonneau, T. Steiner, M.L.Thewalt, E.S. Koteles, J.Y. Chi and B. Elman, Phys. Rev. **B38**, 3583 (1988).

[6.36] R.M. Feenstra and T.C. McGill, Solid State Commun. **36**, 1039 (1980).

[6.37] M. Lax, Phys. Rev. **119**, 1502 (1960).

[6.38] L.C. Andreanni, F. Tassone and F. Bassani, Solid State Commun. **77**, 641 (1991).

[6.39] J.S.Blakemore: Semiconductor Statistics. 2.Ed. Dover Publ., New York 1987.

[6.40] J.P. Bergman, P.O. Holtz, B. Monemar, M. Sundaram, J.L. Merz and A.C. Gossard, Phys. Rev. **B43**, 4771 (1991).

[6.41] C. Klingshirn and H. Haug, Physics Reports **70**, 315 (1981).

[6.42] S. Schmitt-Rink, D.S. Chemla and D.A.B. Miller, Advances in Physics **38**, 89 (1989).

[6.43] Y. Toyozawa, Supplement of the Progress of Theoretical Physics **12** (1959).

[6.44] C. Weisbuch, R. Dingle, A.C. Gossard and W. Wiegmann, J.Vac.Sci. Technol. **17**, 1128 (1980).

[6.45] G. Bastard, C. Delalande, M.H. Meynadier, P.M. Frijlink and M. Voos, Phys. Rev. **B29**, 7042 (1984).

[6.46] P.O. Holz, M. Sundaram, J.L. Merz and A.C. Gossard, Phys.Rev. **B41**, 1489 (1990).

[6.47] B. Monemar, P.O. Holtz, J. P. Bergman, C. I. Harris, H. Kalt, M. Sundaram, J.L. Merz and A.C. Gossard, proceedings EP2DS, Japan 1991, to appear in Surface Science.

[6.48] P.J. Dean, D.D. Manchon and J.J. Hopfield, Phys.Rev.Lett. **25**, 1027 (1970).

[6.49] J.P. Jain, S. Nakashima, N. Jouanne, E. Amzallay and M. Balkanski, Solid State Commun. **33**, 1979 (1980).

Chapter 7

[7.1] D.A.Kleinman, Phys. Rev. **B32**, 3766 (1985).

[7.2] S. Schmitt-Rink and C. Ell, J. Lumin. **30**, 585 (1985) and H. Haug and S. Schmitt-Rink, J. Opt. Soc. Am. **B2**, 1135 (1985).

[7.3] G. Livescu, D.A.B. Miller, D.S. Chemla, H. Ramaswamy, T.Y. Chang, N. Sauer, A.C. Gossard and J.H. English, IEEE J. Quantum Electron. **24**, 1677 (1988) and references therein.

[7.4] S. Schmitt-Rink, C. Ell and H. Haug, Phys. Rev. **B33**, 1183 (1986).

[7.5] G.D. Mahan, Phys. Rev. **153**, 882 (1967).

[7.6] P. Nozieres and C.T. De Dominicis, Phys.Rev. **178**, 1097 (1969) and G.D.Mahan, Phys.Rev. **163**, 612 (1967).

[7.7] A.E.Ruckenstein, S.Schmitt-Rink and R.C.Miller, Phys.Rev.Lett. **56**, 504 (1986) and A.E.Ruckenstein and S. Schmitt-Rink, Phys.Rev. **B35**, 7551 (1987).

[7.8] J.M. Rorison, J. Phys. **C20**, L311 (1987).

[7.9] Ji-Wei Wu, Phys. Rev. **B39**, 7992 (1989).

[7.10] H.Kalt, K.Leo, R.Cingolani and K.Ploog, Phys.Rev. **B40**, 12017 (1989).

[7.11] M.S. Skolnick, J.M. Rorison, K.J. Nash, D.J. Mowbray, P.R. Tapster, S.J. Bass and A.D. Pitt, Phys. Rev. Lett. **58**, 2130 (1987).

[7.12] J.S. Lee, Y. Iwasa and N. Miura, Semicond. Sci. Technol. **2**, 675 (1987).

[7.13] J. Wagner, private communication and J. Wagner, A Ruiz and K.Ploog, Phys. Rev. **B43**, 12134, (1991).

[7.14] A. Chandra, C.E.C. Wood, D.W. Woodward and L.F. Eastman, Solid State Electron. **22**, 645 (1979).

[7.15] C.I. Harris, B. Monemar, G. Brunthaler, H.Kalt and K.Köhler, manuscript accepted for publication in Phys. Rev. B.

[7.16] K.Leo, W.W. Rühle and K.Ploog, Phys. Rev. **B38,** 1947 (1988).

[7.17] See for example, D.J. Thouless, J.Non Cryst.Solids **8-10** ,461 (1972) and R. Abouchacra, D.J. Thouless and P.W. Anderson, J. Phys. **C6**, 1734 (1973).

[7.18] R. Murray, R.C. Newman, M.J.L. Sangster, R.B. Beall, J.J.Harris, P.J. Wright, J. Wagner and M. Ramsteiner, J. Appl. Phys. **66**, 2589 (1989).

[7.19] C.I. Harris, B. Monemar, H. Kalt and K. Köhler submitted to Phys. Rev. B.

[7.20] S.M. Goodnick and P. Lugli, Phys. Rev. **B38**, 10135 (1988).

Chapter 8

[8.1] K. Ploog, A. Fischer, L. Tapfer and B.F. Feuerbacher, Appl.Phys.Lett. **A52**, 135 (1991).

Appendix

List of current publications by the author :

Photoluminescence Study of Reactive-ion-etched Silicon: A New Boron-Related Defect. C.I. Harris, W.D. Sawyer, M. Konuma and J. Weber, Material Science and Engineering **B4**, 457 (1989).

Activation of germanium acceptors during $SiCl_4$ reactive-ion-etching of MOCVD GaAs epitaxial layers. J. Weber, W.D. Sawyer and C.I. Harris, Inst. Phys. Conf. Ser. **106**, 263 (1990).

Variation in the confining potential of doped AlGaAs/GaAs quantum wells with the photon energy of excitation. C.I. Harris, B. Monemar, G. Brunthaler, H. Kalt, K. Köhler and T. Schweizer, Superlattices and Microstructures **9**, 453 (1991).

Dynamics of free and bound excitons in center-doped GaAs/AlGaAs quantum wells. B. Monemar, H. Kalt, C.I. Harris, J.P. Bergman, P.O. Holtz, M. Sundaram, J.L. Merz, A.C. Gossard, K. Köhler and T. Schweizer, Superlattices and Microstructures **9**, 281 (1991).

A Photoluminescence study of the transition from non-degenerate to degenerate doping in n-type silicon doped GaAs/AlGaAs quantum wells. C.I. Harris, B. Monemar, H. Kalt, K. Köhler and T. Schweizer, Proceedings 20th ICPS, World Scientific Publishers, 1378 (1990).

Dynamics of free and bound excitons in acceptor-doped GaAs/AlGaAs quantum wells. B. Monemar, H. Kalt, C.I. Harris, J.P. Bergman, P.O. Holtz, M.

Sundaram, J.L. Merz and A.C. Gossard, Proceedings 20th ICPS, World Scientific Publishers, 1574 (1990).

Picosecond dynamics of exciton capture, emission and recombination at shallow impurities in center-doped GaAs/AlGaAs quantum wells. C.I. Harris, H. Kalt, B. Monemar, P.O. Holtz, J.P. Bergman, M. Sundaram, J.L. Merz, and A.C. Gossard, Materials Science Forum **83-87**, 1363 (1992).

Excitons bound at shallow impurities in GaAs/AlGaAs quantum wells with varying doping level. P.O. Holtz, B. Monemar, M. Sundaram, J.L. Merz, A.C. Gossard, C.I. Harris and H. Kalt, Materials Science Forum **83-87**, 1375 (1992).

Screening and Correlation effects in degenerately center-doped GaAs/AlGaAs single quantum wells. C.I.Harris, H. Kalt, B. Monemar and K. Köhler, to appear in proceedings EP2DS 1991, to appear in Surface Science.

Effect of localisation on optical spectra for shallow acceptors in center-doped GaAs/AlGaAs multiple quantum wells. B. Monemar, P.O. Holtz, P. Bergman, C. I. Harris, H. Kalt, M. Sundaram, J.L. Merz and A.C. Gossard, to appear in proceedings EP2DS 1991, to appear in Surface Science.

Optical spectroscopy of bound excitons in AlGaAS/GaAs quantum wells. B. Monemar, P.O. Holtz, P. Bergman, C. I. Harris, H. Kalt, M. Sundaram, J.L. Merz, A.C. Gossard, K.Köhler and T. Schweizer, to appear in proceedings of workshop on excitons in confined systems Naxos, Sicily, 1991

Optically induced carrier transfer in silicon anti-modulation doped GaAs-$Al_xGa_{1-x}As$ single quantum wells. C.I. Harris, B. Monemar, G. Brunthaler, H. Kalt and K. Köhler, to appear in Phys. Rev. B